A

DISSERTATION ON

DESIGN AND CHARACTERIZATION OF RADIO ASTRONOMY FEEDS

SUBMITTED BY

VISHAKHA V. PENDSE

MO623M02

M.Tech II (E&TC-MICROWAVE)

Guided By:

Mr. A. Praveen Kumar

in partial fulfillment for the award of the degree

of

MASTER OF TECHNOLOGY

IN

ELECTRONICS & TELECOMMUNICATION ENGINEERING

(MICROWAVE ENGINEERING)

COLLEGE OF ENGINEERING PUNE

MAY-2008

COLLEGE OF ENGINEERING PUNE-411005

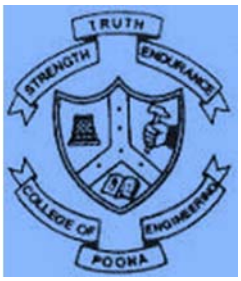

CERTIFICATE

Certified that this dissertation

"DESIGN AND CHARACTERIZATION OF RADIO ASTRONOMY FEEDS"

is the bonafide work of Vishakha Vishwas Pendse who carried out the work under my supervision

during the academic year

2007-2008

Mr. A. Praveen Kumar,
GMRT
TIFR

Prof. V.K.KOKATE
Guide
E & TC Department
COE, Pune

ABSTRACT

The science of Radio astronomy has developed a new perspective in the study of celestial objects. There is a wide variety of radio telescopes all over the world. New ideas are being implemented to improve the quality and sensitivity of radio observations. The need for high sensitivity observations has led to the development of different wideband feed systems. Two such wideband feeds are being introduced in the Giant Metrewave Radio Telescope (GMRT). GMRT is the largest radio telescope in the world operating at metre wavelengths. The wideband feeds include the Eleven feed, designed and developed by Chalmers University of Technology antenna group (Sweden) and a dual band feed designed by CSIRO (Australia), specifically for the GMRT.

This M. Tech. Thesis involves the characterization of these two wideband feeds Also, a coaxial waveguide feed has been designed, fabricated and tested to be used for the 15 metre radio telescope in NCRA (Pune) campus, which is being developed to be used as a lab facility for the radio astronomy students in NCRA. Various tests have been carried out on the wideband feeds in order to characterize their return loss, sensitivity, crosspolarization characteristics, etc. The low noise amplifiers which are used for these feeds are also characterized.

ACKNOWLEDGEMENT

I am very much grateful to Mr. A. Praveen Kumar (GMRT-TIFR) for his valuable technical guidance and suggestions that he provided me at various stages throughout the work. I have learnt a lot while working with him in GMRT.

I thank Prof.V.K.Kokate (Department of E & TC, College Of Engineering Pune) for his support, guidance and the freedom that he gave me while doing this project work.

I take this opportunity to express my sincere thanks to Prof. Jayaram Chengalur and Prof. Yashwant Gupta for believing in my abilities and giving me an opportunity to work for my M. Tech. project in GMRT. It was a valuable experience for me to work with them. I thank Prof. S. Ananthakrishnan for initiating the talks regarding this project work. I thank the management of GMRT-TIFR for all the facilities they provided me including the library and the internet throughout the tenure of my work.

I thank Mr. G. Sankar for helping and guiding me in designing and testing the coaxial feed. His knowledge in antennas and their mechanical aspects was of great help to me. The success of my work would not have been possible without the cooperation of the staff in the Front End Lab of the GMRT. I am deeply thankful to all of them for helping me from time to time. I am thankful to Mr. Subhash Thepane with whom I worked while testing the Eleven feed. I am also grateful to the staff in NCRA and GMRT workshops for their promptness in fabricating and delivering the feed as well as other mechanical items.

My stay in GMRT is a memorable experience for me. I would like to thank all of my friends here for those joyful moments that they shared with me.

TABLE OF CONTENTS

LIST OF FIGURES

Figures

LIST OF TABLES

Table

CHAPTER ONE

Introduction

In the short space of a few decades, Radio Astronomy has advanced our knowledge of the universe in an amazing way. Radio astronomy deals with radio signals originating from the celestial bodies. These signals are very much weak in nature. So in order to capture these signals, the receivers in radio telescopes have to be highly sensitive. One of the most important factors which play a key role in deciding the sensitivity of a radio telescope is the feed antenna.

1.1 Significance of reflector antenna feeds in radio astronomy:

The antenna is at the front end of the radio astronomy receiver. Therefore it plays a vital role in deciding the sensitivity of a radio telescope. The most popular configuration of a radio telescope antenna contains a reflector antenna fed with a feed antenna. A wide variety of feed antennas is available ranging from dipoles to corrugated horns. The feeds are in general designed to maximize the gain as well as the aperture efficiency of the reflector antenna. The feed should be able to efficiently couple the signals reflected from the reflector to the electronics placed after the feed. So an excellent impedance match between the feed and the first stage low noise amplifier is desired. Given these constraints, the bandwidths achieved by the feeds are usually narrow. But high sensitivity astronomical observations require broader bandwidths. Because of these

stringent requirements, the feed is a very important factor in deciding the quality of performance of the radio telescope.

This M. Tech project is on radio astronomy feeds. The project work is carried out at the Giant Metrewave Radio Telescope (GMRT). It involves designing a coaxial waveguide feed working at 700 MHz, for a small radio telescope at NCRA-TIFR (Pune). Also, characterization of two broadband feeds is done. One of the feeds is the 200-800 MHz Eleven feed, which is specifically optimized by the Chalmers antenna group, Sweden for the GMRT. The other feed is the 550-900 MHz part of the dual band feed designed by CSIRO (Australia) again specifically for the GMRT. The project work also involves testing and characterization of the low noise amplifiers designed for these feeds.

1.2 The Giant Metrewave Radio Telescope (GMRT):

The GMRT is situated at Khodad, about 80 km North of Pune. The GMRT consists of an array of 30 antennas. Each antenna is 45 meters in diameter and has been designed to operate at a range of frequencies from 50 MHz to 1450 MHz. the antennas have been constructed using a novel technique(named SMART) and their reflecting surface consists of panels of wire mesh. These panels are attached to rope trusses and by appropriate tensioning of the wires used for attachment the desired parabolic shape is achieved. The design has very low wind loading as well as a very low total weight for each antenna.

The GMRT has a hybrid array configuration, with 12 of its antennas randomly distributed in a central region (about 1 km across), called the Central Square. The remaining antennas are distributed in a roughly Y shaped configuration, with the length

of each arm of the Y being about 14 km. The maximum baseline length between the extreme arm antennas is around 25 km.

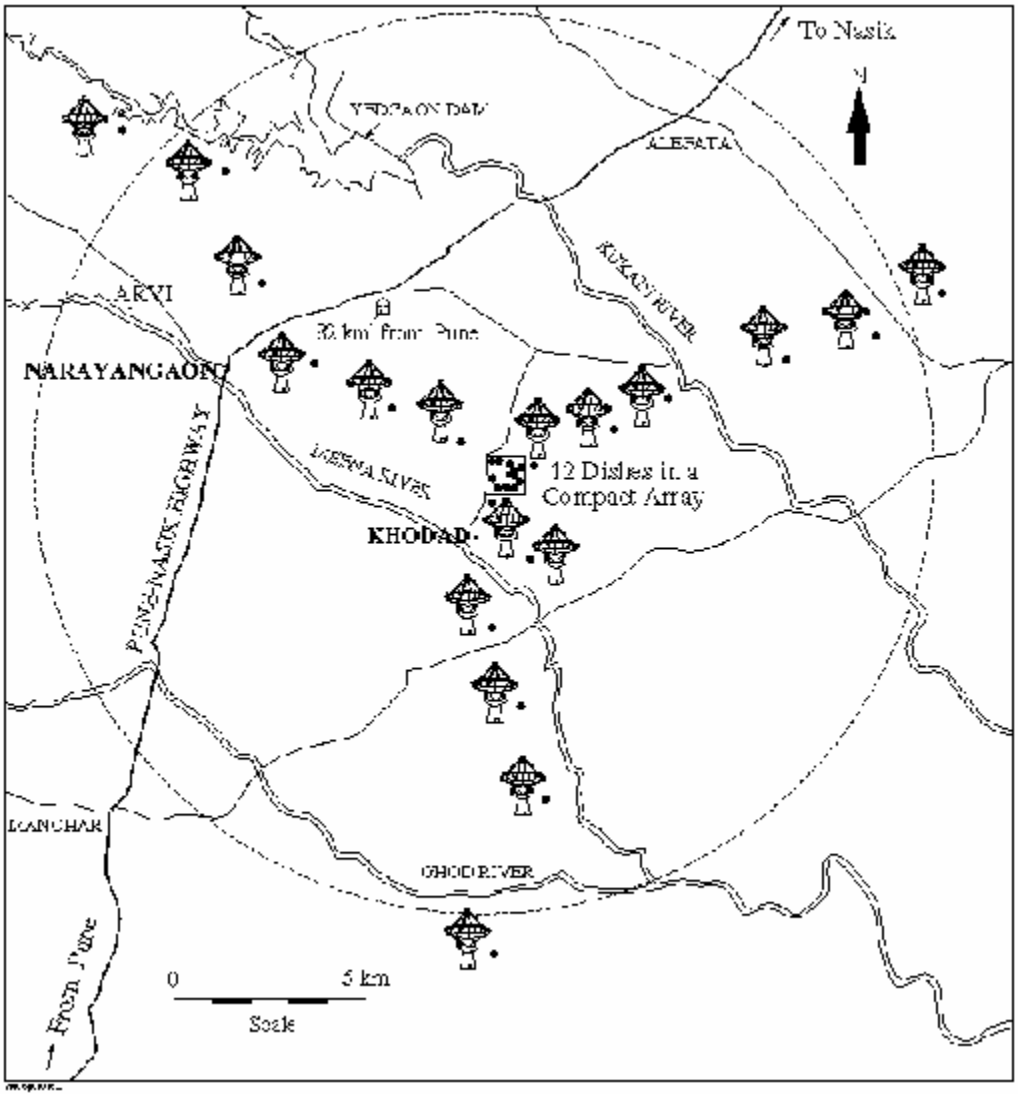

Fig. 1.1 The GMRT array configuration [33]

The GMRT currently operates at 5 different frequencies. The feeds, (except the 1420 feed) are circularly polarized.

The feeds are mounted on four faces of a feed turret placed at the focus of the antenna. The feed turret can be rotated to make any given feed point to the vertex of the antenna.

1.3 Organization of the Thesis:

The second chapter of the thesis introduces some of the basic concepts in radio astronomy. Chapter 3 discusses the key aspects of radio telescope antennas and receivers. Chapter 4 discusses the most widely used radio astronomy antennas - the aperture antennas, their principle of working and the parabolic reflector antennas. Chapter 5 discusses the feeds used for parabolic reflectors. Chapters 6 and 7 describe the testing and characterization of the two broadband feeds, the Eleven feed and the CSIRO dual band feed, respectively. Chapter 8 illustrates the designing of the 700 MHz coaxial waveguide feed. Chapter 9 includes the conclusion and discussion of future work.

CHAPTER TWO

Radio Astronomy Fundamentals

Until a few decades ago man's knowledge of the universe outside the earth came almost entirely from optical astronomy observations. All observations were in the visible band of electromagnetic spectrum in a band about one octave wide. During the 20th century astronomical observations at radio wavelengths created a new branch of astronomy called radio astronomy. The positions of optical astronomy (i.e. in the visible spectrum) and radio astronomy in the electromagnetic spectrum coincide with the two principal transparent bands of the earth's atmosphere and ionosphere. These transparent bands are often called optical and radio windows.

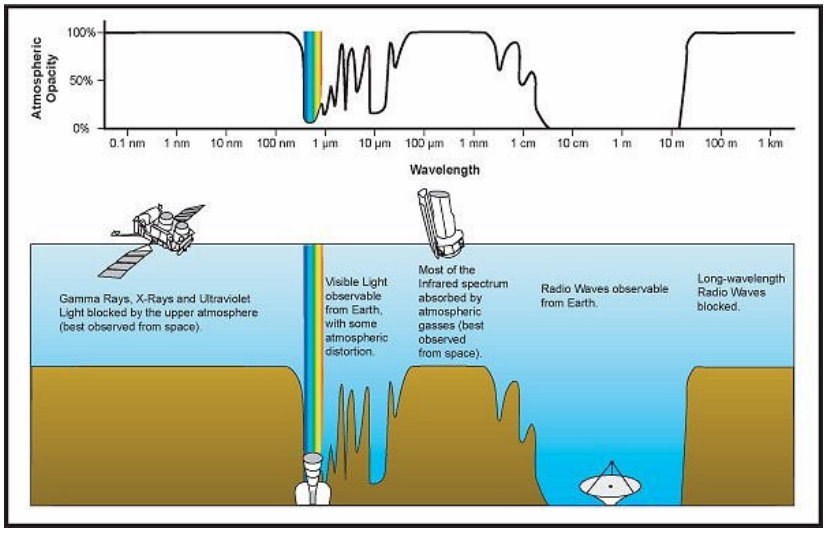

Fig. 2.1 Electromagnetic spectrum showing relative transparency of the earth's atmosphere and ionosphere. [35]

Table 2.1 shows some of the milestones in the development of the science of radio astronomy.

Table 2.1 Historical development of radio astronomy [34]

Year	Development
1931	Karl G. Jansky noticed the disturbances coming from the centre of the Milky way.
1937	Grote Reber constructed the first parabolic reflector antenna 31 ft in diameter. He made the first radio maps of the sky.
1942	J. S. Hey made the first observation of radio emission from the sun.
1944	van de Hulst predicted the presence of neutral hydrogen line in the radio spectrum at 1420 MHz.
1963	Arno Penzias and Robert Wilson discovered the cosmic background radiation.
1967	Jocelyn Bell-Burnell and Anthony Hewish discovered the first Pulsar.

In the next sections, some of the basic terms and concepts in radio astronomy will be discussed.

2.1 Power, Spectral Power and Brightness: [1]

Consider electromagnetic radiation from the sky falling on a flat horizontal area A at the surface of the earth, as shown in the fig. 1.2.

The infinitesimal power dW from a solid angle dΩ of the sky incident on a surface of area dA is

$$\mathbf{dW = B \cos\theta \, d\Omega \, dA \, df} \qquad (2.1)$$

Where dW = infinitesimal power, watts

B = brightness of sky at position of dΩ, watts m^{-2} $Hz^{-1}rad^2$

dΩ = infinitesimal solid angle of sky (sin θ dθ dφ), rad^2

θ = angle between dΩ and zenith, rad

dA = infinitesimal area of surface, m^2

df = infinitesimal element of bandwidth, Hz

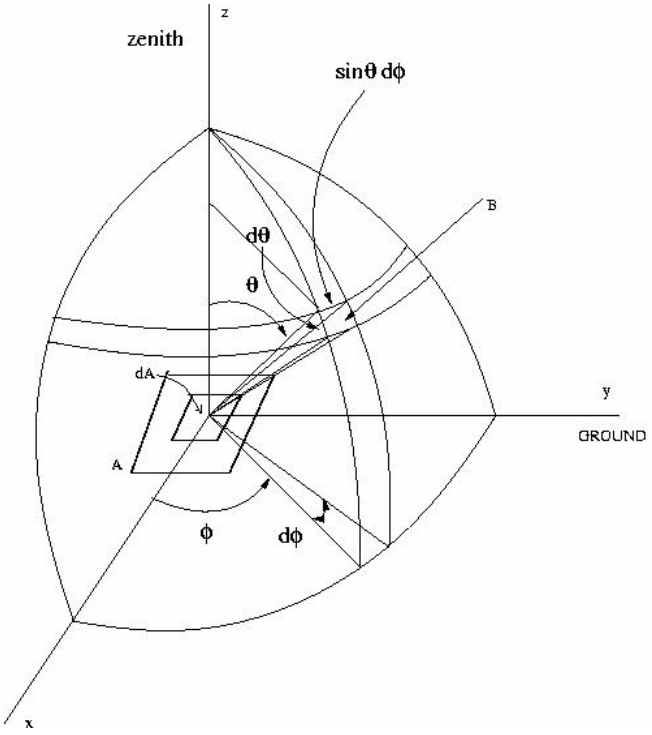

Fig 2.2. Basic geometry for radiation of brightness B incident on a flat area. [1]

The quantity B is called the sky brightness or simply the **brightness**. It is a fundamental quantity of radio and optical astronomy and is a measure of rms power received per unit area per unit solid angle per unit bandwidth. The element of bandwidth lies between a particular frequency f and f+df.

If dW is independent of the position of dA on the surface, the infinitesimal power received by the entire surface A is

$$dW = AB \cos \theta \, d\Omega \, df \tag{2.2}$$

integrating (2), we can obtain the power W received over a bandwidth Δf from a solid angle Ω of the sky.

In general, the brightness is a function of both the position (in the sky) and of the frequency. The variation of the brightness B with frequency is called the brightness spectrum.

The power per unit bandwidth is called the **spectral power**, since its variation with frequency constitutes the power spectrum. Thus, (1) becomes

$$dw = B \cos \theta \, d\Omega \, dA. \tag{2.3}$$

Where dw = spectral power, or infinitesimal power per unit bandwidth, watts per Hz.

We can obtain the spectral power from a solid angle Ω of the sky, by integrating (3).

$$w = A\iint B \cos \theta \, d\Omega \tag{2.4}$$

where w = spectral power, or power per unit bandwidth, watts per Hz.

Brightness Distribution:

Since the sky brightness may vary with direction, it is, in general, a function of angle. This may be expressed by the symbol $B(\theta, \varphi)$ for the brightness. Thus, the spectral power in (4) becomes

$$w = A\iint B(\theta, \varphi) \cos \theta \, d\Omega \quad \text{watts per Hz}$$

2.2 Blackbody Radiation and Planck's Radiation Law: [1]

All objects at temperatures above absolute zero radiate energy in the form of electromagnetic waves. The objects not only radiate electromagnetic energy, but they also may absorb or reflect such energy incident on them. A perfect absorber is called a blackbody and it follows that such a body is also a perfect radiator. A blackbody absorbs all the radiation falling upon it at all wavelengths and the radiation from it is a function of only the temperature and wavelength. Such a body is an idealization, since no body having this property exists.

The brightness of the radiation from a blackbody is given by Planck's radiation law. This law states that the brightness of a blackbody radiator at a temperature T and frequency f is expressed by

$$B = \frac{2hf^3}{C^2} \cdot \frac{1}{e^{hf/kT} - 1} \qquad (2.5)$$

Where B = brightness, watts m^{-2} Hz^{-1} rad^{-2}

h= Planck's constant (= 6.63 X 10^{-34} joule sec)

f = frequency, Hz

c = velocity of light (= 3 X 10^8 m/s)

k = Boltzmann's constant (= 1.38 X 10^{-23} joule K^{-1})

T = temperature, K

Significance of Planck's Law:

The brightness B for a blackbody radiator at four temperatures is shown in the following figure. B tends to zero for large or small frequencies, with its maximum value at an intermediate frequency. Also, the point of maximum brightness shifts to higher frequency as the temperature is increased.

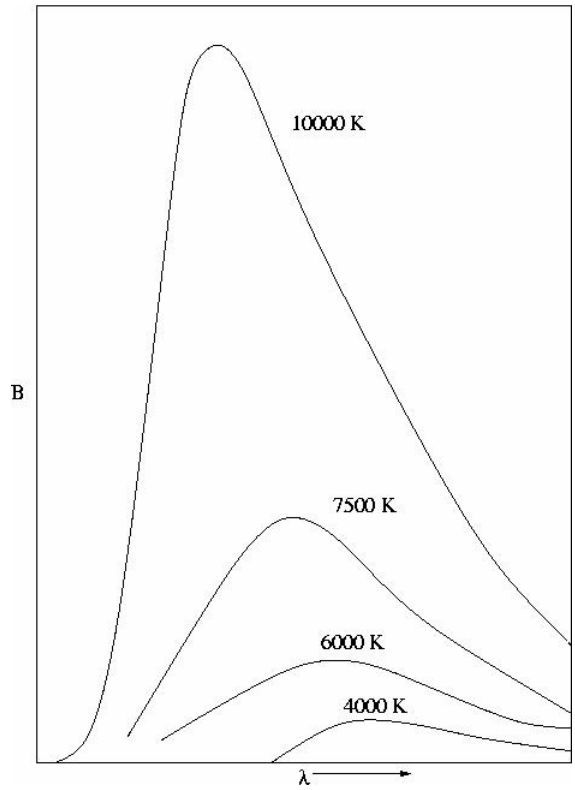

Fig 2.3 .Planck's Radiation law curves for a blackbody radiator as a function of wavelength at four temperatures. [1]

We can also state Planck's radiation law so that the brightness is expressed in power per unit area per unit wavelength per unit solid angle. So, we have

$$B_\lambda = \frac{2hc^2}{\lambda^5} \quad \frac{1}{e^{(hc/kT\lambda)} - 1} \qquad (2.6)$$

Where B_λ = brightness of blackbody radiator in terms of unit wavelength, watts m^{-3} rad^{-2}

To calculate the total brightness of a blackbody radiator, we have to integrate Planck's law over all frequencies. This relation between the total brightness of a blackbody radiator and its temperature is the **Stefan-Boltzmann law**. It states that the total brightness of a blackbody radiator is proportional to the fourth power of its absolute temperature.

Stefan-Boltzmann Law:

$$B' = \sigma T^4 \tag{2.7}$$

Where B' = total brightness, watts m^{-2} rad^{-2}

σ = constant (= 1.80 X 10^{-8} watt m^{-2} K^{-4})

T = temperature of blackbody, K.

An important characteristic of the Planck radiation law curves is that the peak brightness shifts to higher frequency with increase in temperature**. Wien Displacement Law** gives a quantitative expression for this displacement.

Wien Displacement Law:

Under the assumption that $e^{hf/kT} >> 1$, we have for f_m, the frequency at which B is a maximum,

$$(hf_m/kT) = 3.$$

Therefore

$$\boxed{\lambda_m T = \frac{hc}{3k} = 0.0048 \text{ m K}} \tag{2.8}$$

Where λ_m = wavelength at which B is a maximum, m.

Significance of the Wien displacement law:

This law indicates that the wavelength of the maximum or peak brightness varies inversely with the temperature. Due to the simplification of neglecting unity in comparison with $e^{hf/kT}$, the constant 0.0048 is an approximation. A more accurate value, obtained without making this simplification, is 0.0051 m K

If the brightness is expressed in terms of unit wavelength, the wavelength for the peak brightness is not the same as when brightness is expressed in terms of unit bandwidth. So, maximizing (2.6) and simplifying it in the same way as is done while obtaining (2.8) , we obtain (with the assumption that $e^{hf/kT} >> 1$)

$$\lambda_m T = hc/ 5k = 0.00288 \text{ m K}.$$

like (2.8) , this is also an approximation and a more accurate value obtained without simplifying assumptions is 0.0029 m K .

Hence

$\lambda_m T = 0.0051$ m K for brightness in terms of unit frequency

$\lambda_m T = 0.0029$ m K for brightness in terms of unit wavelength.

Rayleigh-Jeans Law and Wien Radiation Law:

In the region of radio wavelengths the product hf may be very small compared to kT ($hf << kT$), so that the second factor on the right side of Planck's radiation law (5) can be reexprssed as:

$$e^{hf/kT} - 1 = 1 + (hf/kT) - 1 = (hf/kT).$$

Thus,

$$B = \frac{2kT}{\lambda^2} \qquad (2.9)$$

This is the **Rayleigh- Jeans Law**, which is a useful approximation in the radio part of the spectrum.

At shorter wavelengths, where hf>>kT, the quantity unity in the denominator of the second factor on the right side of Planck's law (5) can be neglected in comparison with $e^{hf/kT}$, so that the Planck law reduces to

$$B = (2hf^3 / c^2)\, e^{-hf/kT} \qquad (2.10)$$

This approximation is called the Wien radiation law. As indicated in the following figure, the Wien law curve coincides the Planck law curve at wavelengths considerably less than the wavelength of maximum radiation.

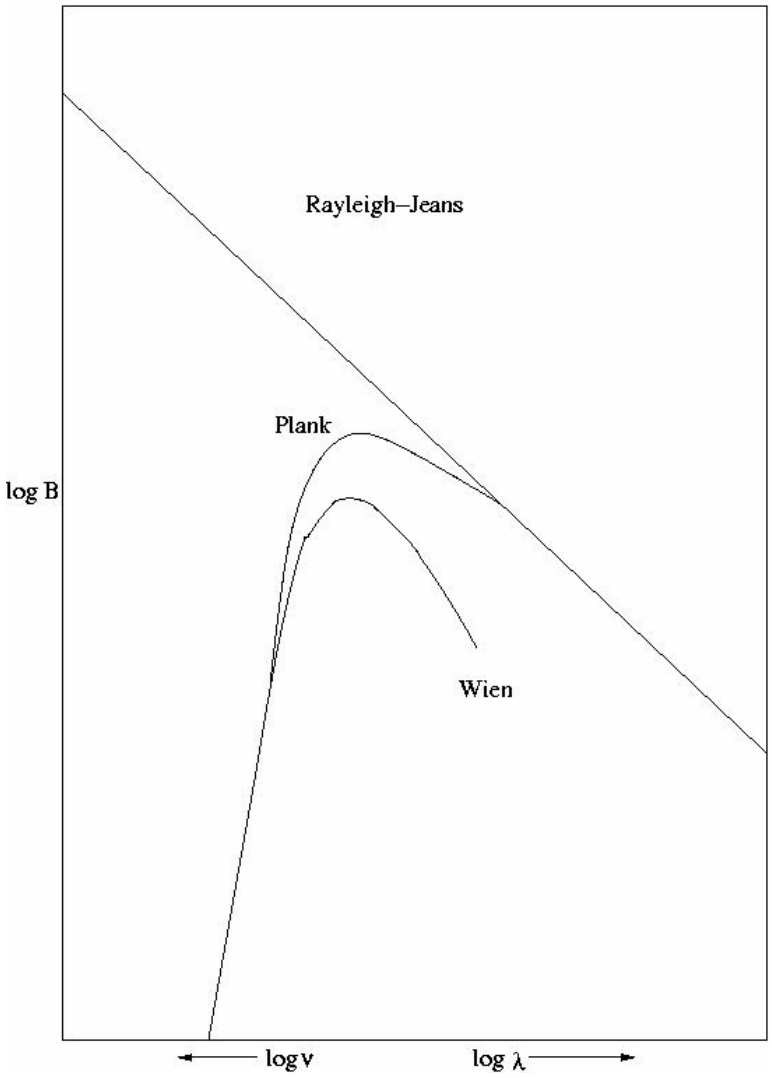

Fig 2.4 The curves of Rayleigh-Jeans law and Wien law of radiation coinciding the Planck's law curve at different parts of the spectrum [1]

The radio astronomy antenna-receiver basically acts like a heat-measuring device, in the sense that the radiation resistance of the antenna measures the equivalent temperature of distant parts of space to which it is projected by the antenna response pattern. Thus the concept of antenna temperature is very important in radio astronomy.

2.3 Antenna Temperature: [1]

The rms noise power per unit bandwidth available at the terminals of a resistor of resistance R and temperature T is given by

$$w = kT. \tag{2.11}$$

Where w = spectral power, watts Hz^{-1}

k = Boltzmann's constant

T = absolute temperature of resistor, K

If the resistor is replaced by a lossless matched antenna of radiation resistance R, the impedance presented at the input is unchanged. However, the noise power will not be the same unless the antenna is receiving from a region at the temperature T. The power per unit bandwidth received by the antenna is

$$w = (1/2)\, A_e \iint B(\theta, \varphi)\, P_n(\theta, \varphi)\, d\Omega \tag{2.12}$$

If the antenna is placed inside a blackbody enclosure at a temperature T, then the brightness will be a constant B_c in all directions. Its value according to Rayleigh-Jeans law will be

$$B(\theta, \varphi) = B_c = (2kT/\lambda^2)$$

Thus

$$w = (kT/\lambda^2)\, A_e\, \Omega_A$$

where $\Omega_A = \int P_n(\theta, \varphi)\, d\Omega$ = the beam area of the antenna which is the angle through which all the power from a transmitting antenna would stream if the power (per unit solid angle) were constant over this angle and equal to its maximum value.

Also, $$A_e\, \Omega_A = \lambda^2$$

Hence

$$w = kT$$

this is the same noise power as for the resistor.

It is not the temperature of the antenna structure which determines the temperature of its radiation resistance. The temperature of the radiation resistance is determined by the region or regions within the antenna beam.

Minimum Detectable Temperature:

The minimum antenna temperature which a radio telescope can detect is limited by fluctuations in the receiver output caused by the statistical nature of the noise waveform. The noise is proportional to the system temperature T_{sys} of the radio telescope, which can be divided in two principal parts, that contributed by antenna T_A and that contributed by the receiver T_R .

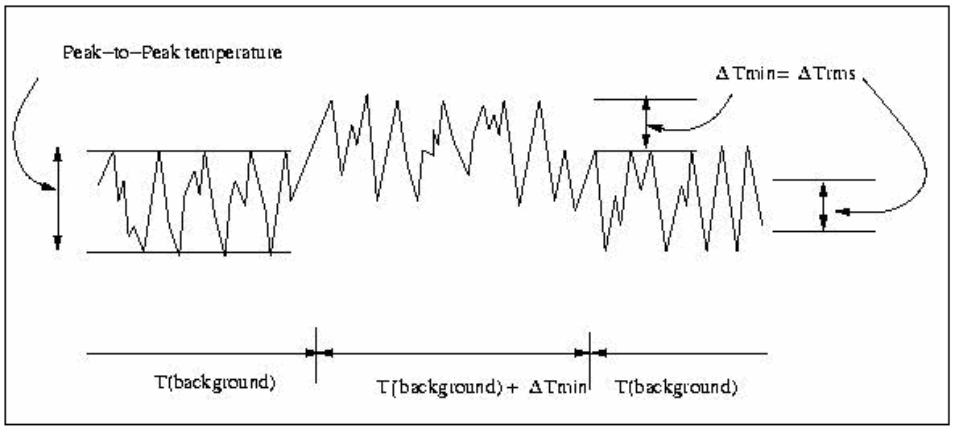

Fig 2.5 Typical radio telescope record showing output fluctuations due to the antenna and receiver noise temperature and due to this temperature plus the minimum detectable temperature ΔT_{min} [1]

The sensitivity or minimum detectable temperature of a radio telescope is equal to the rms noise temperature of the system as given by

$$\Delta T_{min} = \frac{K_s T_{sys}}{\sqrt{(\Delta f\, tn)}} = \Delta T_{rms} \qquad (2.13)$$

Where ΔT_{min} = sensitivity, or minimum detectable temperature, K

ΔT_{rms}= rms system noise temperature, K

T_{sys} = system noise temperature, K

K_s= sensitivity constant, dimensionless.

Δf = predetection bandwidth, Hz

t= postdetection integration time, sec.

n= number of records averaged, dimensionless.

The constant K_s depends on the type of receiver and its mode of operation but is of the order of unity.

Putting (13) in the Rayleigh-Jeans relation, we obtain for the minimum detectable brightness

$$\Delta B_{min} = \frac{2k}{\lambda^2} \frac{K_s T_{sys}}{\sqrt{(\Delta f\, tn)}} \qquad (2.14)$$

2.4 Polarization and Stokes Parameters:[1]

The emission from celestial radio sources extends over a wide frequency range and within any finite bandwidth Δf consists of the superposition of a large number of statistically independent waves of a variety of polarizations. The resultant wave is said to be randomly polarized. The most general situation is one in which the wave is partially polarized, i.e. it may be considered to be of two parts, one completely polarized and the other completely unpolarized. The waves emitted by celestial radio sources are generally of the partially polarized, tending in many cases to completely unpolarized radiation but in other cases a significant amount of polarization. It is convenient to use Stoke's parameters to deal with partial polarization.

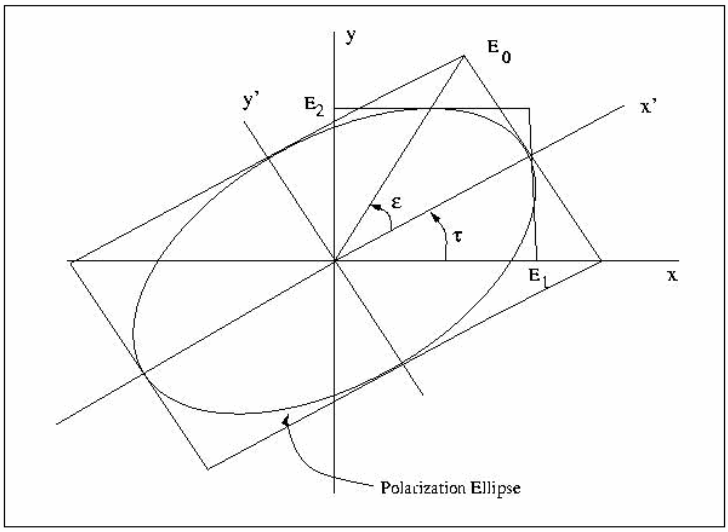

Fig. 2.6 Relation of polarization ellipse axes (x', y') to reference axes (x, y) [1]

Consider a completely polarized wave with polarization ellipse as shown above.

Here, $E_x = E_1 \sin(\omega t - \delta_1)$

$$E_y = E_2 \sin(\omega t - \delta_2)$$

Where $(\delta_1 - \delta_2)$ is the phase difference of E_x and E_y .

The magnitude of the total pointing vector or flux density (watts per square metre) of the wave is

$$S = Sx + S_y$$

$$= (E_1^2 / Z) + (E_2^2 / Z)$$

$$= (E_1^2 + E_2^2) / Z$$

$$S = E_0^2 / Z$$

Where Z is the intrinsic impedance of the medium. S_x represents the Poynting vector for the wave component polarized in the x direction and S_y represents the Poynting vector for the wave component polarized in the y direction.

The Stokes parameters I, Q, U and V are Defined as follows:

$$I = S = S_x + S_y = \frac{E_1^2 + E_2^2}{Z} = \frac{E_0^2}{Z}$$

$$Q = S_x - S_y = \frac{E_1^2 - E_2^2}{Z} = S \cos 2\varepsilon \cos 2\tau$$

$$U = (S_x - S_y) \tan 2\tau = S \cos 2\varepsilon \sin 2\tau$$

$$= 2 \frac{E_1 E_2}{Z} \cos(\delta_1 - \delta_2)$$

$$V = (S_x - S_y) \tan 2\varepsilon \sec 2\tau = S \sin 2\varepsilon$$

$$= 2 \frac{E_1 E_2}{Z} \sin(\delta_1 - \delta_2)$$

It follows that

$$I^2 = Q^2 + U^2 + V^2$$

$$\frac{U}{Q} = \tan 2\tau$$

$$\frac{V}{S} = \sin 2\varepsilon = \frac{V}{\sqrt{Q^2 + U^2 + V^2}}$$

These are the relations for a completely polarized wave.

For a completely unpolarized or partially polarized wave, the x and y components are

$$E_x = E_1(t) \sin [\, \omega t - \delta_1(t)]$$

$$E_y = E_2(t) \sin [\, \omega t - \delta_2(t)]$$

In this case, it is necessary to take time averages.

Hence the Stokes parameters are

$$I = \frac{\langle E_1^2 \rangle}{Z} + \frac{\langle E_2^2 \rangle}{Z} = S_x + S_y = S$$

$$Q = \frac{\langle E_1^2 \rangle}{Z} - \frac{\langle E_2^2 \rangle}{Z} = S_x - S_y$$

$$= S \langle \cos 2\varepsilon \cos 2\tau \rangle$$

$$U = \frac{2}{Z} \langle E_1 E_2 \cos \delta \rangle = S \langle \cos 2\varepsilon \sin 2\tau \rangle$$

$$V = \frac{2}{Z} \langle E_1 E_2 \sin \delta \rangle = S \langle \sin 2\varepsilon \rangle$$

and

$$I^2 \geq Q^2 + U^2 + V^2$$

where

$$\delta = \delta_1 - \delta_2$$

Significance of the Stokes parameters:

- I represents the total power (sum of x and y components).
- Q represents the difference of the x and y power components
- U represents a power proportional to the time average of the real part of $e^{j\delta}$ and the product of the magnitudes the x and y field components.
- V is the same as U except that it involves the imaginary part of $e^{j\delta}$

I and Q can also be regarded as the sum and difference of two autocorrelation functions while U and V can be regarded like the crosscorrelation functions of E_1 and E_2. For a completely unpolarized wave, $S_x = S_y$ and E_1 and E_2 are uncorrelated. Thus, I=S, Q =U =V=0.

The degree of polarization d is defined as the ratio of the completely polarized power to the total power.

$$d = \frac{\text{Polarized Power}}{\text{Total Power}} = \frac{\sqrt{(Q^2 + U^2 + V^2)}}{I} \qquad 0 \le d \le 1 \tag{2.15}$$

The degree of polarization d is unity for a completely polarized wave and is zero for a completely unpolarized wave.

Table 2.2 Stokes parameters for some particular types of waves.

Type of Wave	Stokes Parameters (I, Q, U, V)
Unpolarized wave	(1, 0, 0, 0)
Right Circularly Polarized wave	(1, 0, 0, -1)
Left Circularly Polarized wave	(1, 0, 0, 1)
Completely Linearly Polarized wave With $\tau = 0$, $S_x = S$, $S_y = 0$, $\varepsilon = 0$, AR=∞	(S, S, 0, 0)
Partially Polarized wave, d= (1/3), Completely polarized part linearly polarized With $\tau = 45^0$	(1, 0, 1/3, 0)

CHAPTER THREE
Receivers and Antennas in Radio Astronomy

The function of a radio telescope receiver is to detect and measure the radio emission of celestial sources. In most cases the emission consists of incoherent radiation whose statistical properties do not differ from the noise originating in the receiver or from the background radiation coupled to the receiver by the antenna. The power level of the signal in radio-telescope receivers is quite small, of the order of 10^{-15} to 10^{-20} watts. The power received from the background may be much higher than this, so that both high sensitivity and high stability of the receiver are important requirements. In some cases, however, other receiver characteristics, such as the ability to detect the signal spectrum as a function of time, are important.

The antenna, being at the front end of the radio telescope system, is one of the most crucial components of the system. It plays a vital role in deciding the sensitivity of the radio telescope system. According to the stringent requirements of radio astronomy, antennas having desirable characteristics are chosen and designed.

3.1 A Typical Radio Astronomy Receiver[1]

The most common type of radio astronomy receivers is the superheterodyne receiver. The signal power, having a centre frequency f_{RF} , is coupled to the receiver by an antenna and is first amplified in a radio-frequency amplifier, which is a low noise amplifier (LNA) having a gain of the order of 10 to 30 dB. The next stage is a mixer, where the weak signal is mixed with a strong local oscillator signal at a frequency f_0

producing an output signal on an intermediate frequency (IF), the IF signal power being directly proportional to the RF signal power. The IF signal is then amplified with a gain of the order of 60 to 90 dB. The largest part of the gain in a superheterodyne receiver is obtained in this IF amplifier, which also usually determines the predetector bandwidth of the receiver. The IF amplifier is followed by a detector, which is normally a square-law device in which the dc output voltage is directly proportional to the input-voltage amplitude squared. Thus the output dc voltage of the detector is directly proportional to the output noise power of the predetection section of the receiver. Final stages usually consist of a low-pass filter or integrator and a data-recording system. The integrator integrates the observed signal power for a predetermined length of time. Following is the block diagram for a typical superheterodyne radio astronomy receiver.

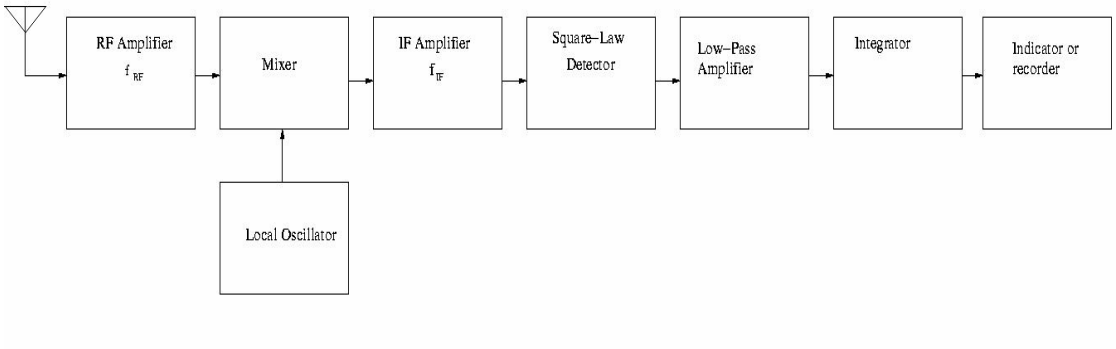

Fig. 3.1 A typical superheterodyne radio astronomy receiver [1]

The section after the mixer is same for all frequencies. Only the RF amplifier, the mixer and the local oscillator must be designed separately for each frequency range. The section before the detector is usually called the high-frequency part of the receiver or the predetection section. The section following the detector is called the low-frequency part or the postdetection section.

3.1.1 Design considerations in receiver:

1. Sensitivity: A receiver's sensitivity is a measure of its ability to discern low-level signals. It is normally taken as the minimum input signal required to produce a specified output signal. As we saw in chapter two, in radio astronomy receivers it is called the minimum detectable temperature and is given as

$$\Delta T_{min} = \frac{K_s T_{sys}}{\sqrt{(\Delta f\, tn)}} = \Delta T_{rms}$$

To achieve better sensitivity, we have to design the receiver so as to achieve one or more of the following.

1. Low system noise temperature.

2. Wide bandwidth of the receiver system.

3. Large postdetection integration time.

But in practice, the integration time cannot be increased beyond the point where it begins to distort a true source profile. Also, bandwidth of the receiver system cannot be increased beyond the bandwidth of the feed-antenna combination. The system noise temperature is made up of the antenna temperature and the receiver noise temperature. The use of high gain, low noise amplifiers can reduce this noise temperature and hence improve the sensitivity. The transmission line losses should also be minimized in order to

minimize the system noise temperature. Broadband feeds and hence broadband receivers, too improve the sensitivity of the system.

2. **Stability:** With the very high gains that are necessary in radio telescope receivers, gain variations are unavoidable. Short- and long-period gain variations can occur that are due, for example to supply voltage variations and to ambient temperature fluctuations. By carefully stabilizing all supply voltages and the operating temperature, gain stability can be achieved to some extent.

Gain instability can reduce the system sensitivity.

3.1.2 Key factors in designing a sensitive and stable radio astronomy receiver[5]

Each of the various blocks in the receiver chain has some gain (or loss) associated with it. That is, the receiver gain is distributed. There are several design considerations in determining the distribution of gain across the receiver.

1. The response of the entire system should remain linear over a wide range of noise temperatures from cold sky to the high antenna temperatures anticipated when observing strong sources like the Sun.

2. The entire receiver system should remain linear even in the presence of strong interference signals. In particular, the intermodulation distortion (IMD) products should remain below a critical threshold. Also the receiver should have a high desensitization dynamic range, which is the power ratio between the level of the strong undesired signal which reduces the SNR by 1 dB and the receiver noise floor.

3. Internally generated spurious products (if any) in the receiver must be very low compared to the receiver noise floor.

4. The receiver should have a good image rejection.

Receiver Calibration: Calibration of radio-astronomy receivers is necessary to provide an absolute scale of antenna temperature. Calibration should be frequently checked because of possible receiver gain and noise temperature variations. To calibrate the gain of the receiver, a standard noise generator can be used to inject a known amount of noise power in the receiver chain.

3.2 Significance of Antennas in Radio Astronomy:

Antennas are at the front end of the radio telescope. The receiver measures the antenna temperature i.e. the temperature of the radiation resistance of the antenna. Antenna temperature depends on the region or regions that are within the antenna beam. Thus, the radiation pattern of the antenna is a very important parameter because it decides the antenna temperature. The antenna should 'look' at the desired radio source and should minimize the noise contribution from undesired locations, for example, the ground. Otherwise the temperature measured by the receiver (which is assumed to be corresponding to the radio source) will not be correct. Also, the signals picked up by the antenna should be efficiently transmitted to the receiver. Hence the impedance match between the antenna (feed) and the first stage low noise amplifier is a crucial point.

The resolving power of the radio telescope is ultimately decided by the antenna radiation pattern and the array configuration. As we saw in the previous section, the sensitivity of the receiver is improved if the antenna (feed) is wideband. The polarization efficiency of the antenna is also an important parameter in radio astronomy receivers.

Thus, antennas are among the most significant factors which decide the performance of the radio telescope.

3.3 Characterization of Antennas:

The IEEE definition of an antenna describes it as 'that part of a transmitting or receiving system that is designed to radiate or receive electromagnetic waves.' Most antennas are reciprocal and behave the same on transmit as on receive.

3.3.1 Classification of Antennas:[3]

Antennas are roughly classified as follows:

Table 3.1 Antenna classification

Type of Antenna	Characteristics	Examples
Electrically Small Antenna	Antenna Structure size much smaller than operating wavelength. Low directivity, low input resistance, high input reactance, low radiation efficiency	Small dipoles and small loops
Resonant Antenna	Operate well at single or selected narrow frequency bands. Low to moderate gain, real input impedance.	Half-wave dipole, microstrip patch antenna, Yagi-Uda antenna
Broadband Antenna	Have an active region which relocates on the antenna as the frequency changes. Constant and real input impedance, low to moderate gain.	Log-periodic and spiral antenna
Aperture Antenna	Have physical aperture through which electromagnetic energy flows. Have high gain increasing with frequency, moderate bandwidth	Horn, waveguide antennas, reflector antennas

3.3.2 Antenna Parameters:

- **Radiation Pattern: [2,3,4]**

A radiation pattern is defined as a mathematical function or a graphical representation of the radiation properties of the antenna as a function of space coordinates. In most cases, radiation pattern is determined in the far-field region and is represented as a function of the directional coordinates. Radiation properties include power flux density, radiation intensity, field strength, directivity, phase or polarization.

Isotropic, directional and omnidirectional patterns:

An isotropic radiator is defined as a hypothetical lossless antenna having equal radiation in all directions. It is often taken as a reference for expressing the directive properties of actual antennas.

A directional antenna is one having the property of radiating or receiving electromagnetic waves more efficiently in some directions than in others.

An omnidirectional antenna is defined as one having an essentially nondirectional pattern in a given plane and a directional pattern in an orthogonal plane. An omnidirectional pattern is a special type of a directional pattern.

Principal Patterns:

Although the total pattern of an antenna is three-dimensional, the pattern in a particular plane is often of interest. The three-dimensional pattern is usually represented in terms of the two-dimensional patterns in two planes that form 90 degree angles with each other, with the origin of a spherical co-ordinate system on their intersection line. The $\Phi = 0^0$ direction is taken to lie along the intersection line and the $\theta = 0^0$ direction is then perpendicular to this line and lies in one of the planes. These are called principal

planes and the patterns in them are the principal plane patterns of the antenna. For linearly polarized antennas, usually one of the principal planes is taken as the plane in which the E-field lies. This plane pattern is called the E-plane pattern and the orthogonal plane pattern is called the H-plane pattern.

As an example, let us consider the radiation pattern of an ideal dipole as shown in the following figure which clearly shows the E- and H-plane radiation patterns.

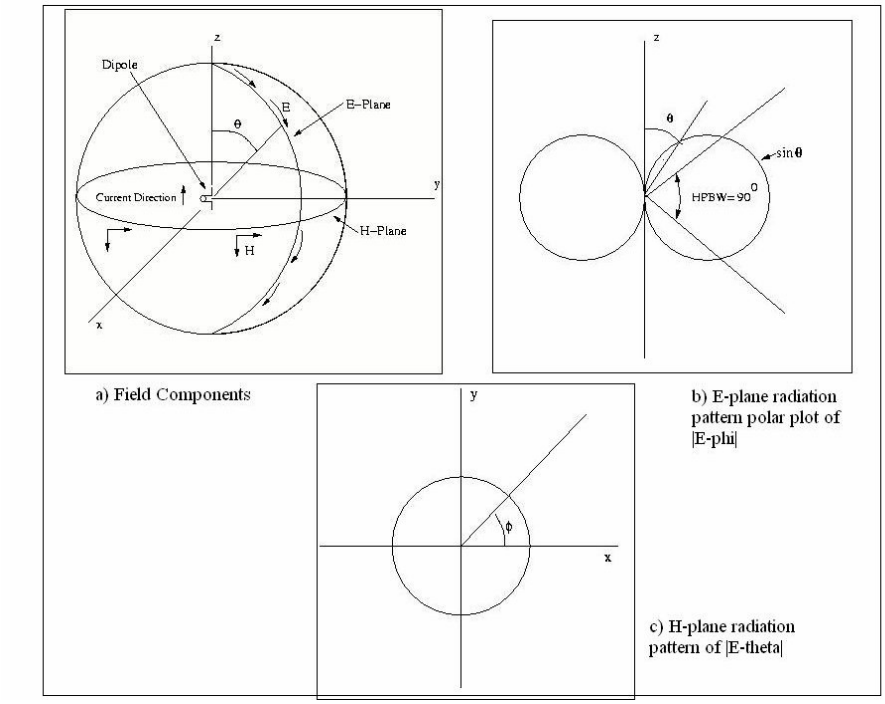

Fig 3.2 Radiation from an ideal dipole.[3]

Radiation pattern lobes:

A typical antenna power pattern is shown in the following figure. It has several lobes.

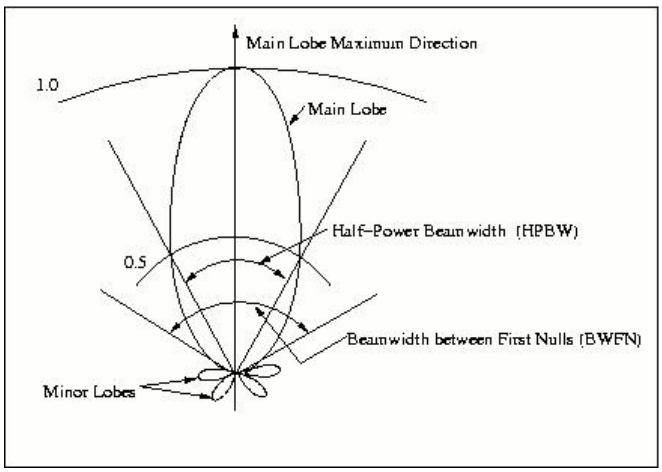

Fig 3.3 A typical power pattern polar plot.[3]

A radiation lobe is a portion of the radiation pattern bounded by regions of relatively weak radiation intensity.

The Main Lobe (or the Main Beam) is the lobe containing the direction of maximum radiation.

Any lobe other than the main lobe is called as a Minor Lobe. Minor lobes are composed of side lobes and back lobes. A side lobe is a radiation lobe in any direction other than the intended lobe. Back Lobes are directly opposite the main lobe.

- **Radiation Power Density:[2]**

Electromagnetic waves are used to transport information through a wireless medium or a guiding structure, from one point to the other. So power and energy are assumed to be associated with electromagnetic fields. The instantaneous Poynting vector, which is define as

$$W = E \times H \tag{3.1}$$

Where

W = instantaneous Poynting Vector, watts m^{-2}.

E = instantaneous electric field intensity.

H= instantaneous magnetic field intensity.

The total power crossing a closed surface can be obtained by integrating the normal component of the Poynting vector over the entire surface.

- **Radiation Intensity: [2]**

Radiation intensity in a given direction is defined as the power radiated from an antenna per unit solid angle. In mathematical form it is expressed as

$$U = r^2 W_{rad} \tag{3.2}$$

Where

U = radiation intensity, watts rad^{-2}

W_{rad} = radiation density, watts m^{-2}

- **Directivity:[2]**

Directivity of an antenna is defined as the ratio of the radiation intensity in a given direction from the antenna to the radiation intensity averaged over all directions.

$$D = \frac{U}{U_0} = \frac{4\pi U}{P_{rad}} \tag{3.3}$$

If the direction is not specified, the direction of maximum radiation intensity is implied

$$D_{max} = D_0 = \frac{U|_{max}}{U_0} = \frac{4\pi U_{max}}{P_{rad}} \tag{3.4}$$

- **Gain:[2,4]**

Although the gain of an antenna is closely related to its directivity, it is a measure that takes into account the efficiency of the antenna as well as its directional capabilities.

Absolute gain of an antenna in a given direction is defined as the ratio of the radiation intensity, in a given direction, to the radiation intensity that would be obtained if the power accepted by the antenna were radiated isotropically. The radiation intensity corresponding to the isotropically radiated power is equal to the power accepted by the antenna divide by 4π.

$$\text{Gain} = \frac{\text{Radiation Intensity}}{\text{Toatal Input (accepted) Power}}$$

$$= 4\pi \frac{U(\theta,\phi)}{P_{in}} \qquad \text{(dimensionless)} \tag{3.5}$$

Relative gain of an antenna is defined as the ratio of the power gain in a given direction to the power gain of a reference antenna in its referenced direction. The power input must be the same for both the antennas.

$$G = \frac{4\pi\, U(\theta,\phi)}{P_{in}\ \text{(Lossless isotropic source)}} \tag{3.6}$$

When the direction is not stated, the power gain is usually taken in the direction of maximum radiation.

- **Antenna Efficiency**:[2]

The total antenna efficiency is used to take into account losses at the input terminals and within the structure of the antenna. Such losses may be due to

1. Reflections because of the mismatch between the transmission line and the antenna.
2. Losses in conductors and dielectric (I^2R losses).

The overall efficiency is

$$\mathbf{e_0 = e_r e_c e_d.} \tag{3.7}$$

Where

e_0 is the total efficiency,

e_r is the reflection (mismatch) efficiency = $(1 - |\Gamma^2|)$

e_c is the conduction efficiency and

e_d is the dielectric efficiency.

Γ is the voltage reflection coefficient at the input terminals of the antenna.

All of these quantities are dimensionless.

- **Half-Power Beamwidth:[2,4]**

In a plane containing the direction of the maximum of a beam, the angle between the two directions in which the radiation intensity is one-half the maximum value of the beam, is called the half-power beamwidth. Sometimes the term beamwidth is used to describe the angle between any two points of the beam, such as the angle between the 10-dB points. In such cases the specific points on the beam must be described to avoid confusion .But the term beamwidth by itself is usually meant to describe the 3-dB beamwidth.

Beamwidth is used to describe the resolution capabilities of the antenna to distinguish between two adjacent radiating sources or radar targets.

- **Beam Efficiency:**

For an antenna with its major lobe directed along the z-axis (θ =0), the beam efficiency is given by the ratio of the power transmitted within cone angle θ, to the total power transmitted by the antenna.

$$\text{Beam Efficiency} = \frac{\text{Power transmitted (recieved) within cone angle } \theta}{\text{Power transmitted (received) by the antenna}} \quad \text{(dimensionles)} \tag{3.8}$$

A very high beam efficiency, usually in 90's, is necessary for antennas used in radiometry, astronomy, radar and other applications where received signals through minor lobes must be minimized.

- **Bandwidth:[2]**

The bandwidth of an antenna is defined as the range of frequencies within which the performance of the antenna with respect to some characteristic, confirms to a specific standard. The terms pattern bandwidth and impedance bandwidth are used to specify the specific characteristic which is being considered.

- **Polarization:[2,3]**

Polarization of an antenna in a given direction is defined as the polarization of the wave transmitted by the antenna. When the direction is not stated, the polarization is taken to be the polarization in the direction of maximum gain.

Polarization of a radiated wave is defined as that property of an electromagnetic wave describing the time varying direction and relative magnitude of the electric field vector. It is the figure traced as a function of time by the extremity of the electric field vector at affixed position in space, and the sense in which it is traced, as observed along the direction of propagation.

Polarization may be classified as linear, circular or elliptical. If the vector that describes the electric field at a point in space as a function of time is always directed along a line, the field is said to be linearly polarized. In general, the figure traced out by the tip of the electric field vector is elliptical. Linear and circular are the special cases of elliptical polarization. The figure may be traced in a clockwise (CW) or counter-clockwise (CCW) sense. Clockwise rotation of the electric field vector is designated as right-hand polarization and counterclockwise as left-hand polarization.

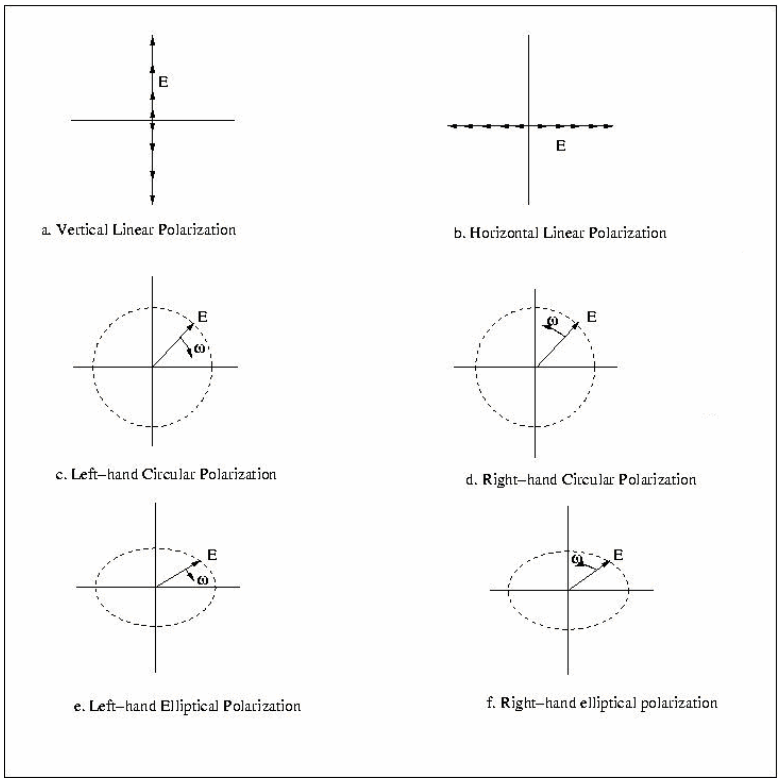

Fig 3.4 Some wave polarization states. The wave is approaching. [3]

Table 3.2 Linear, circular and elliptical polarization[2]

Polarization	Conditions on Electric Field Vector
Linear	1. Only one component or 2. Two orthogonal linear components having phase shift of 0^0 or multiples of 180^0
Circular	1. Two orthogonal linear components and 2.The two components must have equal magnitude and phase shift of odd multiples of 90^0
Elliptical	1. Two orthogonal linear components. 2. The two components can be of same or different magnitude and 3. a) If the two components are of the same magnitude, the time-phase difference between the two components must not be 0^0 or multiples of 180^0) b) If the two components are of the same magnitude, then the time-phase difference between them should not be odd multiples of 90^0

Polarization Efficiency:[2]

The polarization efficiency of an antenna is defined as the ratio of the power received by an antenna from a given plane wave of arbitrary polarization to the power that would be received by the same antenna from a plane wave of the same power flux density and direction of propagation, whose state of polarization has been adjusted for a maximum received power.

$$\text{Polarization Efficiency} = P_e \frac{|\rho_e \cdot E^{inc}|^2}{|\rho_e|^2 \, |E^{inc}|^2} \qquad (3.9)$$

Where

l_e is the vector effective length of the antenna

E^{inc} is the incident electric field

The vector effective length $l_e$is defined as the ratio of the magnitude of the open-circuit voltage developed at the terminals of the antenna to the magnitude of the electric field strength in the direction of the antenna polarization.

- **Antenna Input Impedance:[2]**

It is defined as the impedance presented by an antenna at its terminals or the ratio of the voltage to current at a pair of terminals or the ratio of the appropriate components of the electric to magnetic fields at a point.

$$Z_A = R_A + X_A \tag{3.10}$$

Where

Z_A is the antenna input impedance

R_A is the antenna resistance

X_A is the antenna reactance.

All of the above parameters defined at a pair of terminals.

In general the resistive part of the impedance consists of two components:

$$R_A = R_r + R_L$$

Where R_r is the radiation resistance and

R_L is the loss resistance of the antenna.

- **Antenna Radiation Efficiency:[2]**

The conduction and dielectric losses are represented by R_L, the loss resistance. The conduction-dielectric efficiency or the radiation efficiency of an antenna is defined to

be the ratio of the power delivered to the radiation resistance R_r to the power delivered to R_r and R_L.

Antenna Radiation Efficiency

$$e_{cd} = \left[\frac{R_r}{R_r + R_L} \right] \quad \text{(dimensionless)} \tag{3.11}$$

- **Antenna effective area:[2]**

Antenna effective area is defined as the ratio of the available power at the terminals of a receiving antenna to the power flux density of a plane wave incident on the antenna from that direction, the wave being polarization matched to the antenna. If the direction is not specified, the direction of maximum radiation is implied.

Antenna Effective Area

$$A_e = \frac{P_T}{W_i} = \frac{|I_T|^2 R_T / 2}{W_i} \tag{3.12}$$

Where

A_e = effective area, m^2

P_T = power delivered to load, watts

W_i = power density of incident wave, watts m^{-2}

3.4 Array Theory:[1]

Usually the radiation pattern of a single element is relatively wide and each element provides low values of directivity (gain). In many applications like in Radio Astronomy, it is necessary to design antennas with very directive characteristics (very high gain). This can be accomplished by increasing the electrical size of the antenna.

Instead of enlarging the dimensions of a single antenna, it is often convenient to form an assembly of antennas in an electrical and geometric configuration. This assembly of multiple antennas is called an array. The total field of an array is determined by the vector addition of the fields radiated by the individual elements. There are five controls that can be used to shape the overall pattern of the antenna. They are:

1. The geometrical configuration of the array
2. The relative displacement between the elements.
3. The excitation amplitude of the individual elements.
4. The excitation phase of the individual elements.
5. The relative pattern of the individual elements.

Let us consider an array formed by placing two in-phase point sources at a distance L apart from each other, as shown in the following figure.

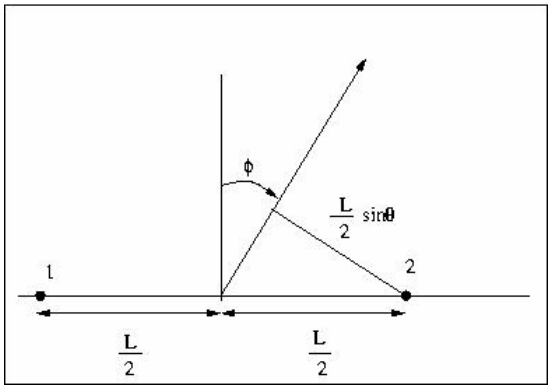

Fig. 3.5 Geometry for array of two isotropic sources. [1]

Taking the reference point for phase halfway between the sources, the far field in the direction Φ is given by

$$E = E_2 e^{j\psi/2} + E_1 e^{-j\psi/2}$$

Where

$$\psi = \beta L \sin \Phi = (2\pi/\lambda) \sin \Phi$$

If $E_1 = E_2 = E_0$,

$$E = 2E_0 (e^{j\psi/2} + e^{-j\psi/2}) / 2.$$

$$E = 2E_0 \cos (\psi/2).$$

$$E = 2E_0 \cos (\pi \sin \Phi /2) \qquad (3.13)$$

For a spacing of $\lambda/2$, the pattern is as shown in the following figure.

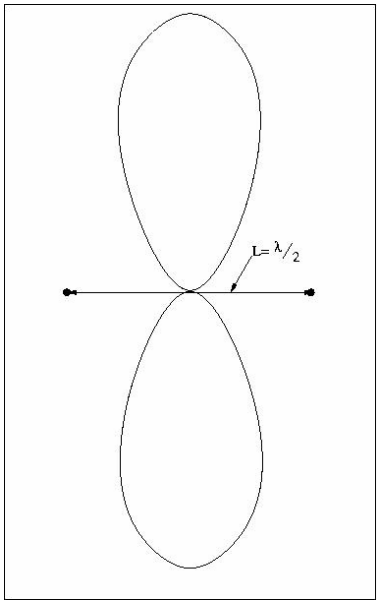

Fig 3.6 Field pattern of two in-phase isotropic point sources with one-half wavelength spacing. [1]

If the individual point sources have directional patterns which are identical, the resultant pattern is given by (3.13), where now E_0 is also a function of angle Φ. The pattern E (Φ) is called as the primary pattern and cos ($\psi/2$) is called as the array factor or the secondary pattern. This is an example of the principle of pattern multiplication, which may be stated more generally as follows:

'The total field pattern of an array of nonisotropic but similar sources is the product of the individual source pattern and the pattern of an array of isotropic point

sources each located at the phase center of the individual source and having the same relative amplitude and phase, while the total phase pattern is the sum of the phase patterns of the individual source and the array of isotropic point sources.'

Let us now consider an array of n isotropic sources, having equal phase and spacing.

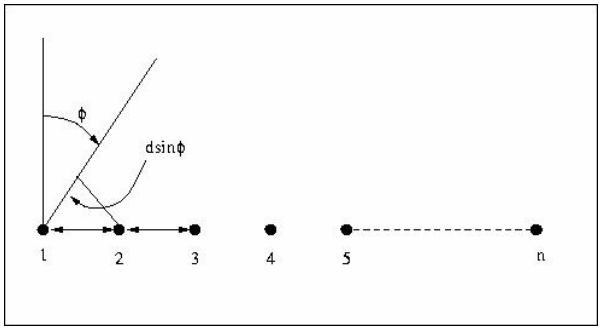

Fig. 3.7 Array of n isotropic sources of equal amplitude and spacing [1]

The far field is obtained as

$$E = E_0 [1 + e^{j\psi} + e^{j2\psi} + e^{j3\psi} + \ . \ . \ . \ + e^{jn\psi}] \tag{3.14}$$

Where $\Psi = \beta d \sin\Phi + \delta$

δ = progressive phase difference between sources

d = spacing between sources

Multiplying (3.8) by $e^{j\psi}$ gives

$$e^{j\psi} E = E_0 [e^{j\psi} + e^{j2\psi} + e^{j3\psi} + \ . \ . \ . \ + e^{jn\psi}] \tag{3.15}$$

Subtracting (3.14) from (2.15) gives

$$E = \frac{1 - e^{jn\psi}}{1 - e^{j\psi}} = E_0 \frac{\sin(n\psi/2)}{\sin(\psi/2)} \angle (n-1)\psi/2 \tag{3.16}$$

If the center of the array is chosen as the reference for the phase, instead of source 1, the phase angle (n-1) Ψ/2 is eliminated. If the sources are nonisotropic but similar, then E_0 will represent the primary or individual source pattern, while sin(nΨ/2)/ sin (Ψ/2) is the array factor.

For isotropic sources and the center of the array as reference the pattern is

$$E = E_0 \frac{\sin (n\psi/2)}{\sin (\psi/2)} \tag{3.17}$$

As ψ tends to zero,

$$E = nE_0 \tag{3.18}$$

This is the maximum value of the field, which is n times the field from a single source. In a broadside array, the beamwidth between first nulls (BWFN) comes out to be

$$BWFN = 2\Phi_{01} = (2/L_\lambda) \text{ rad.} \tag{3.19}$$

Where Φ_{01} are the first nulls, L_λ is the length of array in wavelengths.

The half power beam width (HPBW) is

$$HPBW \approx BWFN/2 = 1/ L_\lambda \text{ rad} \tag{3.20}$$

Continuous Aperture Distribution:

Consider a continuous current sheet or field distribution over an aperture as shown in the fig 3.7.

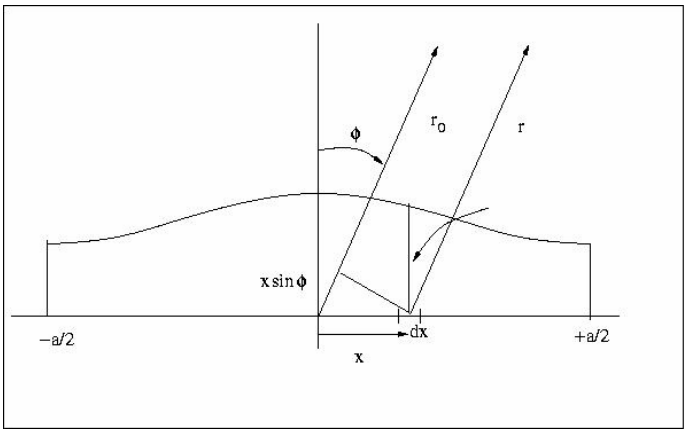

Fig. 3.8 Aperture of width a and amplitude distribution E (x) [1]

Assuming that the current or field is perpendicular to the page (y direction) and is uniform with respect to y, the electric field at a distance r from an elemental aperture dxdy is

$$dE = -\frac{j\omega\mu}{4\pi r}\,\frac{E(x)}{Z}\,e^{-j\beta r}\,dx\,dy \qquad (3.21)$$

Where

j_y = current density, amp m^{-2}

E (x) = aperture electric field distribution, volts m^{-1}

Z = intrinsic impedance of the medium, ohms

$\omega = 2\pi f$, rad sec^{-1}

μ = permeability of medium, henrys m^{-1}

for an aperture with a uniform dimension y_1 perpendicular to the page and with the field distribution over the aperture a function only of x, the electric field as a function of Φ at a large distance from the aperture (r >>a), is .

$$E(\phi) = \frac{-j\omega\mu y_1 e^{-j\beta r_o}}{4\pi r_o Z} \int_{-a/2}^{+a/2} E(x) e^{j\beta x \sin\phi} dx \qquad (3.22)$$

The magnitude of E (Φ) is then

$$|E(\phi)| = \frac{y_1}{2 r_o \lambda} \int_{-a/2}^{+a/2} E(x) e^{j\beta x \sin\phi} dx \qquad (3.23)$$

Where $\beta = (2\pi/\lambda)$.

For a uniform aperture distribution,

$$|E(\phi)| = \frac{y_1 E_a}{2 r_o \lambda} \int_{-a/2}^{+a/2} e^{j\beta x \sin\phi} dx \qquad (3.24)$$

On axis (Φ=0) we have

$$|E(\phi)| = \frac{E_a a y_1}{2 r_o \lambda} = \frac{E_a A}{2 r_o \lambda} \qquad (3.25)$$

Where A= aperture area,

E_a = electric field in aperture plane.

For unidirectional radiation from the aperture (in direction $\Phi = 0^0$ but not in the direction $\Phi = 180^0$), | E (Φ) | is twice the value stated above.

Integration of (3.24) gives

$$\left|E(\phi)\right| = k_o \frac{\sin\left[(\beta a/2)\sin\phi\right]}{(\beta a/2)\sin\phi}$$

where $k_o = \frac{A E_a}{2 r_o \lambda}$

(3.26)

From 3.10, introducing βd sinΦ for ψ, we get the field of a large array of n discrete sources of spacing d is

$$E = n E_o \frac{\sin\left[(\beta a'/2)\sin\phi\right]}{(\beta a'/2)\sin\phi}$$

(3.27)

Where the length of the large array is a' = (n-1) d ≈ nd. Under the condition that Φ is restricted to small values, which will be satisfied when the array is large and only the main lobe and first side lobes are of interest**, it is clear that the field pattern of a large array of discrete sources is the same as the pattern for the continuous array of same length. (a=a').**

3.5 Spatial Frequency Response and Pattern Smoothing: [1]

It will be shown in the next chapter that the Fourier transform of the antenna power pattern is proportional to the complex autocorrelation function of the aperture distribution.

$$\bar{P}(x_{\lambda_o}) = \int E(x_\lambda - x_{\lambda_o})\, E^*(x_\lambda)\, dx_\lambda$$

(3.28)

Where

$\bar{P}(x_{\lambda 0})$ = Fourier transform of antenna power pattern $P_n(\Phi)$

$E(\Phi)$ = field pattern

$E(x_\lambda)$ = aperture distribution

x_λ= distance in wavelengths

$x_{\lambda 0}$ = displacement in wavelengths

The autocorrelation function involves displacement $x_{\lambda 0}$, multiplication, integration. The situation for a uniform aperture distribution is as shown is the following figure. It is apparent that the autocorrelation function is zero for values of $x_{\lambda 0}$ greater than the aperture width a_λ.

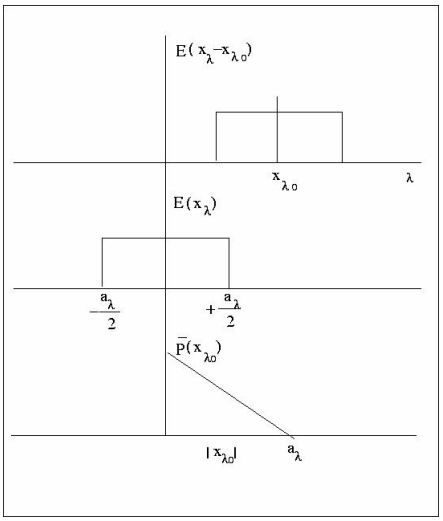

Fig. 3.9 Autocorrelation function of a uniform aperture distribution

The observed response of a radio-telescope antenna to a sky brightness distribution is proportional to the convolution of the antenna power pattern and the brightness distribution.

$$S(\phi_0) = \int B(\phi)\,\bar{P}_n(\phi_0 - \phi)\,d\phi \qquad (3.29)$$

Where

S (Φ_0) = observed flux-density distribution

B (Φ_0) = true source brightness distribution

Φ_0 = displacement, hour angle.

It follows that

$$\bar{S}(x_\lambda) = \bar{B}(x_\lambda)\bar{P}(x_\lambda) \tag{3.30}$$

Where the bars mean the Fourier transform.

There is a cutoff for all values of $x_{\lambda 0}$ greater than a_λ. The quantity $x_{\lambda 0}$ is called the spatial frequency and a_λ its cutoff value.

Thus, $x_{\lambda c} = a_\lambda$

Where x_λ is the spatial frequency cutoff.

Reciprocal of $x_{\lambda c}$ gives an angle.

$\Phi_c = (1/ a_\lambda)$ rad.

Comparing with (3.19), it follows that this cutoff angle is equal to one-half the beam width between first nulls for a uniform aperture distribution. The significance of Φ_c is that structure in the sky brightness distribution having a period of less than BWFN/2 will not appear in the observed response. Half of the beam width between first nulls is equal to the Rayleigh resolution. Thus, two point sources separated by this distance will be just resolved.

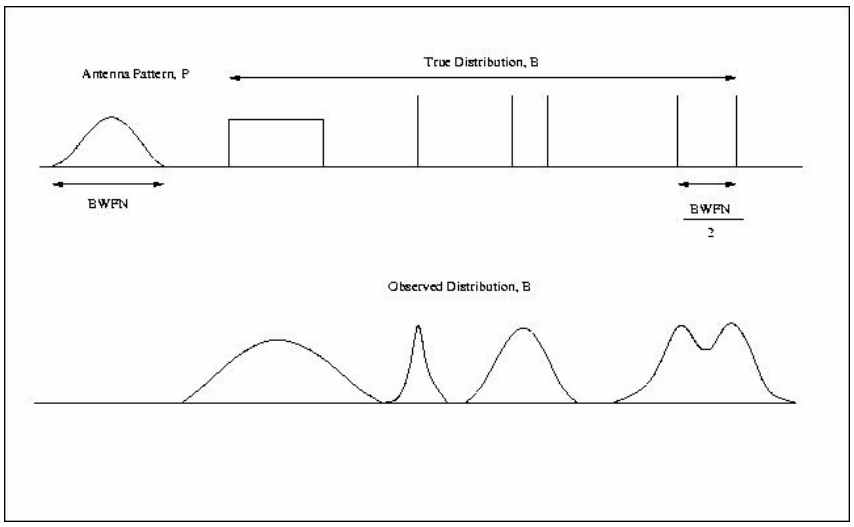

Fig. 3.10 Smoothed distribution S observed with antenna pattern P [1]

3.6 Interferometry [5]

Interferometry is the technique of superimposing (interfering) two or more waves, to detect differences between them. Interferometry works because two waves with the same frequency that have the same phase will add to each other while two waves that have opposite phase will subtract. When the paths differ by an even number of half-wavelengths, the superposed waves are in phase and interfere constructively, increasing the amplitude of the output wave. When they differ by an odd number of half-wavelengths, the combined waves are 180° out of phase and interfere destructively, decreasing the amplitude of the output. Thus anything that changes the phase of one of the beams by only 180°, shifts the interference from a maximum to a minimum. This makes interferometers sensitive measuring instruments for anything that changes the phase of a wave, such as path length.

The Van Cittert-Zernike Theorem: the van Cittert-Zernike Theorem relates the spatial coherence function V (r_1, r_2) = $\langle E(r_1)E^*(r_2)\rangle$ to the distribution of intensity of the incoming radiation, I(s). It shows that the spatial correlation function V (r_1, r_2) depends only on $r_1 - r_2$ and that if all the measurements are in a plane, then

$$V(r_1, r_2) = F\{I(s)\} \tag{3.31}$$

Where F implies taking Fourier transform.

2.6.1 The Need for Interferometry:

The resolution of optical instruments is limited due to the wave nature of light. This idea is based on the Rayleigh's criterion that the angular resolution of a telescope/ microscope is ultimately diffraction limited and is given by

$$\theta \sim \lambda / D \tag{3.32}$$

Where D is some measure of the aperture size. In radio astronomy, the wavelengths are so large that even though the sizes of radio telescopes are very large, the angular resolution is still poor compared to optical instruments. Thus while the human eye has a diffraction limit of ~ 20" and even modest optical telescopes have diffraction limits of 0.1" , even the largest radio telescopes (300 m in dia) have angular resolutions of only ~ 10' at 1 metre wavelength. To achieve higher resolutions, one has to either increase the diameter of the telescope further (which is not practical) or decrease the observing wavelength. The radio telescopes operating at centimetre and milimetre wavelengths are restricted to studying sources which are bright at cm and mm

wavelengths. To achieve high angular resolutions at metre wavelengths one needs telescopes with apertures that are hundreds of kilometres in size. Single telescopes of this size are clearly difficult to build. Instead radio astronomers use a different a technique called aperture synthesis to achieve higher angular resolutions. Aperture synthesis is based on interferometry.

2.6.2 A Two Element Interferometer:

Consider a two element interferometer shown in the following figure.

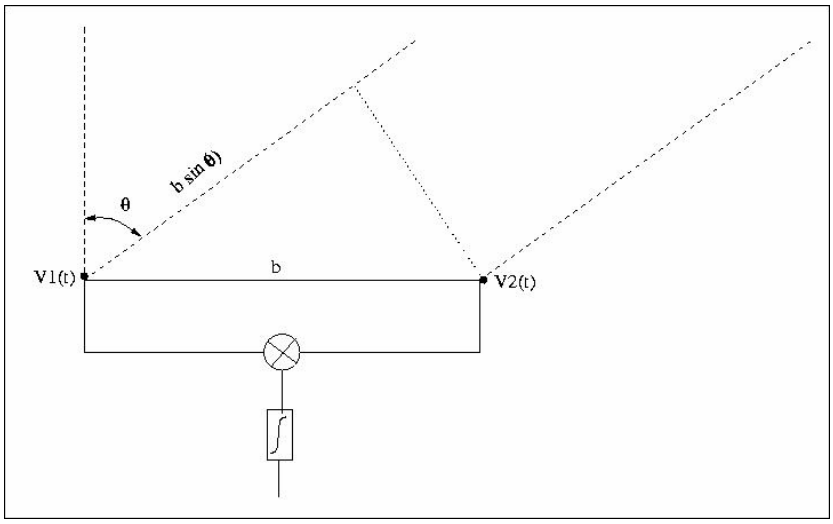

Fig 3.11 A basic two element interferometer. [5]

Two antennas 1, 2 whose vector separation is b, are directed toward a point source of flux density S. The angle between the direction to the point source and the normal to the antenna separation vector is θ. The voltages that are produced at the two antennas due to the electric field from this point source are $v_1(t)$ and $v_2(t)$ respectively. These two

voltages are multiplied together and then averaged. Let the radiation emitted by the source be monochromatic at frequency f. Let the voltage at antenna 1 be

$$v_1(t) = \cos(2\pi ft). \tag{3.33}$$

Since the radio waves from the source have to travel an extra distance b sin θ to reach antenna 2, the voltage there is delayed by the amount b sin θ/ c. this is called the geometric delay, t_g . the voltage at antenna 2 is hence

$$v_2(t) = \cos(2\pi f(t-t_g)). \tag{3.34}$$

Where we have assumed that the antennas have identical gain. The averaged output of the multiplier is

$$\begin{aligned} r(\tau_g) &= \frac{1}{T}\int_{t-T/2}^{t+T/2} \cos(2\pi f t)\cos(2\pi f(t-\tau_g))\,dt \\ &= \frac{1}{T}\int_{t-T/2}^{t+T/2} (\cos(4\pi f t - 2\pi\tau_g) + \cos(2\pi f\tau_g))\,dt \\ &= \cos(2\pi f\tau_g) \end{aligned} \tag{3.35}$$

Where we have assumed that the averaging time T is long compared to 1/f. The cos (4πft) factor hence averages to 0. As the source rises and sets, the angle θ changes. If we assume that the antenna separation vector, i.e. the baseline is exactly east-west and that the source's declination δ_0 is exactly 0, then $\theta = \Omega_E t$, (where Ω_E is the angular frequency of earth's rotation), we have

$$r(t_g) = \cos(2\pi f \times b/c \times \sin(\Omega_E (t - t_Z))) \quad (3.36)$$

Where t_Z is the time at which the source is at the zenith. The output $r(t_g)$, which is also called the fringe, hence varies in a quasi-sinusoidal form, with its instantaneous frequency being maximum when the source is at the zenith and minimum when the source is either rising or setting.

If the source's right ascension was known, then one could compute the time at which the source would be at zenith and hence the time at which the instantaneous fringe frequency would be maximum. (Right Ascension (RA) is the celestial equivalent of terrestrial longitude. For longitude, the zero point is the Prime Meridian; for RA, the zero point is known as the First Point of Aries, which is the place in the sky where the Sun crosses the celestial equator at the March equinox. RA is measured eastward from the March equinox.). If the fringe frequency peaks at some slightly different time, then one knows that assumed right ascension of the source was slightly in error. Thus, in principle at least, from the difference between the actual observed peak time and the expected peak time one could determine the true right ascension of the source. Similarly, if the source were slightly extended, then when the waves from a given point on the source arrive in phase at the two ends of the interferometer, waves arising from adjacent points on the source will arrive slightly out of phase. The observed amplitude of the fringe will hence be less than what would be obtained for a point source of the same total flux. The more extended the source, the lower the fringe amplitude, assuming that the source has a uniform brightness distribution. This is related to the fact that in the double slit experiment, the interference pattern becomes less distinct and then eventually

disappears as the source size is increased. In such circumstances, the interferometer is said to have resolved out the source. When the source size is such that waves from different parts of the source give rise to the same phase lags (within a factor that is small compared to π) then the source will appear as a point source. This condition can be translated into a limit on $\Delta\theta$, the minimum source size that can be resolved by the interferometer, viz.

$$\pi f \Delta \theta \, b/c \leq \pi \quad \rightarrow \quad \Delta\theta \leq \lambda / b \tag{3.37}$$

i.e. the resolution of a two element interferometer is ~ λ / b.

The longer the baseline, the higher the resolution.

Thus observations with a two element interferometer give one information on both the source position and the source size. Interferometers with different baseline lengths and orientations will place different constraints on the source brightness and the Fourier transform in the van Cittert–Zernike theorem can be viewed as a way to put all this information together to obtain source brightness distribution.

With this background, in the next chapter, aperture antennas will be discussed in depth. Their characteristics will be explored with reference to their wide usage in radio astronomy.

CHAPTER FOUR

Aperture Antennas: The most widely used Antennas in Radio Astronomy

As was discussed in the last chapter, performance of a radio telescope depends largely on the antennas that are used. So the choice of antenna is very important. Parabolic reflector with one or more feeds is the most common configuration found in radio telescopes. There is a wide variety of feeds available. The most common are horns, waveguides and dipoles. Horns and waveguides are aperture antennas. Also, parabolic reflector is an aperture antenna. Thus, aperture antennas are the most widely used antennas in radio astronomy. In this chapter we will see the reasons behind this and develop the concepts of radiation from apertures. Also we will thoroughly analyze parabolic reflector antenna since it is of very much importance in the field of radio astronomy.

4.1 Desirable characteristics of aperture antennas

Antennas where the radiation characteristics are determined solely from the electric and magnetic fields across an aperture are called aperture antennas. Following are their important characteristics.

High gain: Aperture antennas have high gain [3]. Radio telescopes need to have high resolution. Resolution depends on the beam width between first nulls (BWFN). Hence higher gains lead to better resolution. This is the main reason of using aperture antennas so widely in radio astronomy.

Increase in gain with increasing frequency: The gain of an aperture antenna increases with the square of frequency if aperture efficiency is constant with frequency [3].

Nearly real-valued input impedance:[3] Real valued input impedance leads to higher radiation efficiency.

A wide variety of aperture antennas is available. Corrugated horns, coaxial waveguides, ridged and flanged circular waveguides are some of the commonly used antennas as feeds for parabolic reflectors which give excellent performance.

Now we will understand the basic concept of radiation from apertures.

4.2 Radiation from apertures:[6]

An electromagnetic field exists over the surface, or the **aperture** of the aperture antennas. The intensity, phase and polarization of the field over this surface are analogous to the current amplitude, phase and direction in wire antennas. When the aperture distribution, i.e. the description of the variation of the field quantities over the aperture is known, it is possible in principle to calculate the radiation pattern. As for radiation due to currents, the analysis of radiation due to the field distribution of an aperture is based on Maxwell's equations. The concept of predicting the radiation from an aperture is particularly important because of the fact that , under certain assumptions, the far-field radiation characteristics and aperture electric or magnetic fields are the Fourier transform of each other. The field equivalence principle or Huygen's principle together with the radiation integral are used to determine the relation between the aperture fields and the radiation patterns.

4.2.1 Field equivalence principle:

The field equivalence principle, as applied to planar apertures, states that if a region of sources (z<0) causes radiated fields (see fig. 4.1), E, H in the region z>0 then the same radiated fields would be obtained by replacing an imaginary surface s at z=0 by a conducting surface on which an electric current density J_s and a magnetic current density J_m flow. The current densities are given by

$$J_s = \hat{u}_z \text{ X } H_a$$

$$J_m = -\hat{u}_z \text{ X } E_a \qquad (4.1)$$

Where E_a and H_a are respectively, the tangential electric and magnetic fields in the aperture. E_a and H_a can be computed by solving the internal problem by a knowledge of the electromagnetic fields and boundary conditions appropriate to the antenna structure. Then the radiated fields can be derived using the current densities.

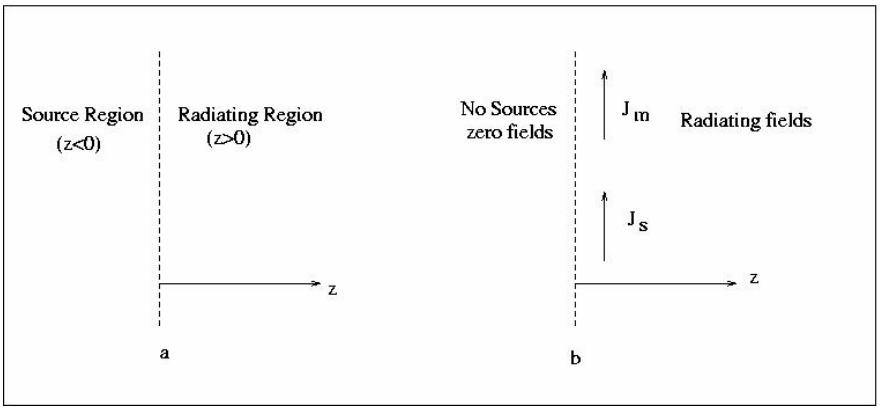

Fig. 4.1 Field-equivalence principle applied to a plane aperture [6]

This is only one of many field-equivalence relations. There are two more versions that are useful. Since the region z<0 contains no fields, it is possible to introduce an imaginary surface without altering J_s or J_m. if a perfect electric conductor is introduced behind the surface s, then according to image theory, there will be an image of J_m and an opposite image of J_s (see fig. 4.2). If the conductor is removed and the images remain, the

result will be a surface s, on which $J_s = 0$ and $J_m = 2(\hat{u}_z \times E_a) = \hat{u}_z \times 2E_a$. This form of field-equivalence principle is particularly useful because it involves only the aperture electric field. It is sometimes referred to as the E-field model. A third form of the principle is the dual of the last version. If a perfect magnetic conductor is introduced behind surface s, the radiated fields can be determined from $J_m = 0$ and $J_s = -\hat{u}_z \times 2H_a$.

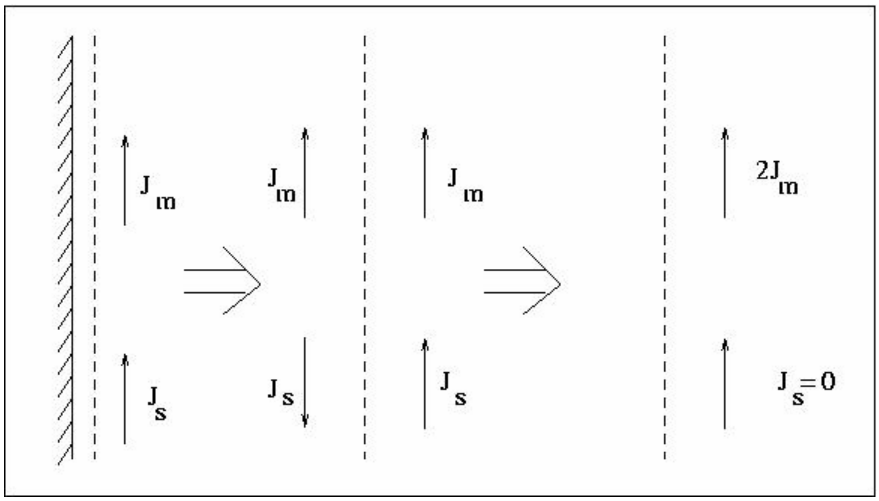

Fig. 4.2 Image plane with field-equivalence principle [6]

In an aperture antenna, the electric and/or magnetic fields (and hence currents) are only known over the aperture. Outside the aperture, assumptions must be made about the extent of the surface s and the currents flowing on it. These assumptions are different for the three versions above and consequently lead to three versions of the radiation equations. In all cases there will either be no actual conducting surface (e. g. a horn with no flange), or a finite conducting surface (e.g. a corrugated horn). In addition the condition $\hat{u}_z \times E_a = (J_m) = 0$ is not a valid boundary condition on a practical conducting sheet and the assumption that the aperture electric fields are undisturbed by the presence of the aperture is approximate.

4.2.2 Radiation Equations:

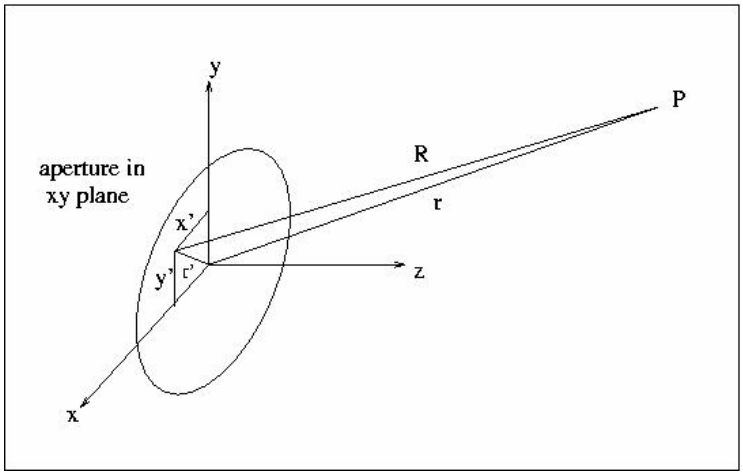

Fig. 4.3 Aperture in xy plane [6]

Consider the geometry in figure 4.3. An aperture is in xy plane. The point of observation is P.

For the first version, using both E_a and H_a the radiation equations are derived as follows. The magnetic vector potential gives the radiation from an electric current density J_s.

$$A = \int_s J_s \frac{e^{-jkR}}{4\pi R} ds \tag{4.2}$$

Similarly the electric vector potential A_m gives the radiation from a magnetic current density J_m.

$$A_m = \int_s J_m \frac{e^{-jkR}}{4\pi R} ds \tag{4.3}$$

In the far-field R = r – r'cos θ and if r' is expressed in terms of the spherical coordinates θ and Φ then equation 4.2 becomes

$$A = \frac{e^{-jkR}}{4\pi R}\,\hat{u}_z \; X \int_{x'}\int_{y'} E_a(x', y')\exp\{(jk(x'\sin\theta\cos\phi + y'\sin\theta\sin\phi)\}dx'dy' \tag{4.4}$$

Similar is true for equation 4.3.

Eqn 4.4 is a two-dimensional Fourier transform and its components are written down as

$$f_x = \int_{x'}\int_{y'} E_{ax}(x', y')\exp\{(jk(x'\sin\theta\cos\phi + y'\sin\theta\sin\phi)\}dx'dy'$$

$$f_y = \int_{x'}\int_{y'} E_{ay}(x', y')\exp\{(jk(x'\sin\theta\cos\phi + y'\sin\theta\sin\phi)\}dx'dy' \tag{4.5}$$

A comparable set of Fourier transform relates the aperture magnetic field to the radiated field.

$$g_x = \int_{x'}\int_{y'} H_{ax}(x', y')\exp\{(jk(x'\sin\theta\cos\phi + y'\sin\theta\sin\phi)\}dx'dy'$$

$$g_y = \int_{x'}\int_{y'} H_{ay}(x', y')\exp\{(jk(x'\sin\theta\cos\phi + y'\sin\theta\sin\phi)\}dx'dy' \tag{4.6}$$

In the far-field the electric and magnetic fields are related by the TEM relation

$$E = \eta_0 H \; X \; \hat{u}_r$$

where η_0 is the free-space wave impedance of 377 Ω. The radiated electric fields are given by

$$E = -j\omega (A + \eta_0 A_m \; X \; \hat{u}_r) \tag{4.7}$$

Combining the above equations and transforming the electric fields into spherical coordinates gives the radiated electric fields using J_s and J_m as

$$E_\theta = \frac{jk_0 \exp(-jk_0 r)}{4\pi R}\{ f_x\cos\phi + f_y \sin\phi + \eta_0 \cos\theta (g_y\cos\phi - g_x \sin\phi)\}$$

$$E_\phi = \frac{j k_0 \exp(-jk_0 r)}{4\pi r}\{ \cos\theta (f_y \cos\phi - f_x \sin\phi) - \eta_0 (g_y \sin\phi + g_x \cos\phi)\} \quad (4.8)$$

A common approximation is to assume that the fields in the aperture are TEM-type fields so that $E_{ax} = \eta_0 H_{ay}$ and $E_{ay} = \eta_0 H_{ax}$. Then the equations simplify to

$$E_\theta = \frac{j k_0 \exp(-jk_0 r)}{4\pi r}\{ (1 + \cos\theta)(f_x\cos\phi + f_y \sin\phi)\}$$

$$E_\phi = \frac{j k_0 \exp(-jk_0 r)}{4\pi r}\{ (1 + \cos\theta)(f_y\cos\phi - f_x \sin\phi)\} \quad (4.9)$$

If an E-field model is used with only $2J_m$ in the aperture, the far-field radiated fields are

$$E_\theta = \frac{jk_0 \exp(-jk_0 r)}{2\pi r}(f_x \cos\phi + f_y \sin\phi)$$

$$E_\phi = \frac{jk_0 \exp(-jk_0 r)}{2\pi r}\cos\theta (f_y \cos\phi - f_x \sin\phi) \quad (4.10)$$

If an H-field model is used with only $2J_s$ in the aperture, the far-field radiated fields are

$$E_\theta = \frac{jk_0 \exp(-jk_0 r)}{2\pi r}\cos\theta (g_y \cos\phi - g_x \sin\phi)$$

$$E_\phi = \frac{jk_0 \exp(-jk_0 r)}{2\pi r}(g_x \cos\phi + g_y \sin\phi) \quad (4.11)$$

For horns and feeds, the linear polarized copular and crosspolar fields are normally required. These can be obtained from the spherical components by

$$E_{co} = E_\theta \sin\Phi + E_\Phi \cos\Phi$$

$$E_{xp} = E_\theta \cos\Phi + E_\Phi \sin\Phi \qquad (4.12)$$

This assumes that the aperture electric field is directed along the y-direction.

The difference between the different models that are presented is most significant for wide radiation angles and small apertures. Potentially most accurate model is eqn 4.8. However, for small aperture, the currents on the outside of the antenna structure influence the radiation. So no model is always better at predicting the correct result. Most common practice is to use either the pure E-field model or the modified E-and H-field model.

4.3 Parabolic Reflector Antennas:

Reflector antennas are the most widely used radio astronomy antennas. They have the following desirable characteristics[3]:

1. Ease in coupling the receiver to the antenna.
2. A gain of about 25 dB for aperture diameters as small as 10λ is easily achievable.
3. Full steerability: Generally either by polar or azimuth-elevation mounting.
4. Operation over a wide range of wavelengths is possible by simply changing the feed.

Let us have a look at the history of development of reflector antennas.

Table 4.1 History of parabolic reflector antennas [6]

Year	Development
1672	Sir Isaac Newton invented the optical reflecting Telescope
1887	Hertz used a cylindrical reflector antenna fed by a dipole to demonstrate a number of fundamental properties of electromagnetic waves.
1931	Marconi used parabolic reflectors to demonstrate a microwave-radio link across the English channel.
1934	Karl Jansky built the first radio telescope using a Paraboloidal reflector.
1937	Grote Reber constructed the first parabolic reflector antenna 31 ft in diameter. He made the first radio maps of the sky.

In the years of Second World War and after that parabolic antennas became more and more popular for scientific, broadcast and communication purposes.

4.3.1 Characteristics of Parabolic Reflectors:[3]

The simplest parabolic antenna consists of a large (relative to a wavelength) reflecting surface which is a paraboloid of revolution and a much smaller feed antenna. A typical arrangement is as shown in the following figure.

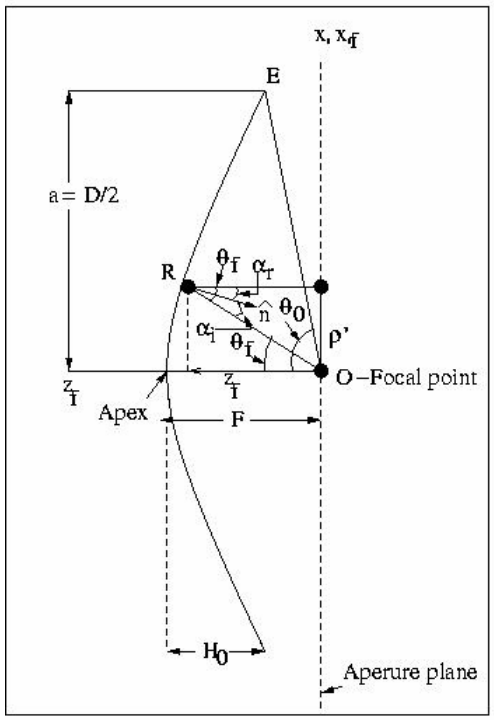

Fig 4.4 A prime-focus parabolic reflector cross-section

The equation describing the parabolic reflector surface shape in the rectangular form using (ρ', z_f) is

$$(\rho')^2 = 4F\,(F - z_f) \qquad \rho' \le a \tag{4.13}$$

The apex of the dish corresponds to $\rho' = 0$ and $z_f = F$, and the edge of the dish to $\rho' = a$ and $z_f = F - a^2/4F$. this means that for a given displacement of ρ' from the axis of the

reflector, the point R on the reflector surface is a distance z_f away from the focal point O. the parabolic curve can also be expressed in polar coordinates (r_f , θ_f) as

$$r_f = 2F/(1+ \cos \theta_f) = F\sec^2 (\theta_f/2) \quad (4.14)$$

The axisymmetric parabolic reflector is completely specified with two parameters, the diameter D and the focal length F. the F/D ratio represents the curvature rate of the dish. In the limit as F/D approaches infinity, the reflector focuses at infinity, i.e. becomes planar.

The angle from the axis to the reflector rim is related to the F/D as

$$F/D = 1/ (4 \tan\theta/2)$$

$$\theta = 2\tan^{-1}(1/ 4(F/D)) \quad (4.15)$$

The important properties that make reflector antenna useful are:

1. All rays leaving the focal point O are collimated after reflection from the reflector and the reflected rays are parallel to the reflector axis.

2. All path lengths from the focal point to the reflector and on to the aperture plane are the same.

When being used in a radio telescope, some properties of antennas, like gain, polarization properties, beam scanning properties are more important than the others. Now we will see how the reflector antenna behaves regarding these properties.

1. Cross-Polarization: For a purely polarized but unbalanced (principal plane patterns unequal) feed, such as a dipole, parabolic reflector induces zero cross-polarization in the principal planes and maximum in the 45^0 planes. With a balanced (principal plane patterns equal) feed positioned with its perfect phase centre at the focus

the reflector produces a very small far-field cross-polarization according to PO analysis. GO analysis produces no far-field cross-polarization. (for PO and GO see section 4.3.3).

The cross-polarization of an axisymmetric reflector decreases with larger F/D. In the case of offset reflectors, as the feed pointing angle increases, cross-polarization increases. Also, for maximum gain, cross-polarization level reaches to a level that is unacceptable in many applications (-23dB for atypical offset reflector).

2. Beam Scanning: Beam scanning is possible by displacing the feed off the focal point. As shown in the following figure, the feed is displaced a distance δ in the focal plane. For a flat reflector, the beam scan angle θ_B equals the feed tilt angle θ_F .for curved reflectors, (F/D finite) the beam scan angle will be less than the feed tilt angle. Scanning is quantified with beam deviation factor (BDF).

$$BDF = (\theta_B / \theta_F)$$

The following approximate relation can be used for small displacements δ:

$$BDF = \{1 + 0.36(4F/D)^{-2} \} / \{1 + (4F/D)^{-2} \} \quad (4.16)$$

3. Gain: The maximum achievable gain for an aperture antenna having a physical aperture A_p is

$$G_{max} = A_p (4\pi/\lambda^2) \quad (4.17)$$

In practice, this ideal gain is not achieved and it is decreased. It is represented as

$$G = \varepsilon_{ap} A_p ((4\pi/\lambda^2) \quad (4.18)$$

Where ε_{ap} is the aperture efficiency.

$$\varepsilon_{ap} = e_r \varepsilon_t \ \varepsilon_s \varepsilon_a \quad (4.19)$$

where

e_r is the radiation efficiency (see chapter 3)

ε_t is the aperture taper efficiency

ε_s is the spillover efficiency

ε_a is the achievement efficiency.

The feed antenna pattern has the greatest influence on reflector antenna gain.

Aperture taper efficiency is obtained by working with that portion of the feed power that reaches the aperture.

$$\varepsilon_t = \frac{4F^2}{\pi a^2} \frac{\left| \int_0^{2\pi} \int_0^{\theta_0} F_f(\theta_f, \phi') \tan\frac{\theta_f}{2} d\theta_f d\phi' \right|^2}{\int_0^{2\pi} \int_0^{\theta_0} \left| F_f(\theta_f, \phi') \right|^2 \sin\theta_f d\theta_f d\phi'} \tag{4.20}$$

Since the feed pattern will extend beyond the rim of the reflector, the associated power will not be redirected by the reflector into the main beam and gain is reduced. This is referred to as spillover and the associated efficiency is called the spillover efficiency, which is defined as the fraction of power radiated by the feed that is intercepted by the main reflector or the subreflector of a dual reflector.

$$\varepsilon_s = \frac{\int_0^{2\pi} \int_0^{\theta_0} \left| F_f(\theta_f, \phi') \right|^2 \sin\theta_f d\theta_f d\phi'}{\int_0^{2\pi} \int_0^{\pi} \left| F_f(\theta_f, \phi') \right|^2 \sin\theta_f d\theta_f d\phi'} \tag{4.21}$$

Taper and spillover efficiencies can be combined to form the illumination efficiency.

The achievement efficiency is expressed as a combination of subefficiencies as:

$$\varepsilon_a = \varepsilon_{rs}\, \varepsilon_{cr}\, \varepsilon_{blk}\, \varepsilon_{phr}\, \varepsilon_{phf} \tag{4.22}$$

where

ε_{rs} is **random surface error efficiency:** It is associated with gain loss from reflector surface errors. Random surface deviations from the ideal shape of a reflector cause gain reduction and side-lobe increase. This is due to the distortions in the aperture phase because of the consequent departure from equal ray path lengths of a focused reflector system. With δ is the rms surface deviation.

$$\varepsilon_{rs} = 685.8\ (\delta/\lambda)^2 \text{ dB} \tag{4.23}$$

ε_{cr} is **cross-polarization efficiency:** It has contributions due to reflector(s) and feed. In a single reflector system, the reflector contributes less in cross-polarization. Feed antennas having a component orthogonal to the desired polarization cause drop in gain.

ε_{blk} is **aperture blockage efficiency:** It is defined as

$$\varepsilon_{blk} = [1- (A_b / \varepsilon_t A_p)]^2 \tag{4.24}$$

where A_b is the blockage area projected onto the physical aperture of area A_p. the blockage is caused because of the structures placed in front of the reflector such as the feed, subreflector and support hardware. They block the rays exiting the aperture and scatter power into the side-lobe region.

ε_{phr} and ε_{phf} are **reflector and feed phase error efficiencies:** Phase errors in the aperture plane lead to gain loss and pattern deterioration. Phase errors arise from one or more of the following reason/s.:

1. Displacement of the phase centre of the feed antenna off the focal point.
2. Deterministic deviations of the reflector from the design shape.
3. An imperfect feed antenna phase centre.
4. Random surface error effects.

4.3.2 Different configurations of parabolic reflectors:[3]

1. Prime-focus parabolic reflector: In this configuration, the feed is placed at the focal point of the reflector and its main beam peak is directed towards the reflector center. This is the simplest configuration. It has some disadvantages:

a) The image-forming quality is poor due to lower f/D ratios.

b) The feed antenna pattern extends beyond the edge of the parabolic reflector and the feed picks up some thermal radiation from ground.

c) The feed and the electronics (if it is placed immediately near the feed) cause blockage of the aperture.

Most radio telescopes are intended to work over a wide frequency spectrum; a Cassegrain or Gregorian reflector system would result in an unacceptably large subreflector at lower frequencies. Therefore a prime-focus system is preferred.

2. Offset Reflector: The geometry of this configuration is as shown in the following figure.

Its primary advantage is that it reduces the blockage of the main reflector aperture caused in the prime-focus reflectors by the feed assembly and associated support structure. Its properties are similar to the axisymmetric counterpart formed by using the diameter of the parent reflector D_p.

The cross-polarization performance is poor as compared to the axisymmetric reflectors.

3. Dual Reflectors: When a subreflector is introduced between the feed and the main reflector, the system becomes a dual reflector system. The most popular dual reflector is the Cassegrain reflector. It is shown in the following figure. The main

reflector is parabolic and the subreflector is hyperbolic. In a Gregorian reflector, the subreflector is concave rather than convex. Cassegrain and Gregorian systems are derived from their optical counterparts and are named after their inventors.

Following

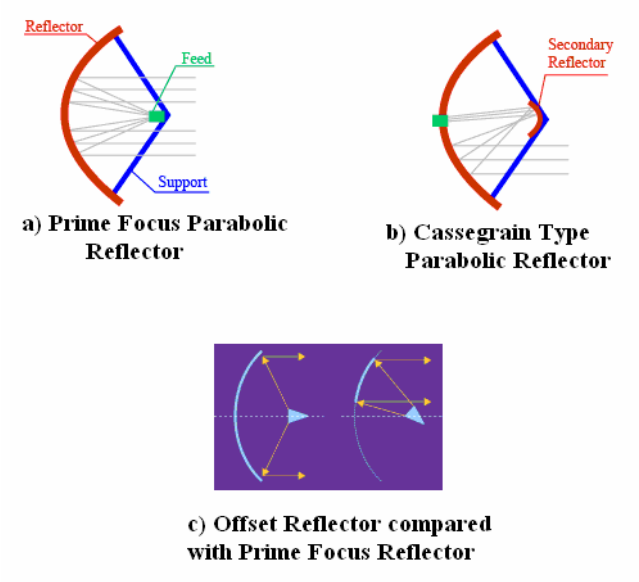

Fig.4.5 Different types of parabolic reflector arrangement [36, 37]

4.3.3 Methods of analyzing parabolic reflectors:[3]

There are two basic techniques for analyzing reflector antennas:

4.3.3.1 Geometrical Optics / Aperture distribution Method:

By this method one can determine the aperture field distribution and then find the far-field radiation pattern using the aperture theory.

Application of this method requires the following to be true:

1. The radius of curvature of the main reflector is large compared to a wavelength and the local region around each reflection point can be treated as planar.

2. the radius of curvature of the incoming wave from the feed is large and can be treated locally at the reflection point as a plane wave.
3. the reflector acts as a perfect conductor so that the incident and reflected wave amplitudes are equal.

First let us assume that the feed is an isotropic radiator. Since all rays from the feed travel the same physical distance to the aperture, the aperture distribution of a parabolic reflector will be of uniform phase. However, there is a nonuniform amplitude distribution introduced. This is due to the fact that the power density of the rays leaving the isotropic feed falls off as $1/r_f^2$ since the wave is spherical. After reflection, there is no spreading loss since the rays are parallel. Hence the aperture field intensity varies as $1/r_f$. Thus there is a natural amplitude taper in the aperture caused by the curvature of the reflector. If the feed is not isotropic, then the effect of its normalized radiation pattern is also included. The entire radiation pattern function of the reflector system can be written as

$$f = V_0 \int_0^{2\pi} \int_0^{a} \frac{F_f(\theta_f, \phi_f)}{r_f} \hat{u}\, e^{jk_0 \rho' \sin\theta \cos(\phi - \phi')} \rho'\, d\rho'\, d\phi' \tag{4.25}$$

And the complete radiation pattern follows from eqn 4.9.

$$E = -j\omega\mu \frac{e^{-j k_0 r}}{4\pi r} \iint_{S_r} [J_s - (J_s \cdot \hat{r})\hat{r}]\, e^{j k_0 \hat{r} \cdot r'}\, dS' \tag{4.26}$$

For a circular projected aperture of radius a = D/2.

The uniform aperture phase and the use of a real-valued feed pattern function leads to a symmetric pattern function since the Fourier transform of a real-valued

function is symmetric. Thus GO formulation always produces symmetric secondary radiation pattern. However, this is not the case always in practice. Hence amore accurate analysis, PO/surface current method is introduced.

4.3.3.2 Physical Optics/ Surface Current Method:

In this method, one uses the current on the metallic reflector generated by the incident fields from the feed antenna. Then one can integrate over that current distribution to obtain the far-field. Using the general expression for the magnetic vector potential appropriate to a surface current in the general far-field electric far-field expression, we have

Where S_r is the surface of the reflector.

Using physical optics approximation one can find the surface current J_s. PO makes use of the assumptions that were listed for GO method to relate the surface current to the incident field. The incident magnetic field from the feed H_i and the magnetic field associated with the reflected wave H_r are related to the surface current as

$$J_s = H_{tan}$$

where H_{tan} is the tangential component of the total magnetic field which is given by

$$H_{tan} = \check{n} \times (H_i + H_r)$$

For a perfect conductor, $H_i = H_r$. so

$$J_s = 2\, \check{n} \times H_i \qquad \text{over the front of the reflector}$$

$$= 0 \qquad \text{on the shadowed side of the reflector}$$

The discontinuity at the rim of the reflector separating the illuminated and shadowed regions is neglected.

For axisymmetric reflectors, the PO and GO methods yield identical results. For offset reflectors, PO produces slightly better results than GO.

Both of these methods give accurate results for the main beam and the first few side lobes. To find the pattern in the far-out side-lobe region, diffraction theory is included along with these two methods. The resultant methods are called as GTD (Geometrical theory of diffraction) and PTD (Physical theory of diffraction).

4.3.4 Significance of Feeds for Parabolic Reflectors:

As we saw in the sections above, feeds contribute significantly in the performance characteristics of the reflector antenna systems. The radiation pattern of the feed contributes to the illumination efficiency of the reflector. Feed's crosspolarization properties influence reflector's polarization efficiency. If the feed's phase centre is not at the focus of the reflector, then it affects the phase efficiency of the system. Feed's mechanical size also influences the aperture efficiency of the reflector because of the aperture blockage that it causes. Reflector in inherently wide-band antenna. Feed limits the bandwidth of the system. Feed's radiation efficiency and impedance match with the electronics (LNA) is important because ultimately it is the feed that couples the signal from the reflector to the electronics.

Thus, in many respects, feed decides the performance of the reflector system. Therefore designing of a feed should be carefully done so as to optimize the performance of the antenna. This involves choosing the type of feed from a wide variety of feeds available, according to the application concerned as well as making compromises on different parameters. For e.g. if symmetrical radiation pattern is more important (in order

to reduce cross-polarization), then one may compromise on aperture blockage or simplicity in construction by going for a corrugated horn.

In next chapter the characteristics of different types of feeds will be explored. Also, the different approaches taken while designing a feed will be discussed.

CHAPTER FIVE

Feeds for Parabolic Reflectors

The feed acts as a primary antenna for the parabolic reflector. Feed's radiation characteristics influence the reflector's radiation characteristics and aperture efficiency to a great extent. Reflector antennas have a wide range of applications in various fields like radio astronomy, satellite communication, radar systems etc. Depending on the requirements, a wide variety of feeds is available. Ranging from microstrip arrays to corrugated horns, feeds having different characteristics have been designed. In this chapter different types of feeds will be discussed. Then the approaches towards designing a feed will be explored. Before concluding, keeping in view the two broadband feeds that have been introduced in GMRT, the importance of using broadband feeds in radio astronomy is stated.

5.1 Different types of feeds and their comparison:

Pure-mode horns and waveguides were the most preferred feeds for reflectors for many years. But later it was understood that the efficiency of the system improves if the feed's distribution is matched to the reflector's focal field distribution. This matching occurs when the radiating surface is corrugated. So corrugated hybrid mode horns came in use. They offer excellent pattern symmetry (hence low cross-polarization), wide bandwidth and good impedance matching.

One drawback of corrugated horns is that they are bulky. The corrugations as well as the orthomode transducer that is used to separate two orthogonal polarizations, increase the overall dimensions of the feed. In many applications dual polarization is a

requirement. So to reduce the size of the feed, coaxial feeds were explored. Although their pattern symmetry and bandwidth characteristics are not as attractive as corrugated horns, they are compact in size. They achieve an aperture illumination equivalent to that of circular waveguide feeds, with much smaller aperture diameter and equivalent impedance match for a shorter cavity length [8]. Ridged waveguides too offer low cutoff frequency, wide bandwidth and good impedance matching characteristics. Microstrip feeds also find their use in many applications because of their light weight and ease of fabrication.

Dipoles with a metallic blocking behind them are also used as feeds for reflectors. But the metallic blocking reduces the aperture efficiency as well as strongly influences cross-polarization. One novel antenna using log-periodic folded dipole arrays above a finite ground plane is the Eleven feed [14].

Thus, there is a wide variety in the types of feeds available. One has to choose the suitable type of feed so as to meet the required specifications of the system.

Following is a comparison of different types of feeds in terms of their performance characteristics.

Table 5.1 Comparison of different types of feeds [6]

Type Of feed	**Shape of Pattern**	**Pattern Symmetry**	**Peak Crosspolar Level**	**Gain**	**Efficiency**	**Bandwidth**	**VSWR**	**Size and Volume**
Pure-mode Horn	Gaussian	Medium	High	Medium	Medium	Medium	Good	Medium
Prime-focus waveguide Feed	Broad	Medium	Medium	Low	High	Medium	Medium	Small
Multimode Horn	Shaped	Medium to good	Medium to low	Medium	Medium	Narrow	Good	Medium
Corrugated Horn	Gaussian	High	Very low	Medium to High	Low	Wide	Good	Large
Dielectric-loaded Horn	Gaussian	High	Very low	Medium	Medium	Wide	Medium	Large
Dielectric-rod feed	Broad	Medium	Medium	Low	High	Medium	Poor	Small
Dipole Feed	Broad	Poor	High	Low	Medium	Narrow	Poor	Small
Microstrip feed	Broad	Medium to poor	High	Low	High	Narrow	Medium	Small

5.2 Designing a Feed:[3]

Designing a feed primarily involves choosing the type of feed according to the application and then deciding its geometrical parameters so as to optimize the reflector's aperture efficiency. Ultimately feed designing becomes a trade-off between taper efficiency and spillover efficiency. A single-reflector antenna usually requires a feed which radiates a broad beam, while a dual-reflector antenna needs a feed with a narrow beam of radiation. Feeds radiating narrower beams have wider apertures and generally give higher-quality radiation characteristics.

If the feed radiation pattern is broad, then taper efficiency is high, but the spillover increases and the spillover efficiency becomes low. If the feed pattern is narrow, the spillover efficiency is high but the edge taper increases and taper efficiency reduces. This is shown in the following figure.

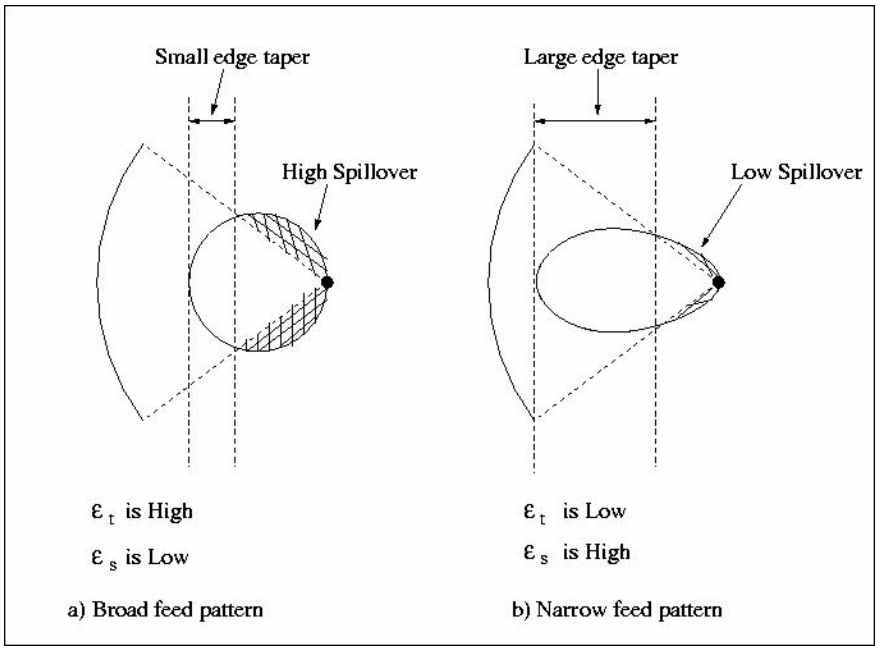

Fig. 5.1 Influence of feed antenna pattern on reflector aperture taper and spillover. [3]

Spillover and taper efficiencies are combined to form illumination efficiency. The optimum trade-off between taper and spillover efficiencies occurs when the reflector edge illumination is about -11dB. At this edge taper, the illumination efficiency is maximum and is equal to 82%. This is shown in the following graph.

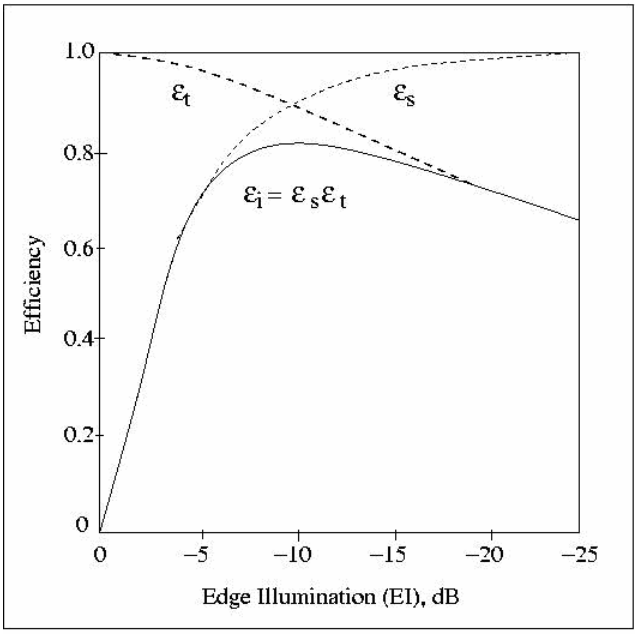

Fig. 5.2 Aperture taper ε_t , spillover ε_s and illumination ε_i efficiencies for a $\cos^2 \theta_f$ pattern as a function of edge illumination [3]

One approach toward feed designing aims at matching the feed radiation pattern to the reflector so as to achieve maximum illumination efficiency. This requires the feed's radiation pattern to be such that the taper at the reflector edge becomes -11dB. The expression for the edge illumination (EI) is as follows:

$$EI = -FT - L_{sph} \qquad (5.1)$$

Where EI = edge illumination, dB

FT = feed taper (at aperture edge) , dB = $-20 \log[F_f(\theta_0)]$

$F_f(\theta_f, \Phi_f)$ is the feed radiation pattern. For a rotationally symmetric pattern, variation with Φ is zero.

L_{sph} = spherical spreading loss at the aperture edge, dB.

$= -20 \log [(1 + \cos \theta_0)/ 2]$

One feed pattern is used to model the patterns of real feeds such as the conical corrugated horns. The pattern function is as follows.

$$F_f(\theta_f) = \cos^q \theta_f \qquad \theta_f \leq (\pi/2)$$

$$= 0 \qquad \theta_f > (\pi/2) \qquad (5.2)$$

The edge illumination for this pattern is

$$EI = [(1 + \cos \theta_0)/2] \cos^q \theta_0 \qquad (5.3)$$

From this expression one can find out the q value for the EI of -11 dB.

Then one has to select a feed antenna that approximates the $\cos^q \theta_f$ pattern with the q value found from (5.3).

The HPBW and -10 dB beam widths for various F/D ratios (hence θ_0 s) that give -11 dB edge illumination are shown in the following figure. So a feed can be designed so as to give the -10 dB or -3 dB beam widths specified in the following figure.

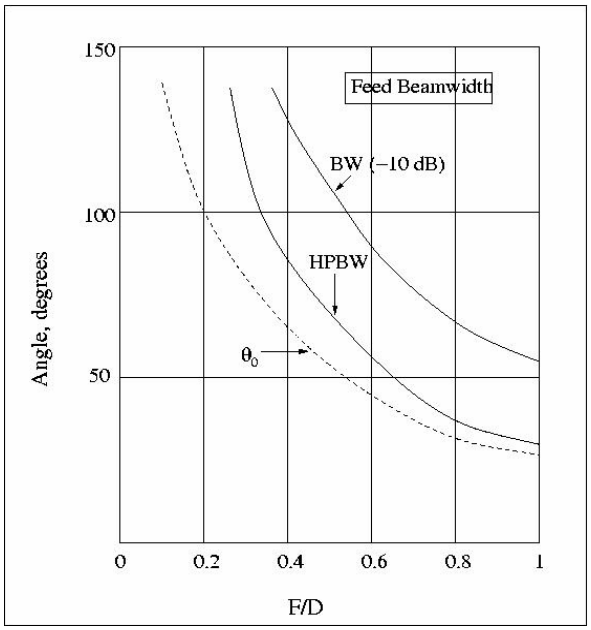

Fig. 5.3 Half-power and -10 dB Beamwidths of feeds to achieve -11 dB edge illumination [3]

The other approach toward feed designing aims to match the aperture distribution of the feed to the focal field distribution of the reflector. It turns out that the focal field distribution of a parabolic reflector is the spatial Fourier transform of the aperture distribution with increasing accuracy with larger F/D. So for a uniform aperture distribution, the focal field distribution is the sync function (sin u /u). The feed having an aperture distribution which matches the focal field distribution will result in 100 % aperture efficiency.

In radio astronomy, the signals come from distant radio sources. So the waves falling on the reflector can be considered as uniform plane waves. This uniform amplitude distribution will create a (sin u)/u type focal field distribution. Hence we need a feed whose aperture distribution would resemble this focal field distribution. However, a feed of infinite extent would be required to collect all these fields. If we call this feed an "ideal feed", then it will have a point phase centre and rotationally symmetric radiation pattern. The pattern would extend only over a cone only out to the reflector rim and would compensate for spherical spreading loss. This pattern is expressed as follows:

$$F_f(\theta_f, \Phi_f) = (\cos^2 \theta_0/2) \sec^2 (\theta_f/2) \qquad \theta_f \leq \theta_0$$

$$= 0 \qquad \theta_f > \theta_0 \qquad (5.4)$$

This ideal feed pattern would lead to 100% aperture efficiency if no ohmic or achievement losses are present. The pattern discontinuity at reflector rim produces the required uniform APD and zero outside.

This feed pattern is impossible to realize. A realistic feed which would maximize the aperture efficiency should have the following characteristics.

- The feed pattern should be rotationally symmetric, or balanced.
- The feed pattern should be such that the reflector edge illumination is about -11 dB.
- The feed should have a point phase centre and the phase centre should be positioned at the focal point of the reflector.
- The feed should be small in order to reduce blockage; it is usually on the order of a wavelength in diameter.
- The feed should have low cross-polarization, usually below -30 dB.
- The above characteristics should hold over the desired operational frequency band.

High sensitivity astronomical observations require broad bandwidths. Two such broadband feeds are being introduced in the GMRT. Before proceeding to the next chapters in which these broadband feeds are specifically explained in detail, we will discuss in general the need for broadband feeds and also look at some commonly used broadband feeds.

5.3 Broadband Feeds: A significant step towards high sensitivity:

As we have seen in chapter 2, the minimum detectable antenna temperature for a radio telescope is

$$\Delta T_{min} = \frac{K_s T_{sys}}{\sqrt{(\Delta f\, tn)}} = \Delta T_{rms}$$

Where ΔT_{min} = sensitivity, or minimum detectable temperature, K

ΔT_{rms}= rms system noise temperature, K

T_{sys} = system noise temperature, K

K_s= sensitivity constant, dimensionless.

Δf = predetection bandwidth, Hz

t= postdetection integration time, sec.

n= number of records averaged, dimensionless

Also, as was discussed in chapter 3, one of the means to improve the sensitivity of a radio telescope is to increase the bandwidth of the feed and hence that of the receiver. It is a challenging task to design a feed antenna which gives good impedance match, low cross-polarization and optimum aperture efficiency over a wide band. The major types of feeds that are broadband in nature are discussed below.

5.3.1. Corrugated Horn: [6], [9], [10]

Corrugated horns have become the preferred choice of feed antenna for reflectors in radio astronomy as well as in radar systems. They produce radiation patterns with high symmetry and low cross-polarization. The corrugations change the fields so as to provide the desirable properties of axial symmetry, low sidelobes and low cross-polarization. $\lambda/4$ deep corrugations are made on the inner wall of the horn. The requirement to produce a radiated field which has a symmetrical main beam and a low crosspolar level can be met only by a horn which produces an aperture electric field in which the fields are nearly linear. A linear electric field cannot be produced by waveguides which support pure TE or TM modes because they have aperture electric fields in which the field lines are

curved. Only a 'hybrid' mode can produce the desired linear aperture field. When the impedance and admittance at the boundary are equal or both of them are zero, the aperture field becomes independent of the angular variable (Φ) and cross-polarized field also becomes zero. Corrugated walls of the horn make the impedance and admittance zero at the boundary.

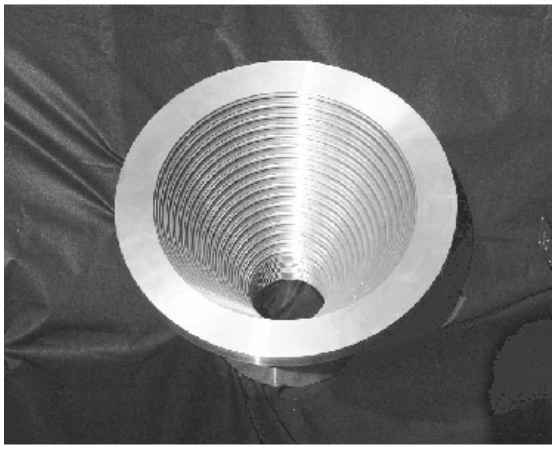

Fig. 5.4 A corrugated horn

Corrugated horns are particularly useful as broadband feeds because the desired properties of low cross-polarization and pattern symmetry are maintained over a broad range of frequencies. Although the principle of operation of corrugated horns depends on λ /4 deep slots, the rate of change of surface impedance with frequency is relatively slow so that even at acceptable frequency distance from λ /4, the good properties still hold. This characteristic is a function of aperture diameter and the bandwidth increases proportionally to aperture diameter. Also, for certain beamwidths it is possible to have a nearly constant beamwidth over a broad bandwidth.

The impedance properties are usually the factors which limit the bandwidth. If there is a smooth and gradual change from a λ /2 to λ /4 slots, the EH_{11} mode propagation is avoided and bandwidth can be increased.

5.3.2. Dielectric-loaded horn: [6],[11],[12]

These are conical horns partially loaded with a dielectric cone. These support hybrid modes similar to those for a conical corrugated horn. The consequence is that they can have the same desirable radiation characteristics as corrugated horns. The dielectric-loaded horns are, in principle, simple to manufacture and can be used as high-performance feeds for parabolic reflectors, particularly at milimetre wavelengths where the corrugated horns are difficult to construct. Developments in plastic technology promise high quality of dielectrics.

Dielectric-loaded horns allow expanding the operating bandwidth because of the absence of resonating elements. One more advantage o this horn is that the desired phase front can be obtained by shaping the front surface of the dielectric core.

However, this horn suffers from higher effective noise temperature.

5.3.3. Ridged waveguide:[13]

The bandwidth of a waveguide or the throat region of a horn is determined by the frequency difference between the cut-off of the dominant mode and the cut-off of the next-highest order mode which will be excited by the geometry of the input section of the waveguide. In a ridged waveguide, the ridges decrease the cut-off frequency of the dominant mode. Hence the bandwidth expands. Ridged waveguides will be discussed in detail in chapter 6.

5.3.4. Log-periodic antenna: [3],[23]

It is a type of frequency-independent antennas. A log-periodic array of dipoles can work on very broad bandwidths. As the name suggests, the frequency response of this type of antenna is periodic over logarithm of frequency. The periodicity of the structure

does not ensure broadband operation. But if the variations of impedance, pattern, directivity, beamwidth etc are made sufficiently small and acceptable for the corresponding bandwidth of the cycle, broadband characteristics are ensured within acceptable limits of variation.

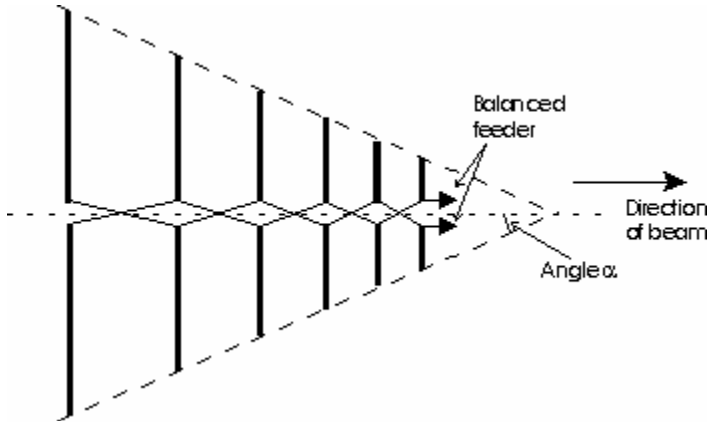

Fig. 5.5 A log-periodic antenna [36]

An **active region** is defined in the case of frequency-independent antennas, which relocates itself on the antenna structure as the operating frequency changes. Consequently, the **phase centre** also changes with the operating frequency. This is undesirable because it affects the aperture efficiency of the parabolic reflector.

A novel feed using log-periodic array of folded dipoles is the Eleven feed. [14] We will see in more detail about log-periodic antennas and the Eleven feed is chapter 7.

CHAPTER SIX

The CSIRO Dual Band Feed

One of the ways to achieve high sensitivity for radio telescopes is to make observations at wide bandwidths. GMRT currently operates at five frequency bands. To improve the sensitivity of the observations, two new wideband feeds are being introduced in GMRT. One of these feeds is the dual band feed operating at 220-240 MHz as well as at 550-900 MHz [19]. This feed has been designed by CSIRO (Australia) specifically for GMRT. The 550-900 MHz band is received by a ridged circular waveguide, whereas the low frequency band is received by a coaxial cavity.

Fig. 6.1 The 550-900 MHz feed mounted at the focus of the C11 antenna of GMRT

The 550-900 MHz part is fabricated and tested. In this chapter theory of ridged waveguides and the orthomode transducer will be discussed in detail. Then we will discuss the testing of the feed in detail.

6.1 Ridged Circular Waveguides:

Ridged circular waveguides are being used as broadband feeds for parabolic reflectors since long back. Shimizu [15] demonstrated an octave bandwidth feed using circular ridged waveguide operating in the fundamental TE_{11} mode. If a TM_{01} mode is excited, it would tend to destroy the radiation pattern symmetry achieved by the TE_{11} mode. The ridges avoid this by increasing the cut-off frequency of the TM_{01} mode and lowering the cut-off frequency of the TE_{11} mode. [16]. It is shown in Fig 6.1. Physically, the gap between the ridges begins to form a parallel-plate waveguide inside the circular waveguide. A parallel-plate waveguide propagates a TEM mode with no low-frequency cut-off so that as the gap is narrowed the cut-off frequency of the TE_{11} mode decreases [13]. The introduction of ridges also splits the TE_{21} mode.

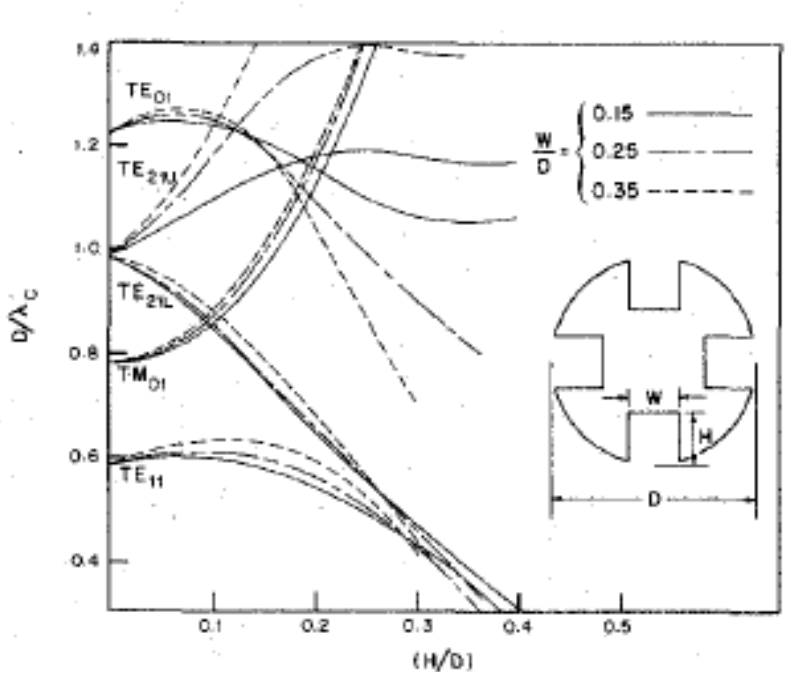

Fig. 6.2 Variation of cut-off wavelengths with heights of ridges in circular ridged waveguide [16]

Chen et. al. [16] have carried out modal analysis of the ridged waveguides (circular and rectangular) by calculating the eigen values and scalar potentials. They demonstrate the dependence of the bandwidth of the ridged circular waveguide on the height of the ridges. In Fig. 6.2, the bandwidth is controlled by the TE_{11} and TM_{01} modes on the left of the peaks and by TE_{11} and TE_{21} modes on the right of the peaks.

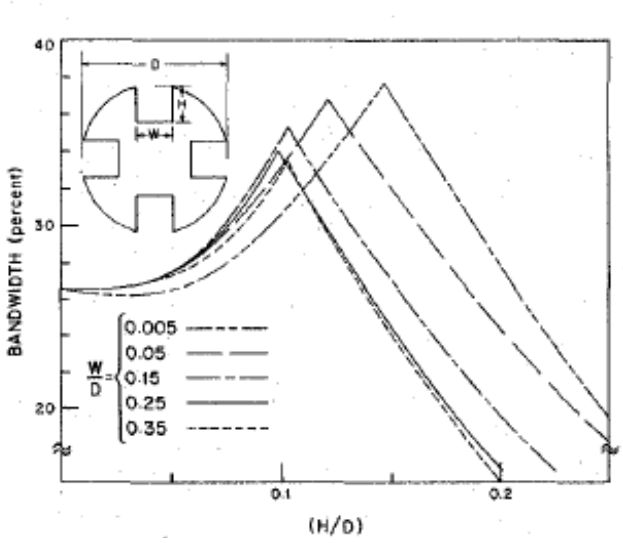

Fig. 6.3 Variation of bandwidth with height and width of ridges [16]

Width of the ridges does not affect the individual modal bandwidths very much. But ridge width is important in determining the maximum bandwidth.

The method of exciting TE_{11} mode in ridged circular waveguides is well developed. When a coaxial line is used to excite a dual- or quad-ridged waveguide feed, the outer conductor is shorted to one of the ridges and the inner conductor protrudes to get connected to the opposite ridge [13].

To extract orthogonally polarized signals, a transition such as orthomode transducer (OMT) is needed. In the CSIRO dual band feed, a stepped OMT is used. In next section we will see the details of it.

6.2 The Orthomode Transducer:

The main performance criteria that is applicable to OMTs and in general to any given antenna system so that the performance becomes acceptable, is stated below [18].

1. Return loss: In applications like radio astronomy, a return loss of even 10 dB is many times unacceptable. A return loss close to 20 dB, at least a minimum of 15 dB is more desirable. This stringent criterion inevitably reduces the bandwidth capability.

2. Isolation: The isolation between the output ports of the OMT is of importance and a figure of at least 30 dB is considered essential where dual polarization is required.

3. Cross-polarization: Higher order modes are inevitably excited to some degree at higher frequencies. One of its serious consequences is the additional level of cross-polarization radiated by the horn antenna used in conjunction with the OMT. Thus, another performance criterion in the OMT design is the increase in the cross-polar field that can be tolerated over that of the inherent level from the horn alone.

4. Insertion loss: the insertion loss of the OMT must be kept to a minimum. Applications like radio astronomy demand a figure considerably low.

Also, criteria like ease of manufacture, size of the OMT are of importance under certain circumstances.

In a quad-ridged OMT, tapered ridges are used inside the waveguide. Two orthogonal pairs of ridges concentrate the field into a small gap in the centre of the guide. This field can then be extracted with the help of coaxial lines passing through the ridges. The main purpose of the quad-ridged OMT is to transform the orthogonally polarized fields in the circular waveguide to a quad-ridged waveguide.

Although the quad-ridged OMT is inherently wideband, its conventional design uses very long (in terms of wavelength) taper from the input to the output probes. Size of the feed is an important criterion for a radio telescope. So for the CSIRO feed [19], a stepped OMT was designed.

A stepped transition is suggested in [17]. Such a stepped OMT reduces the length of the feed, but a compromise has to be made over its bandwidth.

6.3 Testing of the 550-900 MHz CSIRO Feed:

Various tests were carried out in order to characterize the performance of the 550-900 MHz feed. The tests include measurement of return loss, testing of the low noise amplifiers (LNAs) for their linearity, sensitivity test, deflection measurement at antenna base and measurement of HPBW of the feed with reflector system.

6.3.1 Measurement of Return Loss

The return loss of the feed was measured using network analyzer. The feed was kept in open space, facing the sky. Return loss for both the polarizations was measured. It was found that both the polarizations were giving almost identical response. The S11 (in dB) was below -10 dB for the band of 550 to 900 MHz.

The plot of S11 (dB) vs frequency is attached in Appendix B. Also, similar lot for the other prototype of the feed is attached.

6.3.2 Testing of Broadband LNAs for linearity:

Two broadband low noise amplifiers were designed and fabricated for using with the 550-900 MHz CSIRO feed. As was discussed in chapter 3, stability and linearity are the two most basic requirements for an amplifier. Hence, the LNAs were tested for linearity.

1 dB compression point: The compression dynamic range (CDR) of the receiver defines the range of signal levels an amplifier can process linearly. The point at which the amplifier gain falls by 1 dB from the ideal (linear) for a single input signal is a figure of merit known as 1 dB compression point. CDR is the difference in dB between the in-band 1 dB compression point and the minimum discernible signal (MDS) level. [20]

To measure the 1 dB compression point for the LNAs, the input signal level is increased step by step and the output signal levels are measured. Then the output signal level is plotted against the input signal level. The point at which this plot deviates from an ideal linear plot by 1 dB, is the 1 dB compression point. Following figure illustrates the concept.

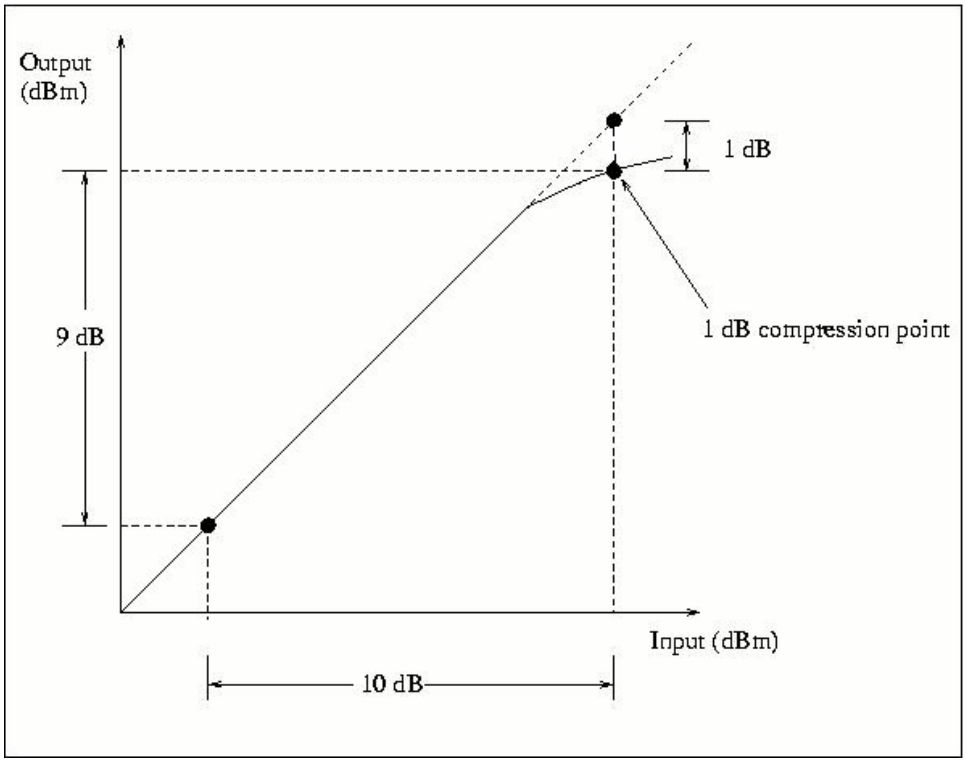

Fig. 6.4 1 dB compression point [20]

1 dB compression point for the LNA came out to be 4 dBm.

Third order intercept point: This concept is used to calculate the amount of third order distortion a device is likely to generate under a particular set of input conditions. The third order intermodulation products result for an input consisting of two signals f_1 and f_2, in producing new signals at ($2f_1$ +/- f_2) and ($2f_2$ +/- f_1). Under small signal conditions well below the compression, the power of a third order IMD product varies by 3 dB per 1 dB change in input power. This allows deriving the Third-order intercept point. A schematic for this measurement is as shown below.

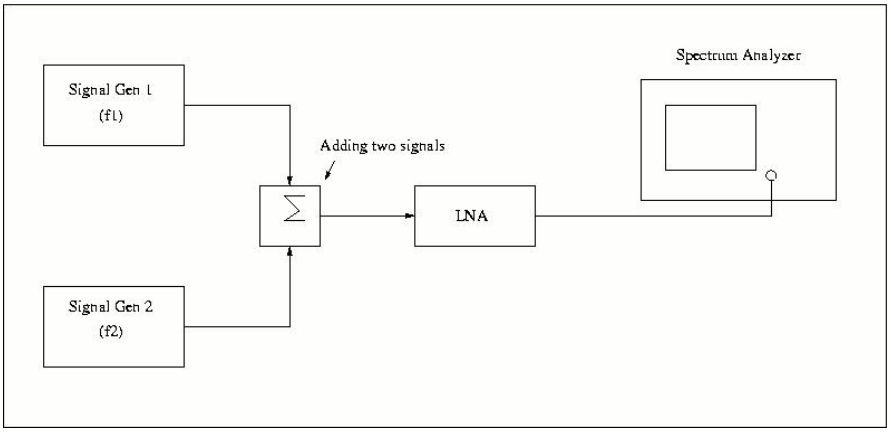

Fig. 6.5 Set up for measuring third order intercept point.

Two tones of equal power are summed and given to the LNA input. The frequencies are f_1= 850 MHz and f_2 =870 MHz. Then the output power (at 850 and 870 MHZ) and the power of the third-order products at $2f_1$- f_2 (830 MHz) and at $2f_2$ – f_1 (890 MHz) are measured.

A typical spectrum analyzer display is as shown in fig. 6.6.

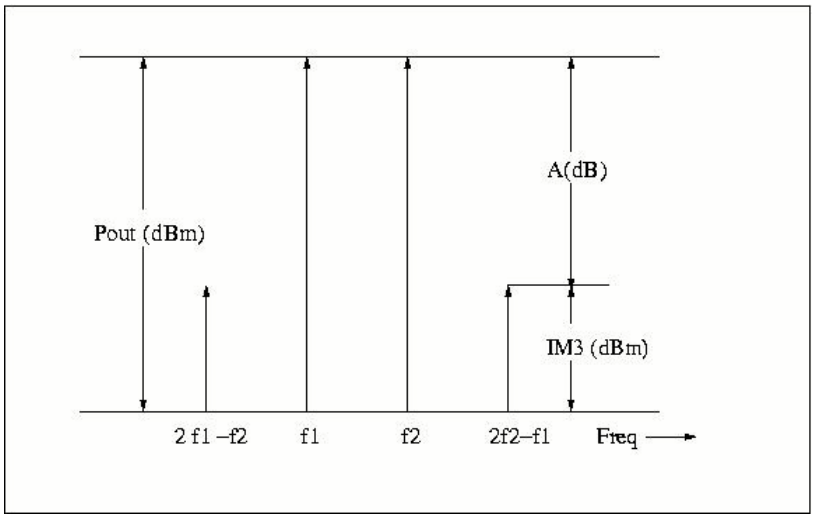

Fig. 6.6 A typical spectrum analyzer display for third order intercept point measurement [20]

Based on the measurements, the third order intercept point was calculated as follows.

$$OIP_3 = P_{out} + (A/2) \text{ dBm.} \quad (6.1)$$

Where P_{out} = output signal level in dBm.

A = the difference between output signal level (P_{out}) and the IMD (P_{IM3}) level in dB.

Here, P_{out} = -3 dBm

P_{IM3} = -57 dBm.

So A = 54 dB

Therefore

OIP_3 = -3 + (54/2)

OIP_3 = 24 dBm.

1 dB compression point and third order intercept point are satisfactory. So the LNAs were installed to the feed.

6.3.3 Measurement of half power beam width (HPBW) of the secondary pattern:

The simulated radiation patterns for the feed were provided by CSIRO. [3] gives the half power beamwidth of the reflector antenna if the edge illumination due to feed is known. Using the method provided in [3] to calculate HPBW, the HPBW for a GMRT antenna with the CSIRO feed at focus was calculated at different frequencies.

HPBW was also measured for some frequencies. The feed was installed on the C11 antenna of GMRT. To measure HPBW, a strong radio source is scanned by the antenna of which HPBW is to be measured. The received power is measured. A typical plot of power against time (in terms of offset from the time of peak power) for azimuth and elevation scans is as shown below.

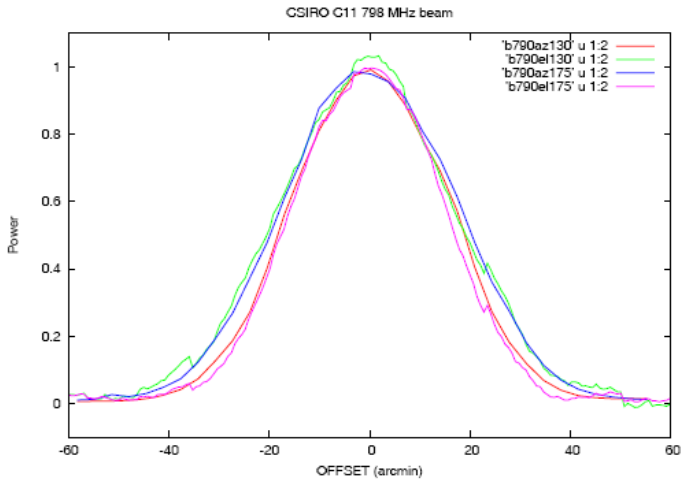

Fig. 6.7 A typical power output plot for an antenna scanning a radio source.

The values on Y axis are normalized power outputs. From this, the HPBW can be calculated. The calculated and measured HPBWs are listed in the following tables.

Table 6.1 Calculated Half power beamwidths for GMRT antenna when illuminated by the 550-900 MHz CSIRO feed

Frequency (MHz)	Edge Illumination (dB)	HPBW (arcmin)
550	-12	48
600	-14	44.7
650	-14	41.25
700	-15	38.64
750	-16	36.44
800	-16	34.38
850	-16	32.07

Table 6.2 Measured Half power beamwidths for GMRT antenna when illuminated by the 550-900 MHz CSIRO feed

	HPBW (arcmin)			
Frequency(MHz)	130az	130el	175az	175el
618	45.7	43.1	44.5	45.1
703		40.1	41.6	40.8
798	36.6	40.4	40.1	33.9

In the measured HPBW table, 130 denotes one channel (polarization) and 175 denotes the other channel. al means the scan in azimuth plane and el means the scan in elevation plane.

6.3.4 Sensitivity test on Feed with C11 antenna:

Sensitivity of the C11 antenna at 610 MHz was measured before and after the feed was changed from the GMRT 610 / 233 MHz dual band feed to the CSIRO feed.

The sensitivity is defined as (Power ON-Power OFF)/Power OFF. Power ON is the power output from the antenna when it is pointed to a radio source (in this case 3C147) and power OFF means the power output from the antenna when it points towards a region of sky where there is no radio source. Two OFF scans were done, one before and one after the ON scan. The sensitivity was computed using the program *ltasens* which fits a linear polynomial to the OFF power scans to account for drifts in the total power. No correction for the sky temperature is made. The experiment was carried out by Dr. Jayaram Chengalur.

The sensitivity plots are attached in Appendix B.

6.3.5 Deflection measurement at antenna base:

When the 550-900 MHz feed was installed on the C11 antenna, at the antenna base, signal was received and seen on spectrum analyzer. Readings were taken for the antenna pointing to blank sky (OFF source) and for the antenna pointing to a radio source Crab (ON source). The deflection in power output (ON-OFF) was measured. The spectrum analyzer plots are attached in Appendix B.

6.3.6 Measurement of return loss along with the 233 MHz part of the feed:

The feed is designed to be dual-band. The lower frequency band is from 220 MHz to 240 MHz. The lower frequency band is received with the outer coaxial waveguide. Initially, as was discussed in section 6.3.1, return loss of the 550-900 MHz part alone was

measured. The effect of the outer 220-240 MHz part on the return loss of 550-900 MHz part was explored by measuring the return loss of the 550-900 MHz part with the 220-240 MHz part put on it. The return loss was found to be improved by nearly 1 dB over most part of the band. The results of this measurement are attached in Appendix B.

CHAPTER SEVEN

The 200-800 MHz Eleven Feed

A novel dual polarized ultra-wideband antenna which employs parallel folded dipoles over a finite ground plane as its basic elements is the Eleven feed invented and developed by the Chalmers antenna group (Sweden) [14]. Optimization of this feed for GMRT is carried out by Yogesh Karandikar [21]. The feed has a wide bandwidth of 200-800 MHz and has almost no phase center variation and almost constant beamwidth throughout this band.

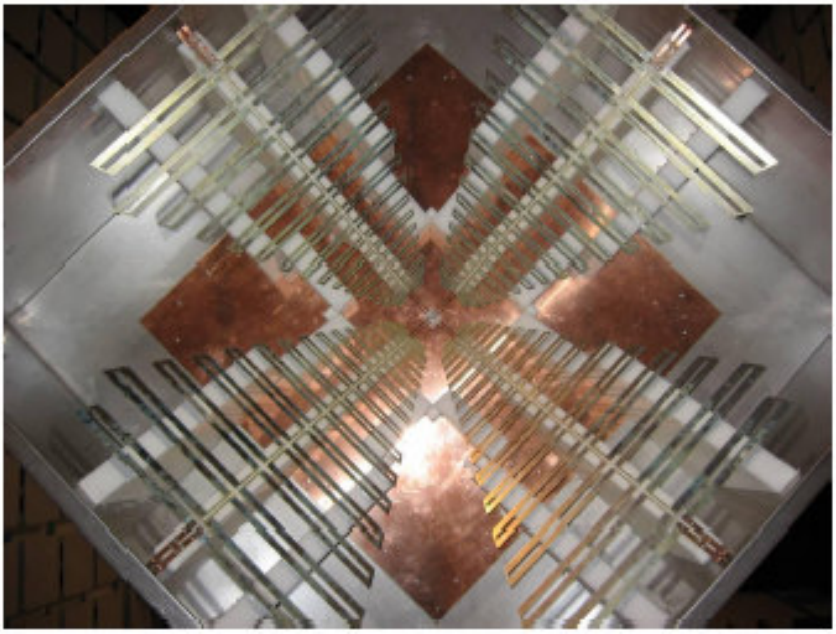

Fig. 7.1 Close up of the Eleven feed

The feed has been named as Eleven antenna because its basic configuration is two parallel dipoles 0.5 wavelengths apart and because it has 11 dB directivity.

7.1 Basic concept behind the Eleven Feed:

An array of two half wavelength dipoles above ground plane can give broadside radiation pattern when both dipoles are excited with equal amplitude and phase [21]. Such an array can be used as a feed for the reflector when infinite ground plane is replaced by a finite one. Eleven feed utilizes this concept by replacing dipoles with log-periodic folded dipole arrays. Hence the characteristics of the Eleven feed include a combination of those of dipoles above a ground plane and those of log-periodic dipole arrays. Log-periodic dipole array is a type of frequency-independent antennas. Therefore it is inherently wideband. So replacing dipoles with log-periodic arrays of folded dipoles increases the bandwidth of the antenna. But the radiation pattern is broadside, which is desired for a feed used for a reflector.

7.2 Dipoles above a ground plane:[21]

The basic element of the Eleven feed is an array of two dipoles placed above a ground plane. Such an array can give a broadside radiation when fed with equal amplitude and phase. When the ground plane is of finite extent, this arrangement can be used as a feed for a reflector. GMRT uses such kind of arrangement for one of its frequency bands. The 150 MHz band feed of GMRT uses folded dipoles placed at half a wavelength apart from each other above a ground plane.

A two element array of folded dipoles is shown in Fig. 7.2 below. It can be fully defined by three variables as

1. Length of the dipole (L)

2. Separation between two dipoles (DP)

3. Height of the dipoles above ground plane (H).

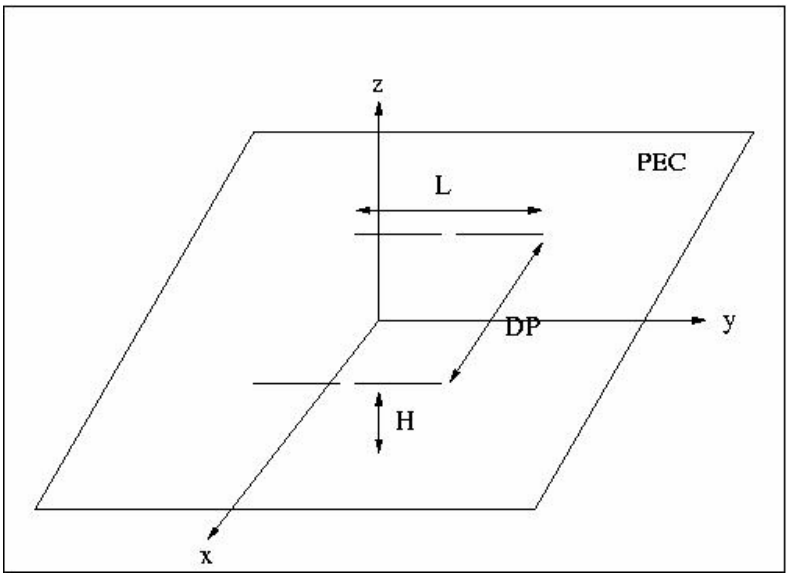

Fig. 7.2 Geometry of array of two dipoles above a ground plane [21]

The complete far-field function of the array over infinite ground plane can be written as

$$G(\theta, \varphi) = C.\ AF(\theta, \varphi).\ GPF(\theta, \varphi).\ j(\theta, \varphi).\ ISF(\theta, \varphi) \quad (7.1)$$

Where

C = constant

AF (θ, φ) = Array factor

GPF (θ, φ) = Ground plane factor

j (θ, φ) = Fourier transform of the current distribution on dipole

ISF (θ, φ) = Incremental source factor

[2] gives the expressions for the factors mentioned above.

$C = 2.2j.\ (2/k).\ C_k\ \eta\ I_0$

$AF(\theta, \varphi) = \cos(\pi\ DP \sin\theta \sin\varphi)$

$GPF(\theta, \varphi) = \sin(2\pi\ H \cos\theta)$

$j(\theta, \varphi) = \cos[(\pi/2) \sin\theta \sin\varphi] \,/\, [1 - (\sin\theta \sin\varphi)^2]$

ISF $(\theta, \varphi) = [\cos\theta \sin\varphi \tilde{\theta} + \cos\varphi \tilde{\varphi}]$

This total far-field function after normalizing can be written as sum of θ and φ components as

$$G^n(\theta, \varphi) = G_\theta^n(\theta, \varphi)\,\tilde{\theta} + G_\varphi^n(\theta, \varphi)\,\tilde{\varphi} \qquad (7.2)$$

Where

$G_\theta^n(\theta, \varphi) = AF(G_\theta^n(\theta, \varphi)\, GPF(G_\theta^n(\theta, \varphi)\, j(\theta, \varphi) \cos\theta \sin\varphi$

$G_\varphi^n(\theta, \varphi) = AF(G_\theta^n(\theta, \varphi)\, GPF(G_\theta^n(\theta, \varphi)\, j(\theta, \varphi) \cos\varphi$

Eqn (7.2) gives the final expression for normalized far-field function of the two element broadside dipole array above infinite ground plane. It is clear from the equation that for half wavelength dipole the far-field function of the array depends only on separation between two dipoles (DP) and height of dipoles above ground plane (H). So it is possible to obtain the desirable pattern by choosing the values of DP and H expressed in wavelengths.

The values of DP, H and the size of finite ground plane are varied and optimum values are chosen for maximizing the aperture efficiency [21].

7.3 Log-Periodic Antennas:[21], [23]

Making antenna performance independent of frequency makes the antennas broadband. The impedance, polarization, pattern, etc are invariant to a change of scale that is in proportion to the change in wavelength, provided the antenna is made up of practically perfect conductors and dielectrics. Thus any lossless system composed of mixture of dielectrics and metals which follows geometrical scaling principle will have its electrical performance independent of frequency when all of its dimensions are scaled in inverse proportion of frequency, i.e. its dimensions measured in wavelengths kept

constant. Planar and conical spirals had been tried which are convenient at centimeter wavelengths but become impractical at longer wavelengths.

Duhamel and Isbell first demonstrated another type of antenna whose shape was not solely determined by angles, hence not truly frequency independent antenna but still having broadband behavior. This type of antenna is called as log-periodic antenna because the impedance ant pattern are periodic over a logarithm of frequency. Isbell succeeded in developing a log-periodic array of dipoles, in which he introduced an extra 180^0 phase shift from one dipole to next by switching the connections of transmission line feeding the dipoles. This modification reduced the variation of the radiation pattern over a period which was seen in the earlier versions.

Conventional log periodic array of dipoles is formed by log periodically loading a transmission line by dipoles. The lengths of dipoles, radius of wire and distance between them are scaled by a factor $\tau < 1$. the array is then fed at the shortest element, i.e. the element corresponding to the highest geometrical frequency. The connections from one dipole to the next are switched so as to provide an extra phase shit of 180^0. A typical log-periodic dipole array is shown in fig. 7.3.

The spacing d_n between one dipole to the next plays an important role in array operation. At particular value of d_n the phase delay in the transmission line combined with the 180^0 phase shift due to switching the connections gives a total phase shift of $360^0 (1- d_n / \lambda)$. This causes the radiated fields from two dipoles which are d_n apart be in phase in backward direction. This results in a beam coming out of the apex of the array giving endfire radiation.

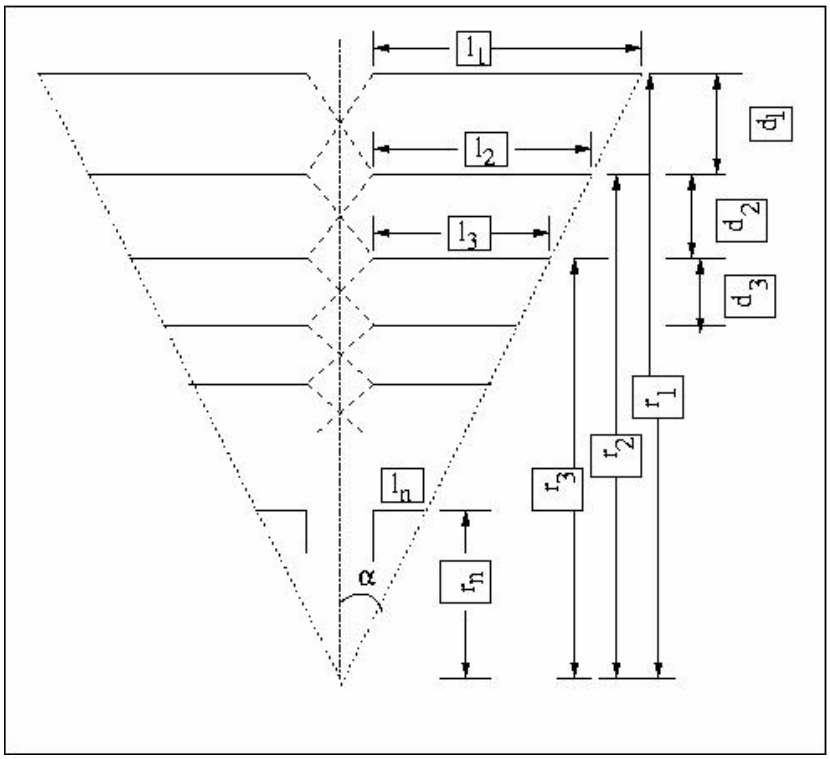

Fig. 7.3 A conventional log-periodic antenna[21]

Theoretically this antenna to be frequency independent, all dimensions should be scaled in proportion to the distance from the origin. This also applies to the transmission line feeding the dipoles, so ideally it should be biconical. But if the spacing between the parallel wire line is negligible as compared to the shortest wavelength of operation then the parallel wire line is equivalent to biconical line. So practically we need not to scale the transmission line and hence the feed gap of all dipoles, if the spacing is small compared to shortest wavelength ($s << \lambda_{min}$). Also in practical realizations the radius of wire forming the dipole is kept constant.

The geometrical relations in the log-periodic dipole array are as follows:

l_n = length of n^{th} element

r_n = distance from origin to n^{th} element.

d_n = Spacing between n^{th} and $(n+1)^{th}$ element.

The values of following parameters should be known in order to specify the entire geometry of the log-periodic dipole array.

f_{min} = lowest geometrical frequency

N = Number of elements in an array

τ = Scaling factor (<1) which decides next geometrical frequency

σ = spacing factor deciding distance between consecutive dipoles (in terms of λ)

α = Opening angle of array

R = Radius of wire forming the dipole (in terms of λ).

l_n , r_n , d_n are interrelated as follows:

$$\frac{l_{n+1}}{l_n} = \frac{r_{n+1}}{r_n} = \frac{d_{n+1}}{d_n} = \frac{R_{n+1}}{R_n} = \tau$$

Also,

$d_n = r_n - r_{n-1} = (1-\tau)\, r_n$

$\sigma = d_n / \lambda_n = (1- \tau)\, r_n / \lambda_n$

$\tan \alpha = l_1 / r_1 = l_n / r_n$

7.4 The optimized Eleven feed:

Eleven feed combines the desirable characteristics of conventional log-periodic arrays with those of an array of two dipoles placed above a ground plane.

Instead of common half-wave dipoles, Eleven feed uses folded dipoles in log-periodic array. Folded dipoles have their input impedance about 4 times that of the half-

wave dipole. Hence it is easy to match the impedance with the high characteristic impedance of the parallel wire line. Also, a half wavelength long folded dipole gives a phase shift of approximately 180^0 from its port 1 (input port) to port 2 (output port) (if we consider folded dipole as a two port network).[21].

Eleven feed uses a finite ground plane. Finite ground causes scattering at the edges, causing back lobes. Thus spill over increases. There exists a trade-off on the size of ground plane. Because lowering the size increases spill over and increasing the size increases aperture blockage. In the optimized Eleven feed for GMRT, though the aperture blockage is not optimized, the effect of the ground plane size on spill over is thoroughly analyzed.

Parallel plate line is used to feed the FDLPA (Folded Dipole Log Periodic Array). A parallel plate line is designed so as to have a characteristic impedance of 200 Ω. The FDLPA is designed to have a characteristic impedance of 200 Ω. When two such arrays are connected in parallel on a parallel plate line, the effective impedance is 100 Ω in odd mode. It gives 50 Ω on each line. So it easily matches with the standard transmission line impedance. At the same time it puts a constraint that the coupled line parallel to the ground should have characteristic impedance of 100 Ω, which depends on its height above the ground plane. Eleven feed in GMRT is a dual polarized feed. So there are two such parallel plate lines, one for each polarization. Both cannot be at the same height above the ground plane. So, only one line can be accurately designed for a 100 Ω impedance. It has an adverse effect on the return loss of other polarization since the line feeding those FDLPAs is not having 100 Ω characteristic impedance.

There are 21 optimization parameters for the Eleven feed. The Eleven feed is fully specified by these optimization parameters. They are listed in table 7.1.

Table 7.1 Optimization parameters for the Eleven feed and their actual values for the feed at GMRT[21]

	Parameter	Description	Value for Eleven feed
1	f_{min}	Lowest Geometrical Frequency (Hz)	175 MHz
2	N	Number of elements in an array.	16
3	T	Scaling Factor (<1)	0.883
4	Σ	Spacing Constant (<1)	0.055
5	*L*	Length of folded dipole from symmetry plane (λ)	0.232
6	w_1	Width of plate at port 1 of folded dipole (λ)	0.01
7	w_2	Width of plate at port 2 of folded dipole (λ)	0.01
8	w_3	Width of shorting plate (λ)	2mm
9	G	Gap between two parallel plates of folded dipole (λ)	0.008
10	K1	Low Frequency Truncation Constant	0.8
11	K2	High Frequency Truncation Constant	0.8
12	S	Length of shorting stub on longest folded dipole (λ)	0.0182
13	Fg	Width of feed gap for all folded dipoles (mm)	6 mm
14	Ws	Width of stripe feeding all folded dipoles (mm)	3 mm
15	T	Thickness of the metal plates (mm)	2 mm
16	DP	Distance of folded dipoles from symmetry plane (λ)	0.25
17	Ψ	Elevation angle of FDLPA (Degrees)	33^0
18	C	Height of the stripe parallel to the ground (mm)	5 mm
19	L	Length of stripe parallel to the ground (mm)	15mm
20	WG	Width of square ground plane (λ max)	1.46 m
21	Hm	Height of metal walls from feed enclosure (m)	0.5 m

Eleven feed is enclosed in a metal box by making vertical walls of metal on the edges of the ground plane. The shorting stub on the last folded dipole is connected to the vertical wall of the metal box, thus giving thermal conductivity in entire structure. To support the FDLPAs, low loss Rohacell Foam is used. It has a dielectric constant of 1.001.

Based on the simulation, the total feed efficiency is calculated to be -3 dB or better over large part of the band. Also, the aperture efficiency is calculated to be approx. -2.2 dB for 63^0 semi-rim angle of the GMRT dish. Peak crosspol level is calculated to be -15.

7.5 Testing of the Eleven feed:

Various tests were carried out on the 200-800 MHz Eleven feed. The tests include measurement of return loss, testing and tuning of LNAs, measurement of HPBW of GMRT antenna with Eleven feed.

7.5.1 Measurement of return loss:

For measuring the return loss, the feed is kept in open space, facing the sky. There are four feeding points for the feed, two for each polarization (one for each FDLPA). A hybrid (see chapter 8 for details) is used to feed each polarization. Return loss is measured by connecting the network analyzer's reflection port to the input of hybrid.

The plots of S11 (dB) against frequency for both the polarizations are attached in Appendix C. The plots show S11 below -8 dB for most of the band. S11 of Polarization B is slightly worse than that of polarization A. This is expected because as mentioned is section 7.4, one of the parallel plate line will be having slightly different characteristic impedance than the other.

7.5.2 Testing and tuning of narrowband LNAs for accurate phase matching:

The LNAs that are used in GMRT for its 610 MHz band were used for the Eleven feed. So effectively the feed was tested in a narrow band of 32 MHz only.

It is required for the Eleven feed to have 2 pairs of LNAs, LNAs in each pair having exactly similar characteristics, in terms of their gain and phase response. So such 4 LNAs were tuned and tested to give gains differing by not more than 0.5 dB and phase response differing by not more than 3^0 (within one pair). LNAs were tuned mainly by changing the matching inductors' values.

7.5.3 Measurement of half power beam width (HPBW) of the secondary pattern:

The Eleven feed was installed on the C2 antenna of GMRT. Power outputs were taken for the antenna scanning in elevation as well as in azimuth direction. The results of the scans are plotted below. Note that the Y axis is proportional to voltage output. The frequency of observation is 610 MHz.

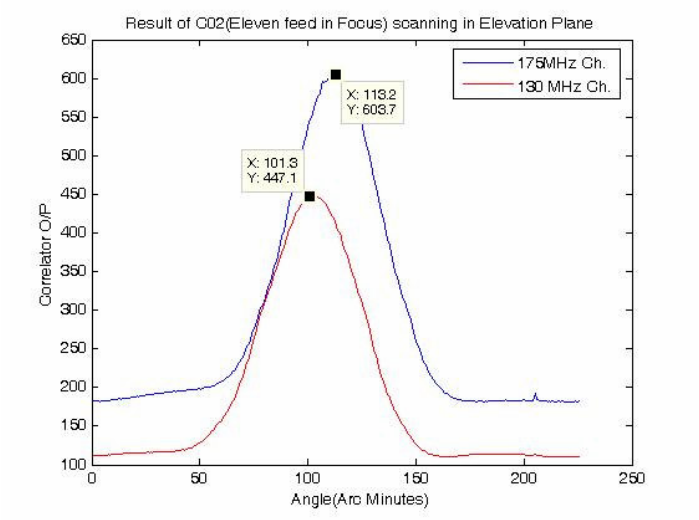

Fig. 7.4 Beam plot of (C02 + Eleven feed) scanning in elevation plane.

The HPBWs are: 45 arcmin for 130 MHz channel

43 arcmin for 175 MHz channel.

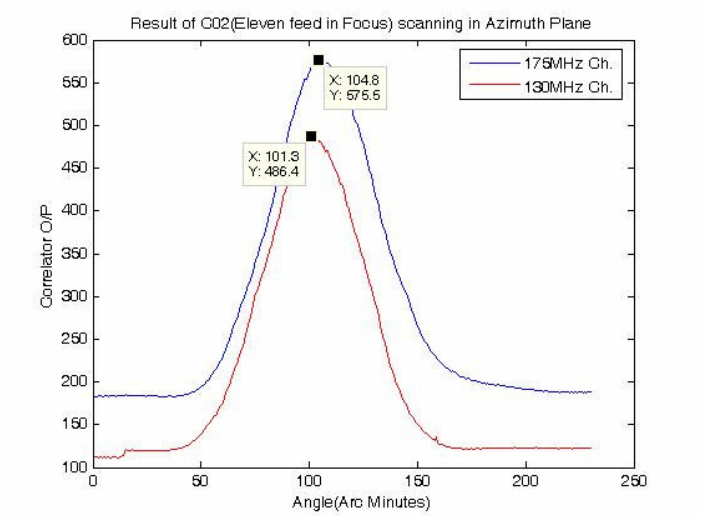

Fig. 7.5 Beam plot of (C02 + Eleven feed) scanning in azimuth plane.

The HPBWs are: 47 arcmin for130 MHz channel

49 arcmin for 175 MHz channel

6.5.4 Deflection measurement at antenna base:

When the feed was installed on the C02 antenna of GMRT, the signal was received and observed on spectrum analyzer. The antenna was pointed to a radio source Virgo and readings were taken for the power output when antenna was pointing towards the source (ON source) and when antenna was pointing towards clear sky (OFF source). The deflection (On source power –OFF source power) was measured. The spectrum analyzer plots are attached in Appendix C.

CHAPTER EIGHT

Design of 700 MHz Coaxial Waveguide Feed

In this chapter the historical development of coaxial waveguide feed will be discussed as well as the previous work done on it will be reviewed. The basic concepts in radiation from a coaxial waveguide will be developed. Then the actual design and testing of the 700 MHz coaxial waveguide feed will be explained. A compensated balun is also designed in order to excite a TE_{11} mode in the coaxial waveguide. Details of its design and testing will also be discussed before concluding the chapter.

8.1 Need for a 700 MHz Feed:

The feed is intended to be used with a parabolic reflector of 15 m diameter, which is to be operated as a small radio telescope as a lab facility for the students in NCRA (National Centre for Radio Astrophysics –TIFR), Pune.

A feed working at 1420 MHz is already in use for another reflector of 4.5m diameter, which is presently being used as a lab facility for the radio astronomy students. A feed working at a lower frequency was required in order to study pulsars which are bright at lower frequencies. Also, to have a reasonably high gain of the reflector, the frequency was not to be too low. So 700 MHz was chosen to be the frequency of operation.

8.2 History and previous work done in coaxial waveguide feeds:

Coaxial waveguides had not found much attention to be used as primary feeds for parabolic reflectors until Koch [26] studied the possibility of generating sector-shaped patterns using multiple coaxial radiating waveguide rings. The geometries considered consisted of a central circular waveguide surrounded by one or more coaxial rings, which were excited through slots on the wall of the waveguide. His analysis of the radiation pattern was based on the Kirchoff-Huygens principle and results in good agreement with experiment were obtained, provided the aperture dimensions were not too small. The experimentally optimized feeds provided good pattern symmetry and excellent reflector efficiencies. However, the geometries considered were too complex and the radiation was due to a combination of circular and coaxial waveguides.

Kraus and Profera [28] studied the radiation characteristics of a TE_{11} mode excited coaxial waveguide. They used a modal expansion method to determine the waveguide aperture field and used Kirchoff-Huygens principle for obtaining the radiation field. Their analysis indicated that the co-polar patterns of a coaxial waveguide lack the desired azimuthal symmetry. To improve the pattern symmetry, they used a loading circular iris on the waveguide aperture. The aperture field was again determined by the modal expansion method. This method is satisfactory for determining the radiation field of large apertures but is inadequate for coaxial waveguides because their aperture sizes are generally small. Also, the currents induced on the waveguide outer surface are significant and affect the radiation field considerably.

James [31] treated both corrugated as well as coaxial waveguides using modal expansion method. The radiation field data for smooth wall coaxial waveguide was obtained using the geometrical theory of diffraction, which provides more accurate results. However, the outer wall thickness was assumed to be 0.5 λ which is too large and it affects the radiation field, in particular, the cross-polar radiation.

Livingston [8] provided the design curves for a coaxial waveguide. They provide the 10 dB beamwidth in both E- and H-plane of a coaxial cavity as a function of the cut-off frequency for the TE_{11} mode. The curves are based on a compilation of empirical data measured on a number of different coaxial cavities, all with a 2 to 1 outer to inner conductor diameter ratio.

Shafai and Kishk [24] used a numerical method. They determined the currents on the conducting walls of the waveguide by a numerical solution of certain integral equations. These computed currents were then utilized to evaluate the radiation fields. They also showed that the radiation field of a coaxial waveguide has high side and back lobe levels which can be reduced by using quarter wavelength chokes on the waveguide wall. The chokes also reduce the surface current on the outer walls of the waveguide which causes oscillations in the radiation pattern.

Bird [27] analyzed the coaxial waveguides wherein the center conductor was in general of infinite extent. Solutions for mutual admittance and radiated fields were obtained for all asymptotic modes.

On the foundation of the literature that is discussed, some characteristics of radiation from coaxial feeds are discussed in the next section.

8.3 Radiation from Coaxial waveguide feeds:

Coaxial waveguide feeds are generally used for narrowband applications as well as for applications where multifrequency capability is desired. [8] When operated in TE_{11} mode, coaxial feeds can produce high aperture efficiency and near optimum radiation patterns.

By incorporation of quarter-wavelength chokes (on the outer surface of the outer conductor), radiation pattern symmetry (and hence low cross-pol level) is obtained. Since a coaxial waveguide has two conductor radii, a variety of radiation patterns can be obtained simply by selecting different aperture dimensions. In particular, a satisfactory pattern symmetry can be found by selecting proper conductor radii and without the need for a corrugated wall or flange. For any given ratio of conductor radii, an outer conductor radius can be found to equalize the E- and H-plane pattern. [24] Pattern symmetry is an important requirement for a feed, because it lowers the cross-polarization. This requirement can be fulfilled by a coaxial feed.

Because of the absence of corrugations, the feed diameter remains small and hence reduces the aperture blockage. This helps to improve the aperture efficiency of the reflector.

As was stated in chapter 5, the optimum feed aperture distribution so as to obtain 100% reflector aperture efficiency is sin u /u type distribution. Koch [26] showed that this type of aperture distribution is possible to obtain in coaxial feeds.

Livingston [8] gives the method to excite TE_{11} mode in a coaxial waveguide. The TE_{11} mode is excited by balanced probes fed in phase opposition. As long as there is no

phase or amplitude imbalance between probes, complete mode symmetry is obtained at the feed aperture. This method of excitation is shown in the following figure.

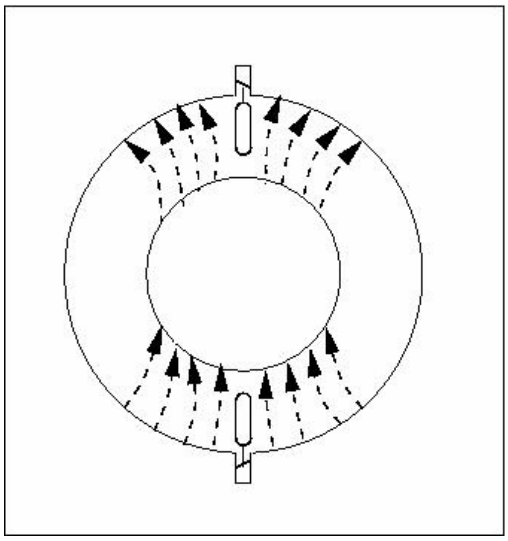

Fig. 8.1 Method of exciting TE_{11} mode in a coaxial waveguide [8]

Livingston [8] also gives the calculated characteristic impedance of a coaxial waveguide (for outer-to-inner conductor diameter ratio as 2:1) as well as the mismatch to free space at the cavity aperture as a function of TE_{11} mode cut-off frequency. The characteristic impedance is relatively constant over the region from 1.15 f_c to 1.85 f_c, varying from 75 to 100 ohms. The mean values of both characteristic impedance and free space mismatch occur between 1.4 and 1.5 times the cut-off frequency. Thus maximum bandwidth would be expected for an operating band centered in this region. However, the free-space mismatch is quite high, varying from 3.5:1 to 5:1. Thus, although it is relatively simple to match the input transmission line to the cavity, matching the cavity to the free space is considerably more difficult. Making the cavity very long is one way to match the system with the free space, but it is undesirable in many applications to have a long feed (because of the aperture blockage).

Bird [27] investigated the coaxial waveguide feeds for the aperture (free-space) mismatch and suggested means for reducing it by extending the centre conductor beyond the aperture plane.

With the background of the literature discussed above, the design of the 700 MHz coaxial waveguide feed was carried out.

8.4 Design of the 700 MHz feed:

The specifications provided for the feed are:

1. The reflector F/D ratio: 0.4

2. Frequency of operation: 700 MHz

3. Bandwidth: 100 MHz.

The feed has to be dual polarized.

From the reflector F/D ratio, we can fine out the semi-rim angle of the reflector from eqn. 4.15.

$$\theta = 2\tan^{-1}(1/4(F/D))$$

for F/D = 0.4,

$$\theta = 64^0 \qquad (8.1)$$

as we saw in chapter 5, for optimum aperture efficiency of the reflector, the edge illumination should be -11dB. Fig. 5.3 gives the feed's 3 dB and 10 dB beamwidths so as to achieve -11 dB edge illumination of the reflector.

The desired 10 dB beamwidth (half-angle) is thus $\mathbf{62^0}$

From this 10 dB beamwidth, a/b ratio is to be determined.

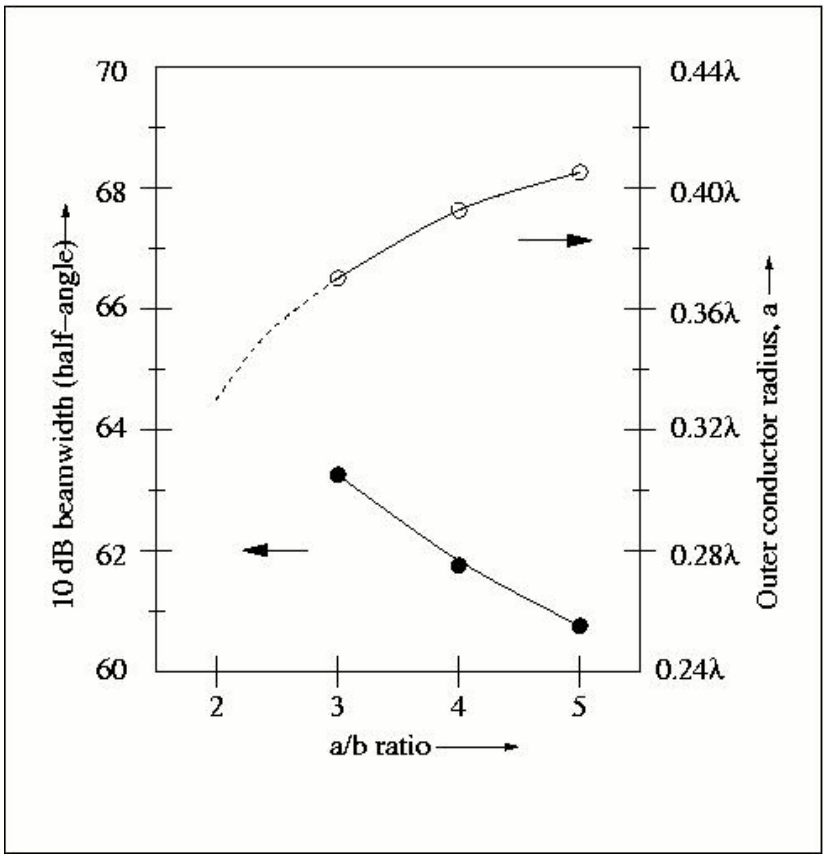

Fig. 8.2 10 dB beamwidths and outer conductor radii as functions of a/b ratio. [25]

The figure shows the 10 dB beamwidth obtained for different a/b ratios. It also gives the outer conductor radius to achieve the 10 dB beamwidth.

To achieve this 10-dB beamwidth of 62^0, the outer-to inner conductor diameter ratio (a/b) was chosen as **3.75.**

The geometry was then simulated in the antenna designing software Concerto. The outer conductor radius was then optimized to be 150mm. With a/b ratio as 3.75, the inner conductor radius came out to be 40mm.

The dimensions of the feed are:

Outer conductor radius: 150mm

Inner conductor radius: 40mm

Length of the feed: 420mm

Length of the chokes: 105mm

First, two prototypes were fabricated, one with the above mentioned dimensions and one with the dimensions manually determined. To reduce surface currents and to achieve a symmetrical radiation pattern, quarter-wavelength chokes were incorporated. The prototypes were tested in terms of their return loss.

The aim of fabricating these prototypes was to decide the position of the excitation probes to excite the feed, so as to have minimum return loss. Depending on the return loss of both the feeds when excited at different positions, the feed with above mentioned dimensions was finalized with the position of excitation probes at 176 mm from the rear end.

The feed was then fabricated. Yet the probe dimensions were not determined. After trying different combinations, final probe dimensions were determined as we will see in the following section.

The detailed geometry of the feed, the position and geometry of the probes are attached. Also, the S11 (return loss) of the feed is attached.

The testing of the feed is discussed in detail in section 8.6.

8.5 Designing a Balun for the coaxial waveguide feed:

As mentioned above, the excitation so as to have TE_{11} mode in the coaxial feed has to be balanced (equal in magnitude but opposite in phase). But the transmission line that is usually used is coaxial line, which is unbalanced one. Hence a balanced-to-unbalanced transformer (balun) is needed.

The compensated balun (also known as Roberts balun) was selected because it is wideband, easy to implement and has low loss.

8.5.1 The compensated wide-band balun:

This type of balun, which was first described by Marchand and later reinvented by Roberts, is known to have a wide bandwidth. The wide bandwidth is obtained by the use of a quarter-wave transmission line section which is placed inside one of the balanced arms, thereby minimizing the over-all physical length.

A schematic diagram of the balun is shown in figure 8.3. Also shown is the equivalent circuit of the balun.

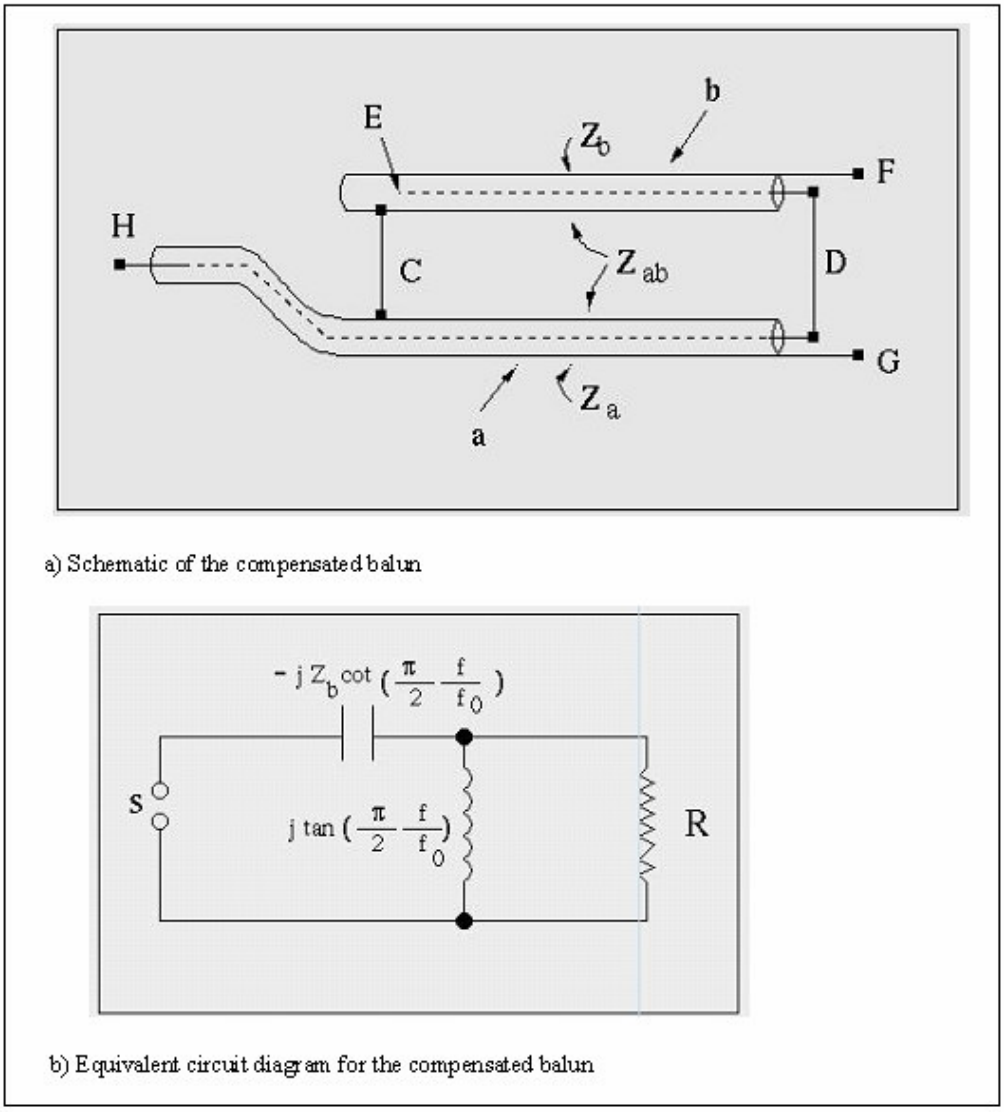

Fig. 8.3 The compensated balun [29], [30]

The device is composed of two lengths of coaxial transmission line, a and b, suitably connected. The symbols Z_a and Z_b represent the characteristic impedance of lines a and b, respectively, considering the waves propagated within each line. Z_{ab} is the characteristic impedance of the balanced transmission line ab, composed of the outer conductors of transmission lines a and b. the coaxial terminal H is the connection for the external unbalanced source (or load). The terminals F and G are the points of attachment of the balanced load (or source). Centre conductors of a and b are connected at D, while outer conductors are connected at C. the centre conductor of line b ends at E.

Figure 8.4 shows the equivalent circuit of the balun for the purpose of studying the impedance.

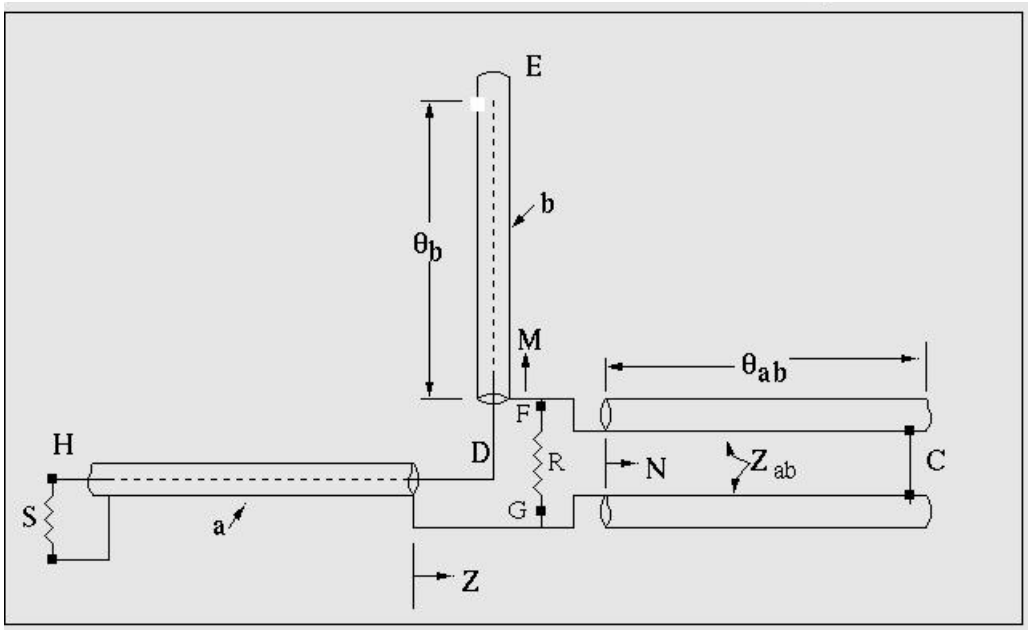

Fig. 8.4 The equivalent circuit of the compensated balun showing different impedances [29]

The terminals F, G and H are the same as in the previous figure. S and R are the external impedances which may be connected to the balun. M is the impedance looking into coaxial line b toward the open circuit at E N is the impedance looking from FG along

the open transmission line ab toward the short-circuit at C. If the transmission losses are neglected,

$$M = -j\, Z_b \cot \theta_b$$

$$N = j\, Z_{ab} \tan \theta_{ab} \qquad (8.2)$$

Where θ_b and θ_{ab} are the electrical lengths of transmission lines b and ab.

Let the electrical lengths of line segments b and ab be equal, making $\theta_b = \theta_{ab} = \theta$ and let characteristic impedance $Z_{ab} = R$ and $Z_a = Z_b = S$. Then

$$Z = R \sin^2 \theta + j (\cot \theta) (R \sin^2 \theta - S) \qquad (8.3)$$

The reactive component of the impedance is zero when $\cot \theta = 0$, (for which Z equals R) and also when $\sin^2 \theta = S/R$ (for which Z becomes S). Following figure is the sketch of the variation of resistance and reactance in the neighbourhood of the lowest-frequency band of interest. The physical lengths being fixed, θ varies directly with frequency.

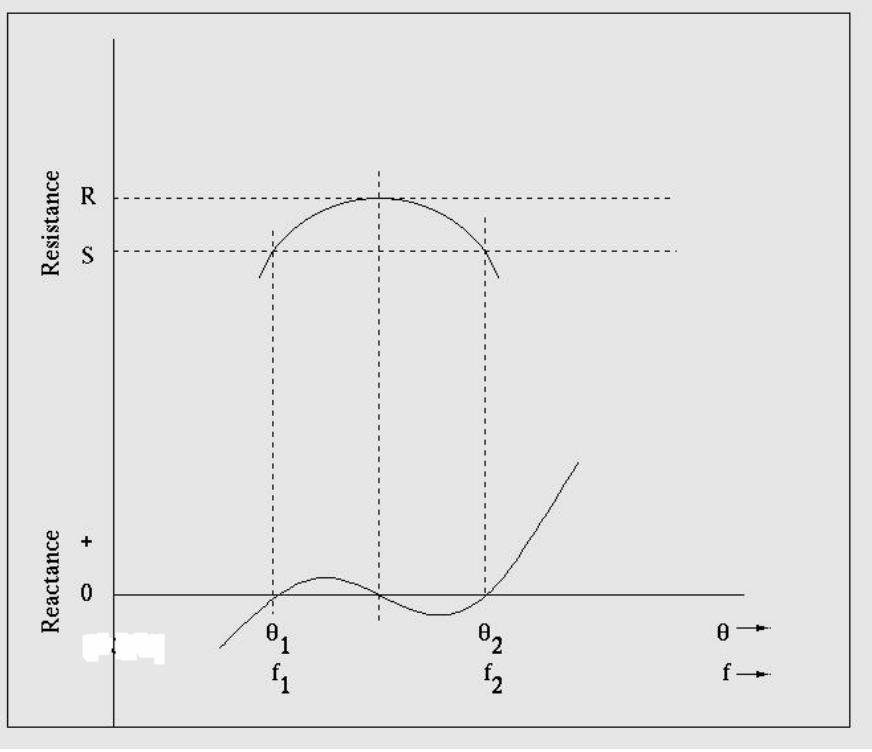

Fig. 8.5 The input resistance and reactance at the point Z of Fig. 8.4 [29]

The region $\theta_2 - \theta_1$ locates a frequency band $f_2 - f_1$ over which the balun has impedance matching characteristics of a desirable nature. cot θ marks the centre of the band and corresponds to an electrical length of 90^0.

Thus the balun serves to transform from a resistance R to a resistance S with a perfect impedance match at frequencies f_1 and f_2. There is an approximate match in the band of frequencies within this interval and also at frequencies somewhat outside. The midband standing wave ratio increases with the ratio of R/s, hence the balun is particularly interesting for balanced to unbalanced transformations where the desired impedance transformation ratio is low.

8.5.2 Design of the Balun:

The specifications for the balun are:

S= 50 Ω, R = 70 Ω.

$Z_b = Z_a = 50\ \Omega$, $Z_{ab} = 70\ \Omega$

The value 70 Ω for the parallel- wire transmission line impedance was chosen because it offers low loss.

The designing of the balun involves determining the dimensions of the two-wire transmission line (having impedance Z_{ab}) as well as those of the coaxial lines a and b (having impedance $Z_a = Z_b$)

To obtain $Z_{ab} = 70\ \Omega$, we have the characteristic impedance of a two-wire balanced transmission line as [32]

$Z_{ab} = 120 \cosh^{-1} (D/d)$

Where D is the spacing between the two wires and d is the individual wire diameter.

For Z_{ab} =70,

(D/d) = cosh (70 / 120)

= 1.175

The suitable available copper tubes are having the external diameter of 16mm.

Therefore, d = 16 mm.

Hence, D = 18.8 mm.

For $Z_a = Z_b = 50\ \Omega$, we have

Characteristic impedance of the coaxial line [10]

$Z_0 = (138/\sqrt{\varepsilon}) \log_{10} (D/d)$

Where D is the outer conductor diameter and d is the inner conductor diameter.

So for $Z_0 = 50\ \Omega$ and air as the dielectric (ε =1),

D/d = 2.303.

Here, the outer conductor diameter is the inner diameter of the copper tube used for the parallel-wire transmission line, which is 12.5 mm.

Hence the inner conductor diameter comes out to be 5.427mm.

At 700 MHz, λ = 428.57 mm

So the length of the quarter-wavelength long line segment (which is hosted inside one of the two arms of the balanced line) is

l = (428.57)/4 = 107.1 mm.

The cut-off frequencies (f_1 and f_2) are calculated as follows:

As shown in Fig. 8.4, the balun offers a perfect impedance match at frequencies for which

$$\sin^2 \theta = S/R \quad (8.4)$$

$$= 50/70$$

$$\theta = 58^0, 122^0$$

Now, the physical lengths of the transmission lines, as seen from Fig. 8.3 are λ /4, i.e. 107.1 mm, where λ is the wavelength at 700 MHz.

The electrical length θ is defined as

$$\theta = 360^0 \text{ x } (l / \lambda) \quad (8.5)$$

$$= 360^0 \text{ x } (l / c) \text{ x } f$$

Hence,

$$\theta_1 = 360^0 \text{ x } (l / c) \text{ x } f_1 \quad (8.5)$$

$$\theta_2 = 360^0 \text{ x } (l / c) \text{ x } f_2 \quad (8.6)$$

Putting $\theta_1 = 58^0$ and $\theta_2 = 122^0$ in (8.5) and (8.6) respectively,

We get

$$f_1 = 451.11 \text{ MHz} \quad (8.7)$$

$$f_2 = 949.27 \text{ MHz} \quad (8.8)$$

These are the frequencies over which the balun will provide the impedance match, with a perfect match at frequencies f_1 and f_2. the centre frequency is 700 MHz.

A detailed drawing of the balun is attached.

A shorting plate is involved. It serves to short the two-wire transmission line. The shorting point is denoted as C in the above figures. This shorting point is kept movable so as to have a chance to optimize the return loss (have optimum impedance match).

8.6 Testing of the 700 MHz feed:

In this section we will see in detail the procedure of determining the final dimensions of the feed as well as the position and dimensions of exciting probes for the feed.

8.6.1 Testing of the prototypes:

Two prototypes were fabricated, one having the dimensions determined by simulation and one having the dimensions determined manually. These prototypes are shown in the following photographs.

Fig 8.6 The two prototypes of the 700 MHz coaxial feed

As shown in the Fig. 8.6, various holes were made on the feeds to fit the probes at various positions. The distance between adjacent holes is 2.5 cm. Up to 22.5 cm from the rear end, such holes were made.

The setup for measuring the return loss is as shown in the figure below. Note that the probes are fitted inside the feed. They are shown just for the sake of understanding the geometry.

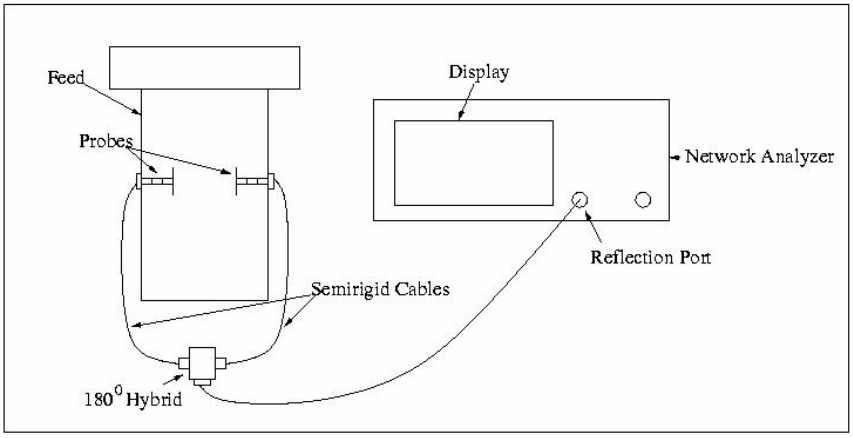

Fig. 8.7 Set up for measuring return loss of the feed

The probe used to excite the coaxial feed consists of a rod and a disc. While testing these first prototypes, brass rods, each of 15mm length, 10mm in diameter and threaded at the ends (so as to fit in one another) were made. Also, aluminum discs of different diameters were made. They are as shown in the following figure.

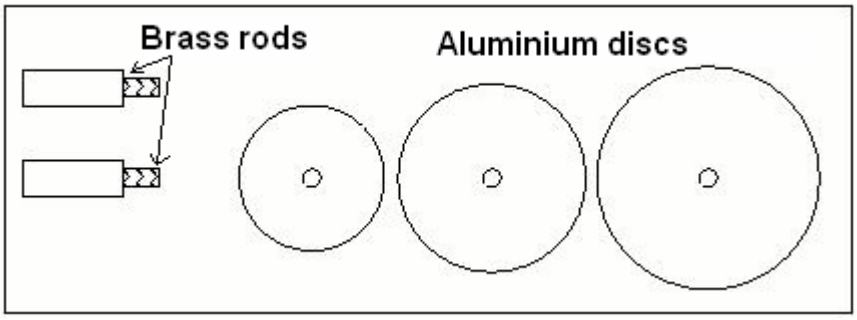

Fig. 8.8 Rods and discs to make probes of different sizes.

Return loss of both these feeds was measured by fixing the probes in each pair of the holes, as well as by changing the length of the probe (by changing the number of brass rod pieces).

To excite TE_{11} mode in a coaxial feed, it is required that the probes should be excited with voltages equal in magnitude but opposite in phase (180^0 out of phase). Usually, a balun (balanced to unbalanced transformer) is used for this purpose. While testing these prototypes, instead of a balun, a 180^0 hybrid was used. This component splits the input into two outputs, with equal amplitudes but having 180^0 phase shift between each other.

It was observed that the prototype with above mentioned dimensions (P2 in the above photograph) gives the minimum return loss, when fed at 176 mm from its rear end. Hence, a final feed was fabricated, with the same dimensions as P2 and having a facility to fit the probes at 176 mm from its rear end.

8.6.2 Testing of the finalized feed:

As mentioned in the specifications above, the feed has to be dual polarized. So two orthogonal pairs of probes are needed (one pair for each polarization). Hence provision is made on the feed to fix two orthogonal pairs of probes.

The dimensions of the probes were not yet finalized. 4 pairs of rods of 10mm diameter and of different lengths and 3 pairs of discs of different diameters were prepared. Return loss of the feed was optimized by testing with different combinations of rods and discs. The best response was observed when a pair of discs 100 mm in diameter and rods of 30 mm of length were used. Hence these dimensions were finalized and two

pairs of probes where the rod and disc are welded (so as to have better and robust connection) were fabricated.

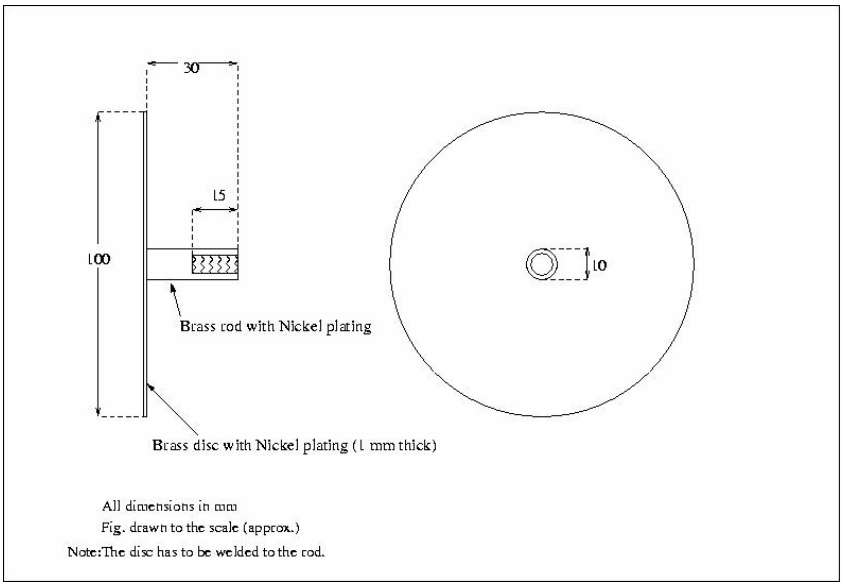

Fig. 8.9 Probe for the coaxial feed with optimized dimensions

8.6.3 Testing of the feed with the Balun:

The fabricated balun was connected to the 700 MHz coaxial waveguide feed and the combination was tested for the return loss.

The balun had to be "tuned" in order to have an optimum return loss. Tuning involves adjusting the position of the shorting plate as well as adjusting the position of the dielectric (Teflon) spacers.

Also, the balun was tested for its return loss with terminating its balanced end with a 50 Ω chip resistor.

The results of testing the feed with the balun and the hybrid are attached in Appendix A.

CHAPTER NINE
Conclusion and Future Work

The aim of this M. Tech. project was to design, fabricate and characterize a feed working at 700 MHz as well as to characterize the 550-900 MHz CSIRO feed and the 200-800 MHz Eleven feed.

The aim has been achieved with significant success. The 700 MHz feed has been successfully designed, fabricated and tested. Its return loss is acceptable for a feed to work in radio astronomy. The baluns for this feed are also designed, fabricated and tested.

The 550-900 MHz CSIRO feed has been characterized in terms of its return loss, HPBW with GMRT antenna and sensitivity. The LNAs used with this feed are characterized in terms of their 1 dB compression point and third order intercept point.

The 200-800 MHz feed has been characterized in terms of its return loss and HPBW with GMRT antenna. The LNAs used with the feed are tested for their gain and phase characteristics.

Future Work:

The 700 MHz feed has to be integrated with the LNAs and rest of the receiver. It has to be installed on the 15m parabolic dish in NCRA, Pune. Tests such as cross-polarization characteristics are to be carried out. Its radiation pattern is yet to be measured.

The eleven feed has to be characterized in terms of its polarization characteristics, sensitivity of GMRT antenna with it. Its radiation pattern has to be measured.

The 550-900 MHz CSIRO feed's second prototype has to be installed on the GMRT antenna and it has to be characterized as was done with the first prototype. The radiation patterns are also to be measured.

REFERENCES

1. John. D. Kraus. 'Radio astronomy', McGraw-Hill Book Company, 1986.

2. Constantine A. Balanis, 'Antenna Theory, analysis and design', Second edition, John Wiley & Sons, Inc., 1982.

3. Warren L. Stutzman, Gary A. Thiele, 'Antenna Theory and Design', Second Edition, John Wiley & sons, Inc., 1998.

4. Lamont V. Blake, 'Antennas', John Wiley & sons, Inc.,1966.

5. A. Praveen Kumar, "GMRT Receivers" ,

   A. P. Rao,"Interferometry and Aperture Synthesis",

   Jayaram Chengalur , "Two Element Interferometers",

   in 'Low Frequency Radio Astronomy' , Third Edition, NCRA-TIFR, edited by Jayaram N. Chengalur, Yashwant Gupta, K. S. Dwarkanath.,2007.

6. A. D. Olver, P.J.B. Clarricoats, A.A. Kishk, L. Shafai, 'Microwave Horns and Feeds', IEE Electromagnetic Waves Series.,1994.

7. G.Sankar, "GMRT Antennas and Feeds" in 'Low Frequency Radio Astronomy', Third Edition, NCRA-TIFR, edited by Jayaram N. Chengalur, Yashwant Gupta, K. S. Dwarkanath.,2007.

8. Marvin L. Livingston, "Multifrequency Coaxial Cavity Apex Feeds", *Microwave Journal, Oct 1979.*

9. Christophe Granet and Graeme L. James, "Design of Corrugated Horns: A Primer", *Antenna Designer's Notebook, Tom Miligan*

10. A. D. Olver, "Corrugated Horns", *Electronics and Communication Engineering Journal, February 1992.*

11. K. Raghavan, A. D. Olver, P. J. B. Clarricoats, "Compact Dual-Mode Dielectric-loaded Horn", *Electronics Letters, 9th October, 1986, Vol. 22, No. 21.*

12. F. F. Dubrovka, O. O. Krupnov, Ya. O. Rospopa, "Analysis of Partially Dielectric-loaded Coaxial Horn Antennas, *International Conference of Antenna Theory and Techniques,* September 2003.

13. Milligan, T. A. 'Modern antenna design', Wiley- IEEE press, 2005.

14. Olsson R., Kildal P.S., Weinreb S., "The Eleven Antenna: A Compact Low-Profile Decade Bandwidth Dual Polarized Feed for Reflector Antennas", *IEEE Transactions on Antennas and Propagation, Vol. 54, No. 2, February 2006.*

15. Shimizu, J. K., "Octave Bandwidth Feed horn for Paraboloid", *IEEE Transactions on Antennas and Propagation, March 1961.*

16. Chen M. H, Tsandoulas G. N., Willwerth F.G., Modal Characteristics of Quadruple-Ridged Circular and Square Waveguides, "*IEEE Transactions on Microwave Theory and Techniques, Short Papers, August 1974.*

17. Samual Hopfer, "The Design of Ridged Waveguides", *IRE Transactions-Microwave Theory and Techniques, October1955.*

18. Stefen J. Skinner, Graeme L. Games, " Wideband Orthomode Transducers", *IEEE Transactions on Microwave Theory and Techniques, Vol. 39, No. 2, February 1991.*

19. Christophe Granet, Ian M. Davis, A. Ross Forsyth, Trevor S. Bird,' Design of a Prime-focus Dual-Band Feed for the GMRT, India: Final Report, 2005.

20. A. Praveen Kumar, Anil Raut, “Improvement of GMRT receiver for Better Dynamic Range”, Int. Tech. report, GMRT-TIFR.,2003

21. Yogesh B. Karandikar, ’Optimization of 200-800 MHz Eleven feed for GMRT.’ Master Thesis at Chalmers University of Technology, Sweden., 2006.

22. Graeme L. James, " Wideband Feed Systems for Radio Telescopes", 1992 IEEE MTT-S Digest.

23. Victor H. Rumsey, ‘Frequency Independent Antennas’, Academic Press, 1966.

24. Lotfollah Shafai, Ahmed A. Kishk, “Coaxial Waveguides as Primary Feeds for Reflector Antennas and Their Comparison with Circular Waveguides, *AEU, Band 39, Heft 1. (1985).*

25. G. Sankar, A. Praveenkumar, “Dual Frequency Coaxial Waveguide Feed- Design Calculations”, GMRT-TIFR., 1990

26. Gerhard F. Koch, “Coaxial Feeds for High Aperture Efficiency and Low Spillover of Paraboloidal Reflector Antennas”, *IEEE Transactions on Antennas and Propagation, Vol. AP-21, No.2, March 1973.*

27. Trevor S. Bird, Graeme L. James, Stefen J. Skinner, “Input Mismatch of TE_{11} mode Coaxial Waveguide Feeds”, *IEEE Transactions on Antennas and Propagation, Vol. AP-34, No. 8, August 1986.*

28. Lester A. Kraus, Charles E. Profera, “A Technique for Obtaining Pattern Symmetry and Low Sidelobes from a TE_{11} Mode Coaxial Radiator, *IEEE Transactions on Antennas and Propagation, May 1977, Succinct Papers.*

29. Willmar K. Roberts, “A new Wide-band Balun”, *Proceedings of the IRE, December 1957.*

30. Grorge Oltman, “The Compensated Balun”, *IEEE Transactions on Microwave Theory and Techniques, Vol. MTT-14, No. 3, March 1966.*

31. Graeme L. James, “Propagation and Radiation Properties of Corrugated Cylindrical Coaxial Waveguides”, *IEEE Transactions on Antennas and Propagation, Vol. AP-31, No.3, May 1983.*

32. Reference Data For Engineers.

33. www.gmrt.ncra.tifr.res.in

34. www.haystack.edu

35. www.ipac.caltech.edu

36. www.radio-electronics.com

APPENDIX A

SIMULATION AND TEST RESULTS FOR THE 700 MHz COAXIAL FEED

The 700 MHz Coaxial Feed

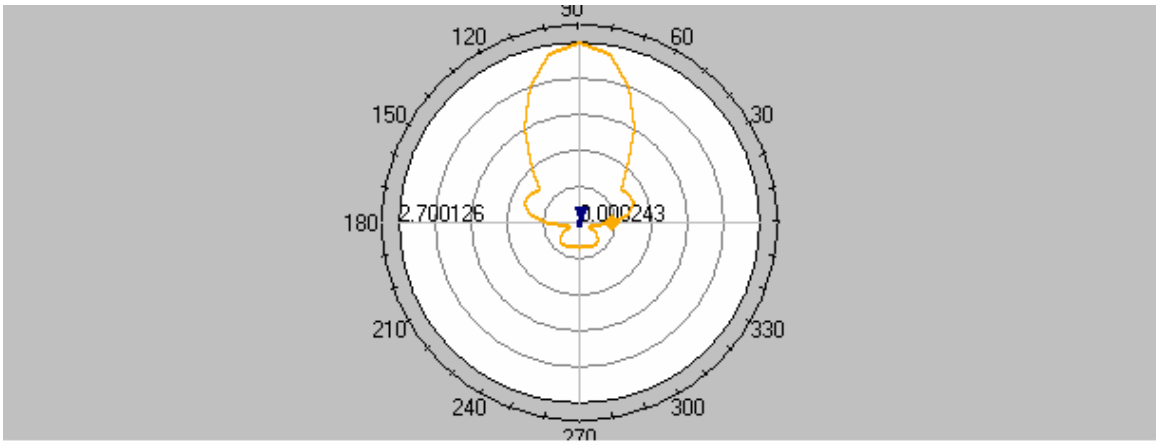

RADIATION PATTERN OF THE FEED(Displayed component =Ephi)

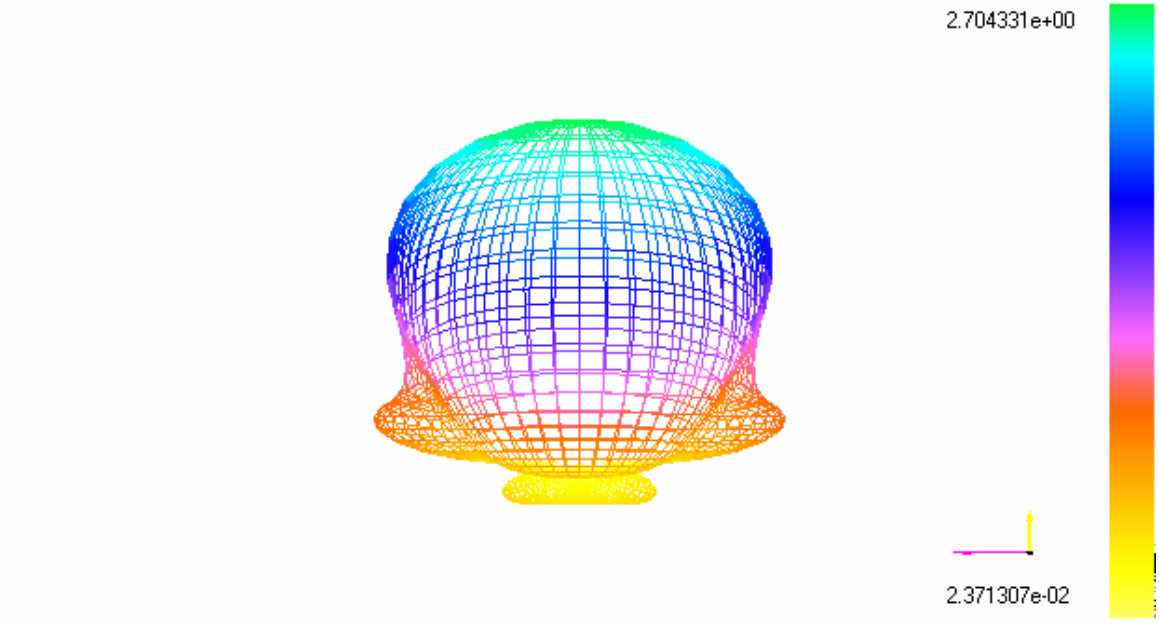

3D RADIATION PATTERN OF THE FEED(Viewed from X axis)

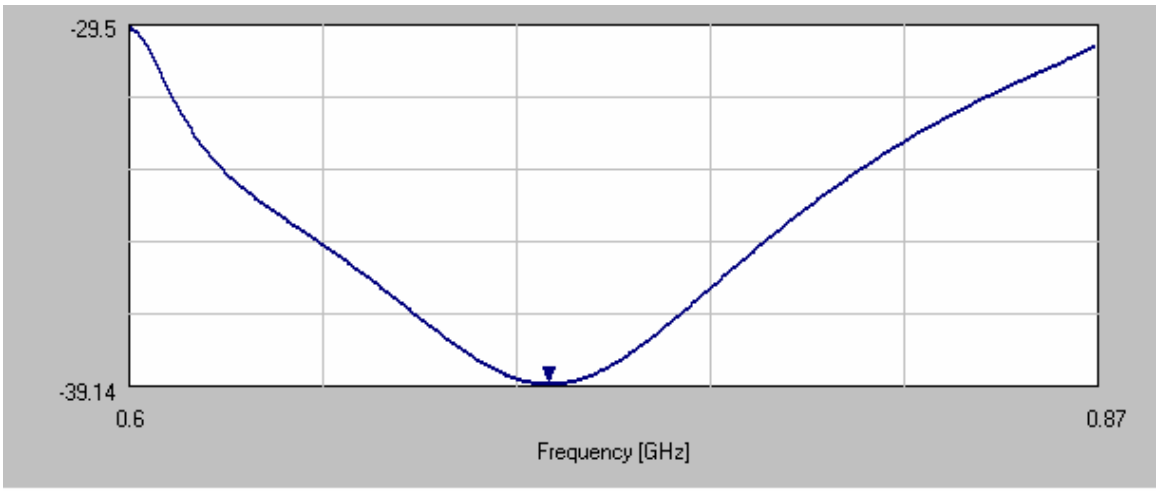

S11 OF THE FEED (Freq Pointed=717 MHz)

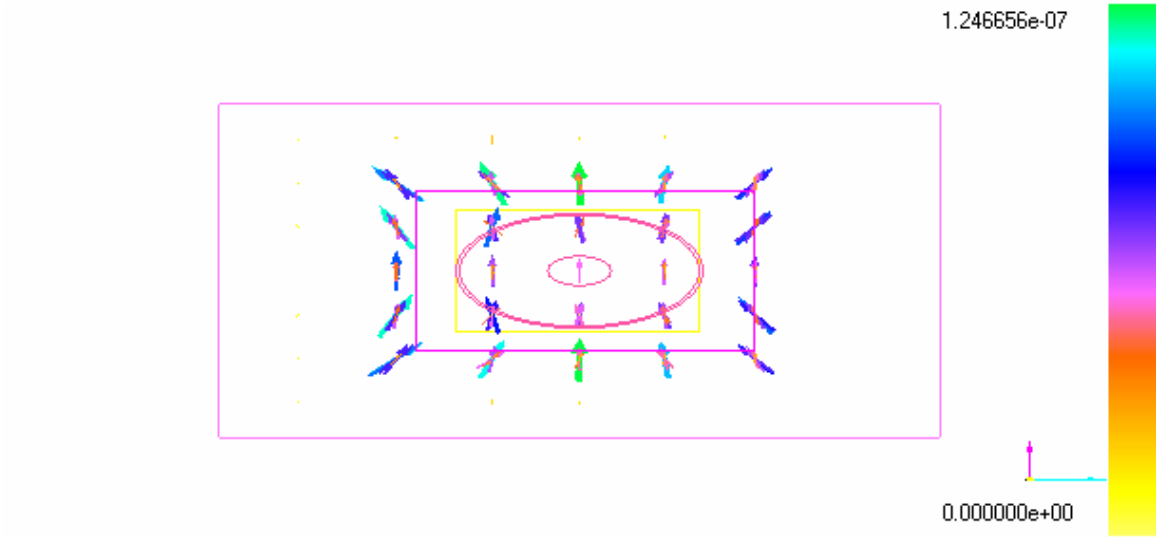

VECTORS REPRESENTING ELECTRIC FIELD DISTRIBUTION

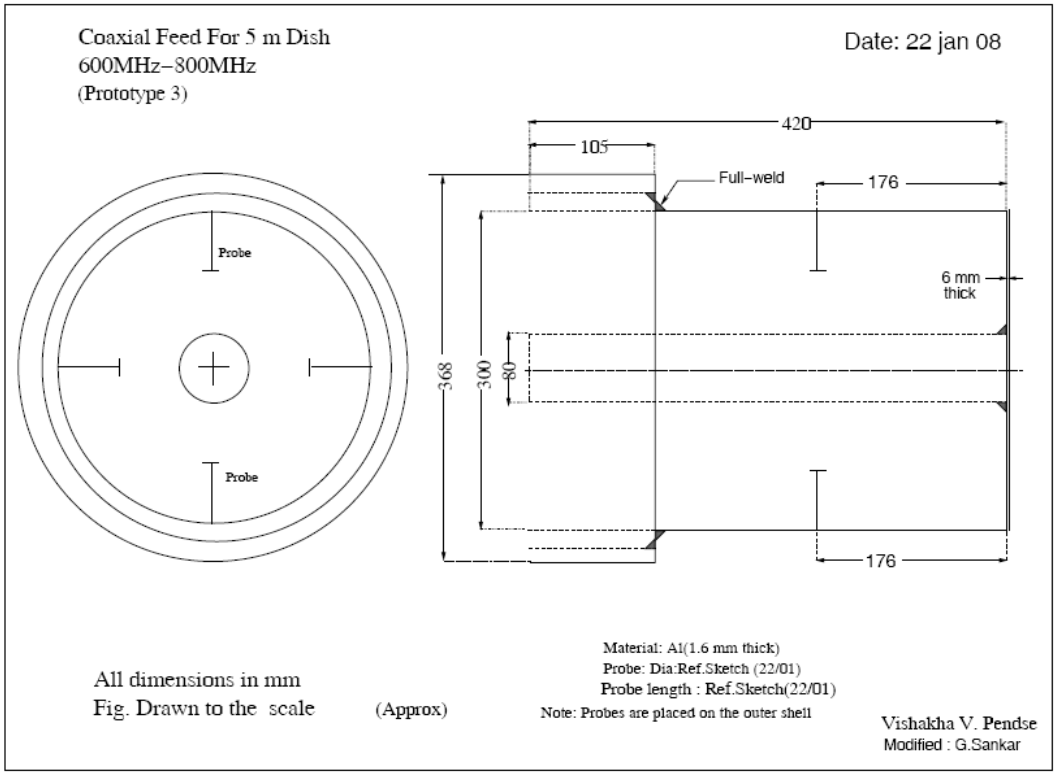

The drawing of the 700 MHz coaxial feed given to the workshop for fabrication.

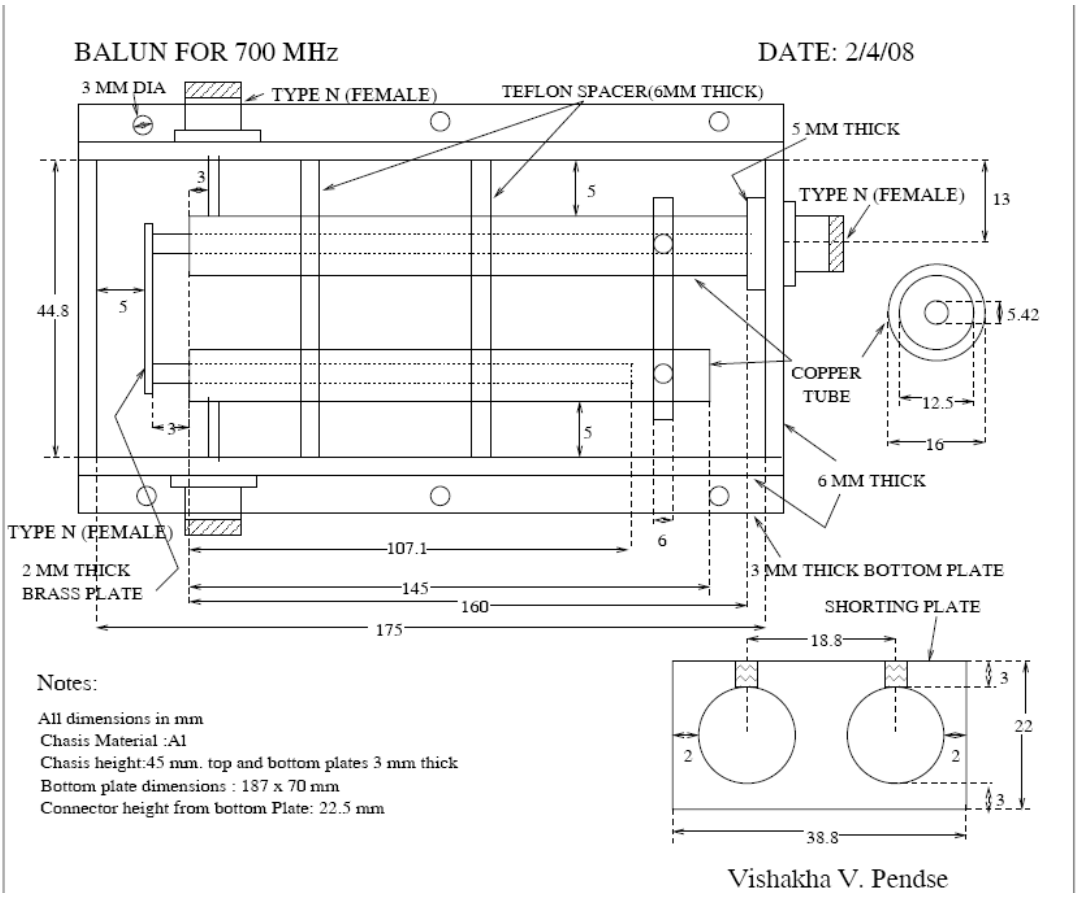

The drawing of the balun given to the workshop for fabrication.

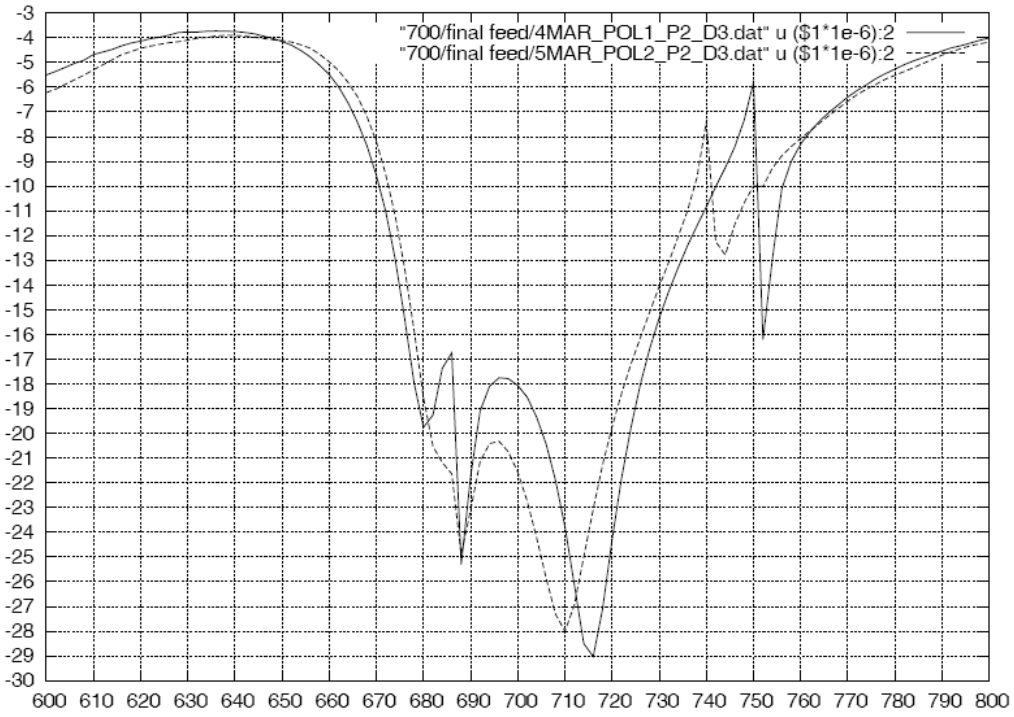

S11 (dB) vs frequency (MHz) of the 700 MHz coaxial feed with 180^0 hybrid for both polarizations.

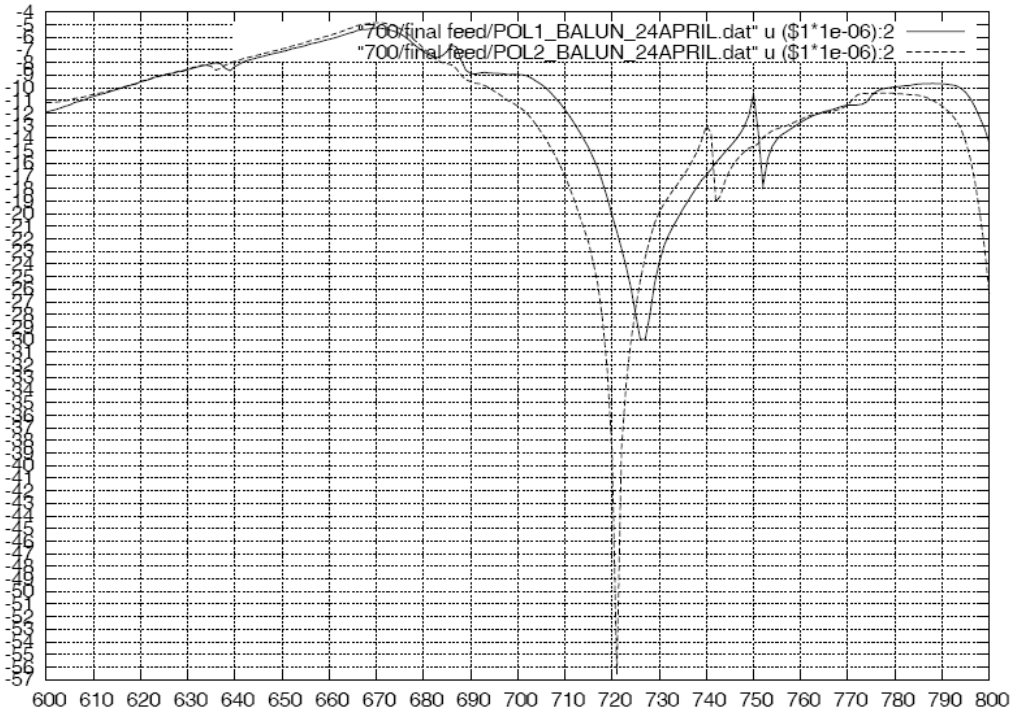

S11 (dB) vs frequency (MHz) of the 700 MHz coaxial feed with balun for both the polarizations.

APPENDIX B

TEST RESULTS FOR THE CSIRO 550-900 MHz FEED

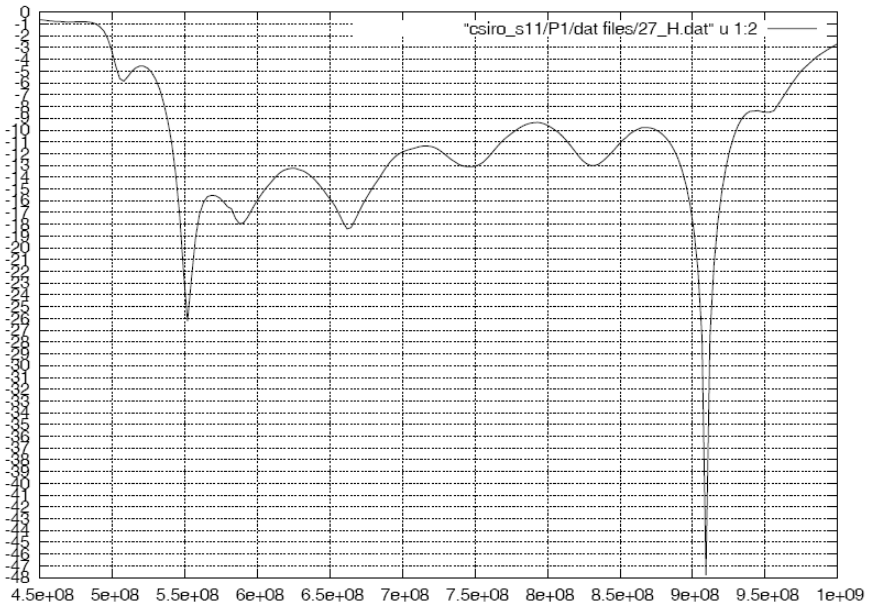

S11 (dB) vs frequency (Hz) of the prototype 1 of the CSIRO 550-900 MHz feed (polarization H)

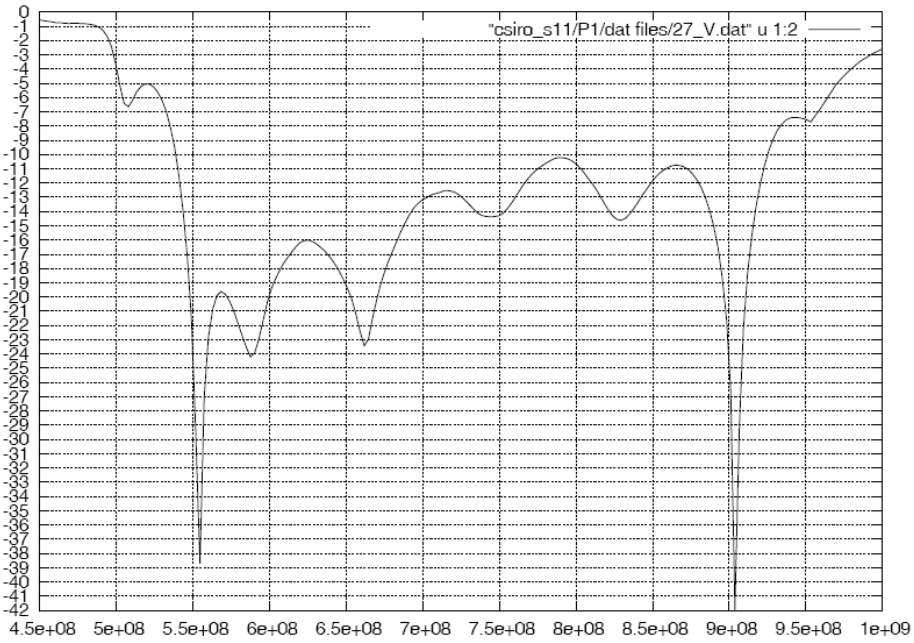

S11 (dB) vs frequency (Hz) of the prototype 1 of the CSIRO 550-900 MHz feed (polarization V)

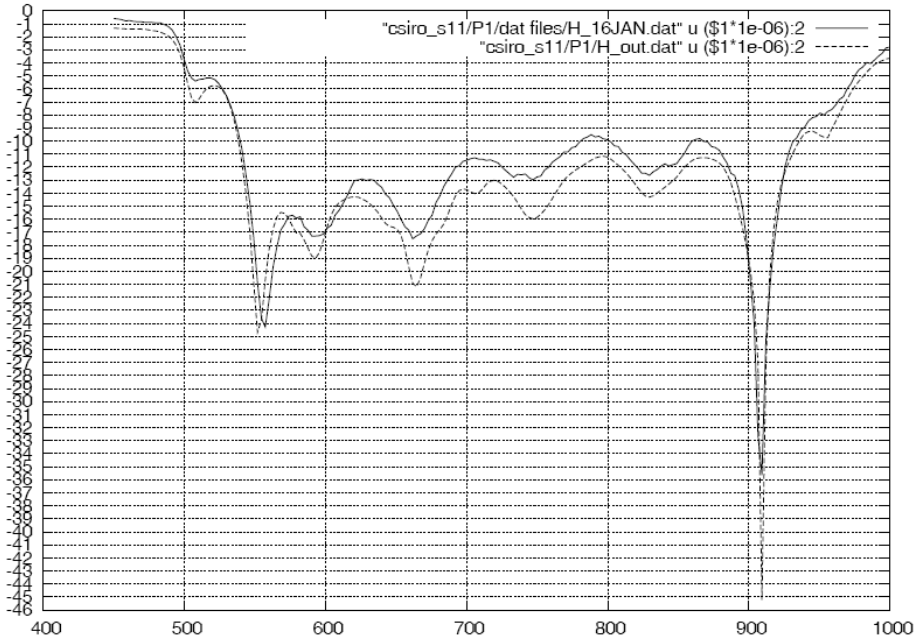

S11 (dB) vs frequency (MHz) of the prototype1 of the CSIRO 550-900 MHz feed (polarization H), with and without the outer low-frequency part.

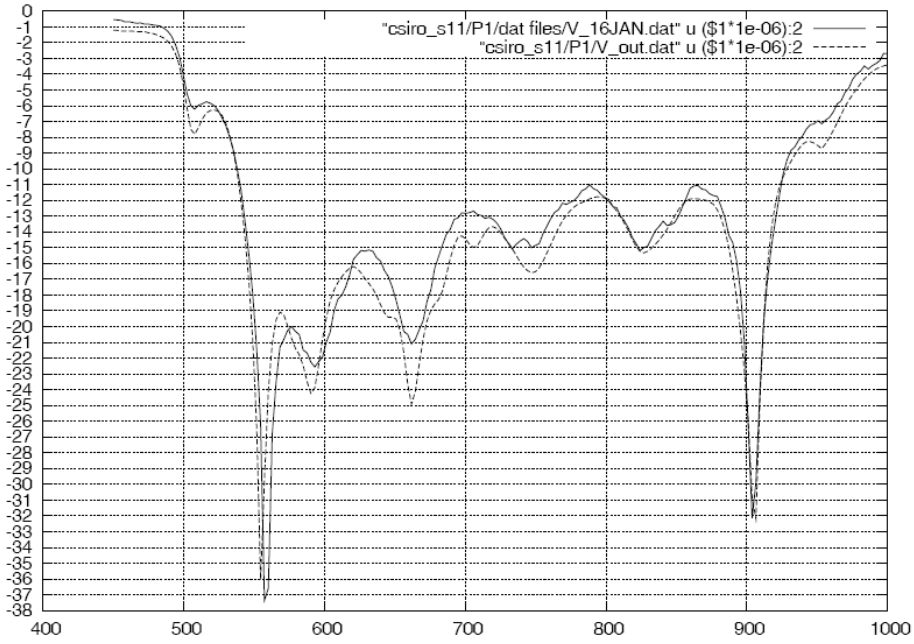

S11 (dB) vs frequency (MHz) of the prototype1 of the CSIRO 550-900 MHz feed (polarization V), with and without the outer low-frequency part.

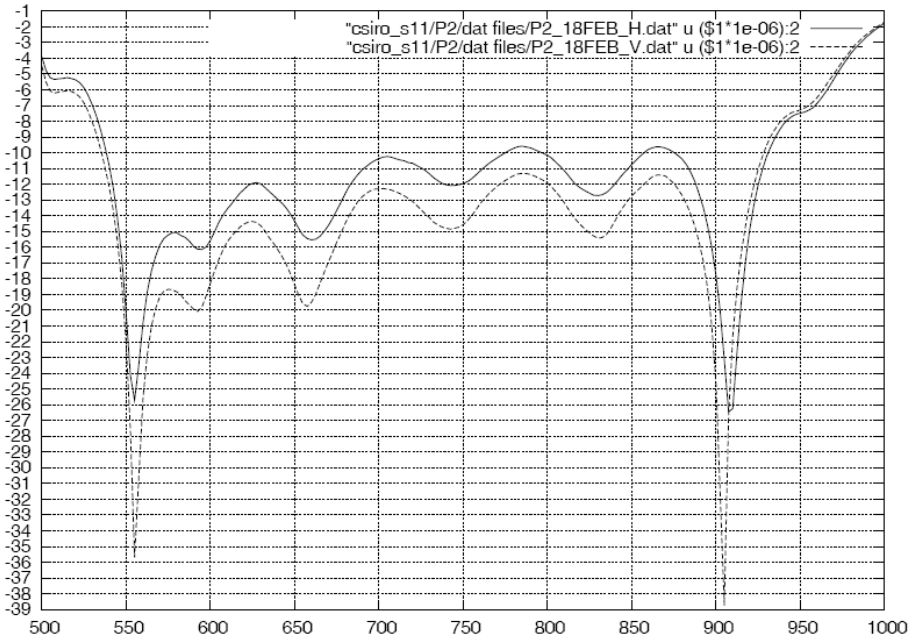

S11 (dB) vs frequency (MHz) of the CSIRO 550-900 MHz feed prototype 2 (Polarizations H and V)

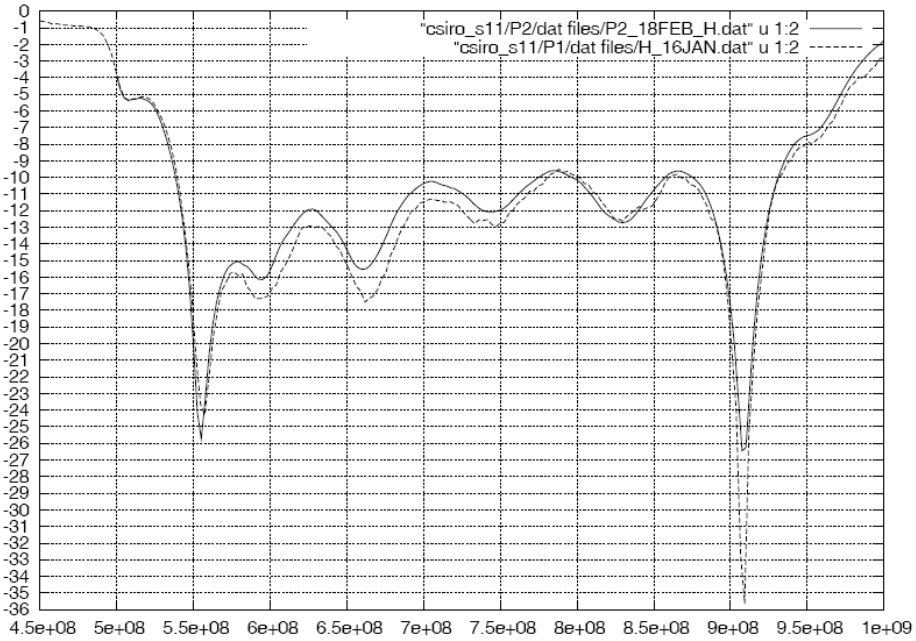

S11 (dB) vs frequency (Hz) of the two prototypes of the CSIRO 550-900 MHz feed (polarization H)

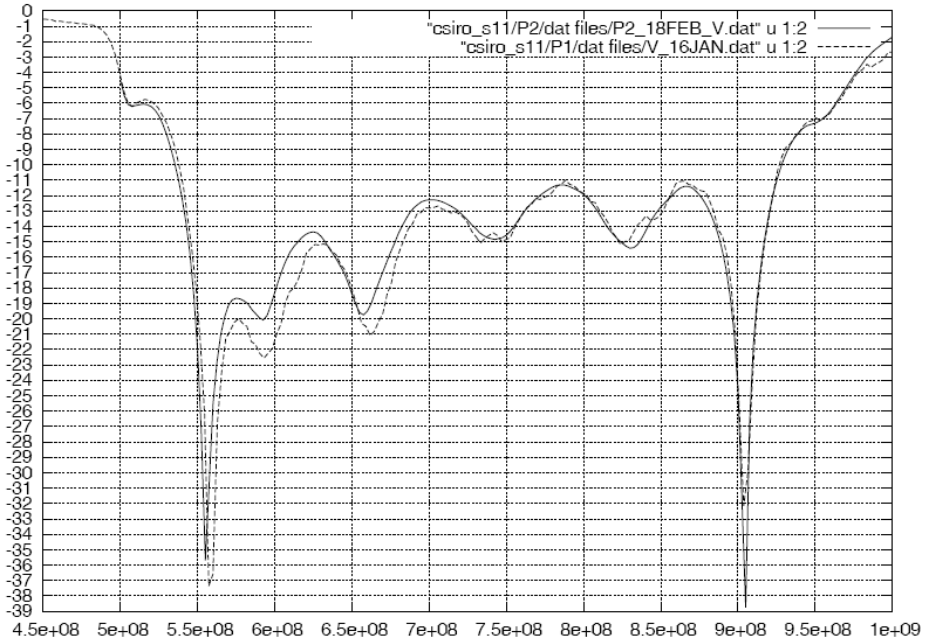

S11 (dB) vs frequency (Hz) of the two prototypes of the CSIRO 550-900 MHz feed (polarization V)

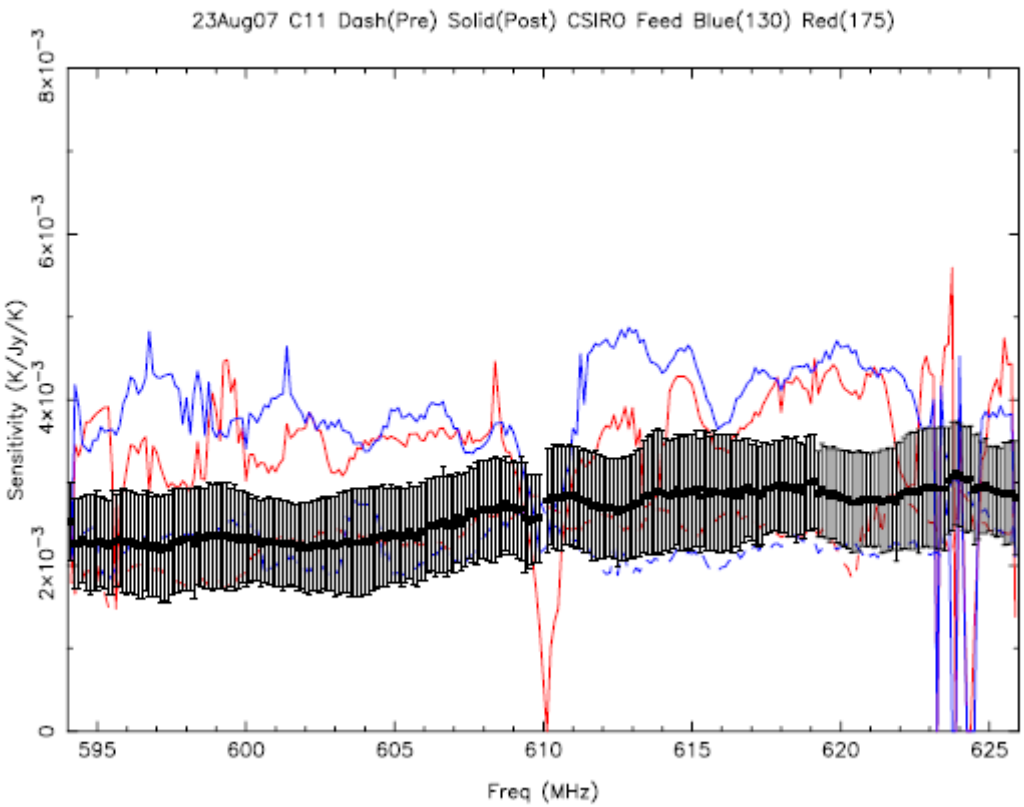

Sensitivity of the C11 antenna at 610 MHz before and after the feed was changed from the GMRT dual feed to the CSIRO feed. The sensitivity is defined as (Power ON-Power OFF)/Power OFF. All measurements are for 3C147. Two OFF scans were done, one before and one after the ON scan. The sensitivity was computed using the program *ltasens* which fits a linear polynomial to the OFF power scans to account for drifts in the total power and corrects for the source flux assuming a spectral index. No correction for the sky temperature is made. The dashed lines are the sensitivity before the CSIRO feed was mounted (i.e. the sensitivity of the existing GMRT dual feed) while the solid lines are the sensitivity with the CSIRO feed. The dots with the error bars are the average sensitivity of all antennas. Note that the CSIRO feed measures linear polarization. The expected Tsys is about 100K.

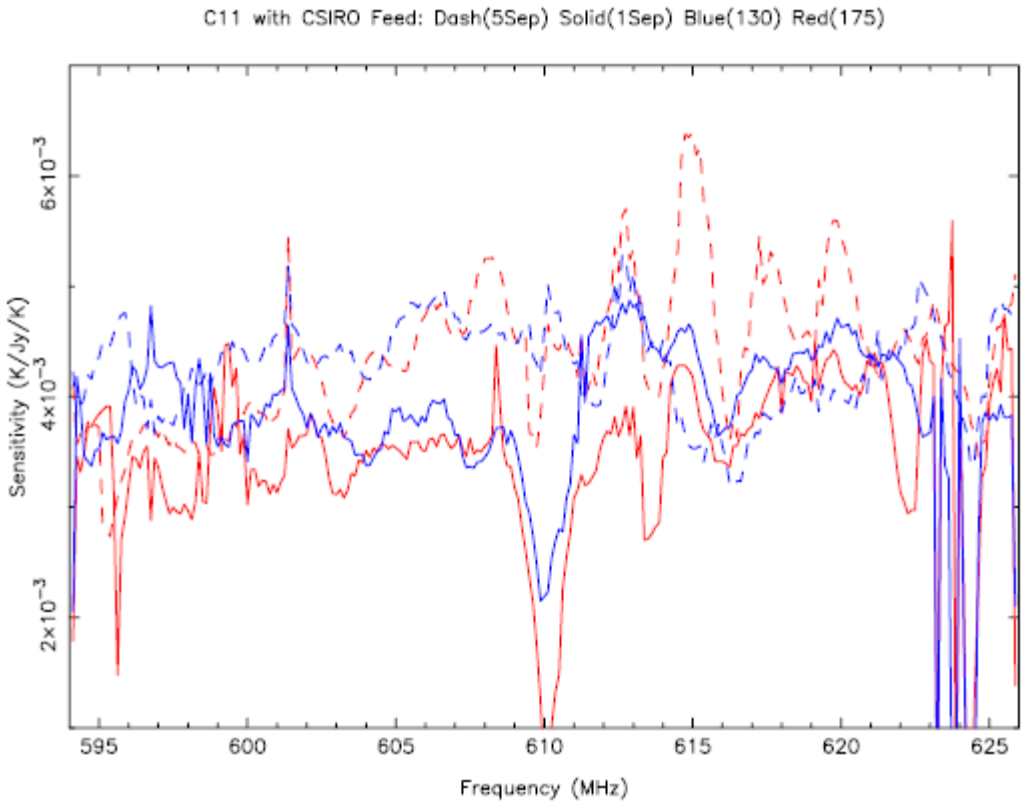

The C11+CSIRO sensitivity shows large ripples. The ripples are different in the different polarizations and also different on different days. The cause of this is currently unclear.

30/08/07

CH. I

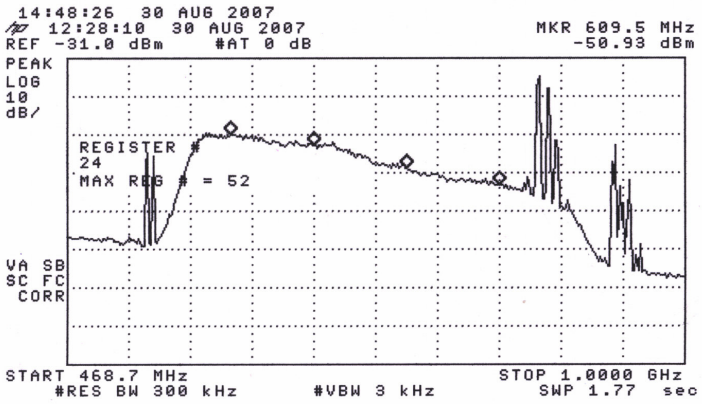

ON-source

source 1- CRAB

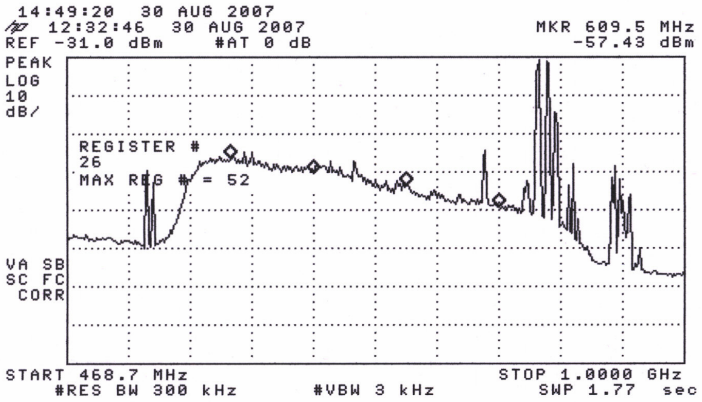

OFF-source

Marker	Frequency	Deflection (dB)
1	609.5 MHz	7.1
2	681.2 MHz	5.2
3	760.9 MHz	5.5
4	840.6 MHz	6.04

Expected (current) deflection at 610 MHz for crab is 6.9 dB

30108107

CH-II

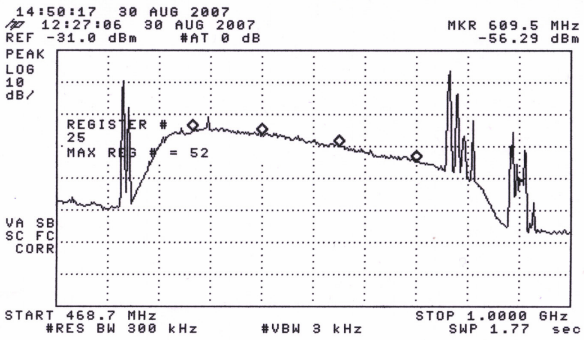

ON-source

source-CRAB

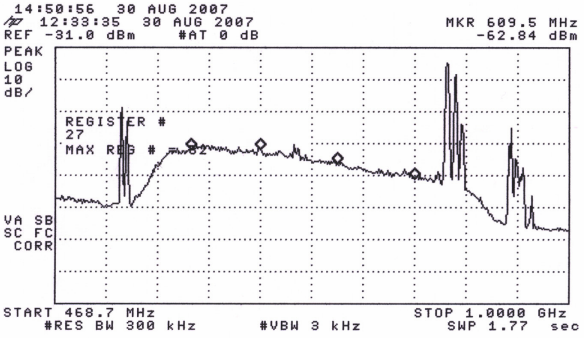

OFF-source

Marker	Frequency	Deflection (dB)
1	609.5 MHz	7.3
2	681.2 MHz	7.18
3	760.9 MHz	7.26
4	840.6 MHz	5.75

Expected (current) deflection at 610 MHz for Crab is 6.9 dB

ON-Source and OFF-source Spectrum analyzer plots for CSIRO feed +C11 antenna

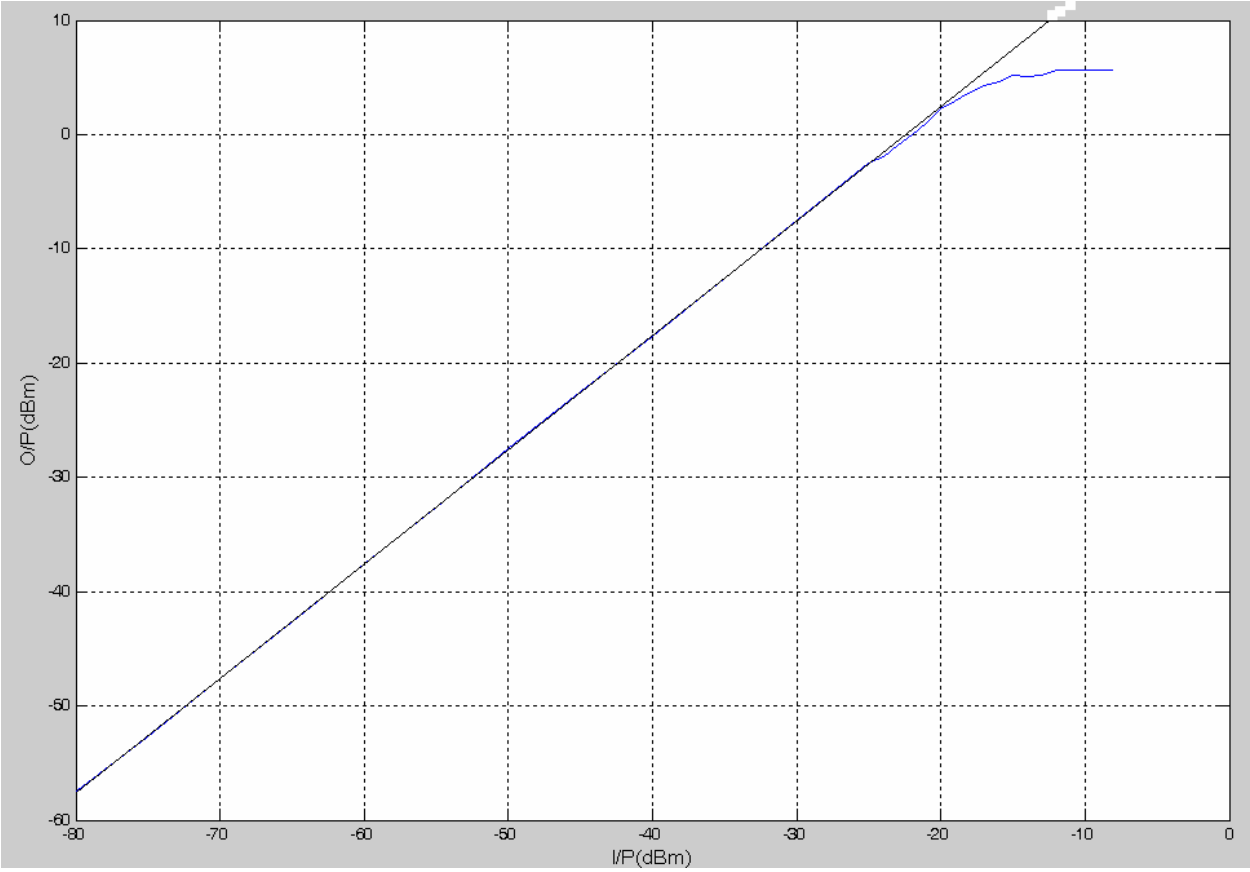

Output power (dBm) vs input power (dBm) for the LNA used for the 550-900 MHz CSIRO feed. The graph coincides with the straight line for low power inputs and deviates from it as the input power increases.

APPENDIX C

TEST RESULTS FOR THE 200-800 MHz ELEVEN FEED

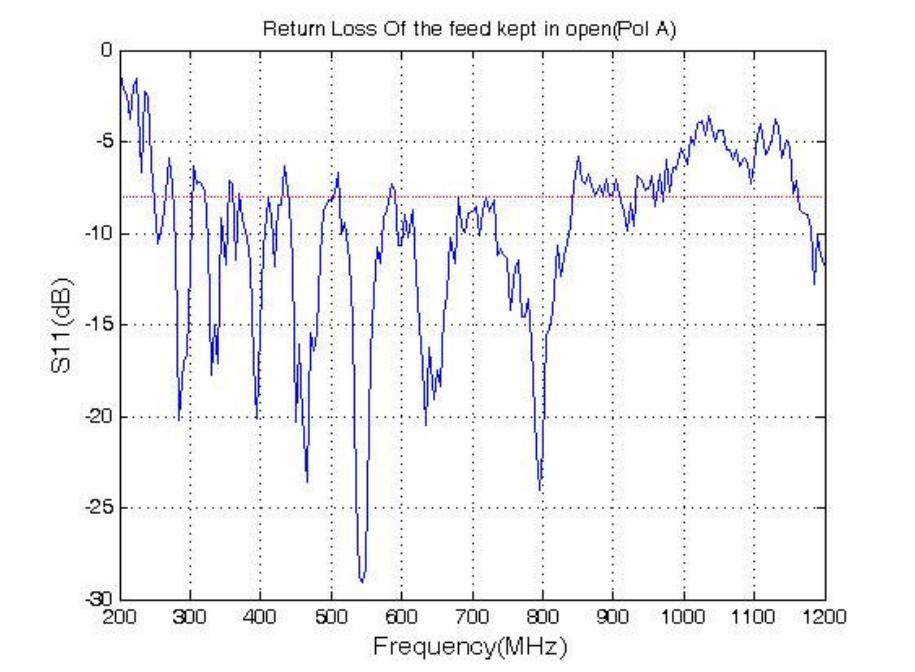

S11 (dB) vs frequency (MHz) of the 200-800 MHz Eleven feed (polarization A)

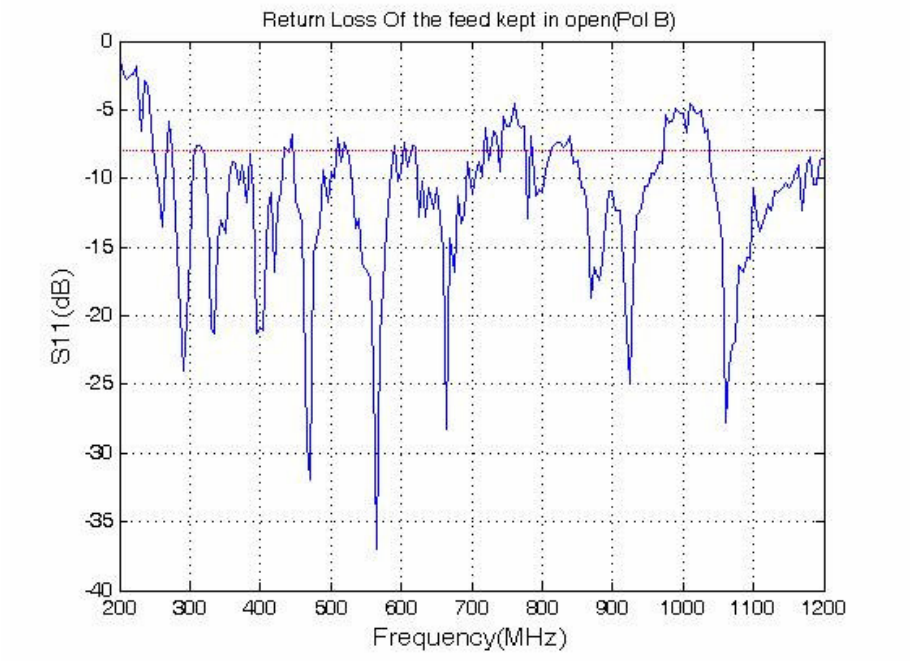

S11 (dB) vs frequency (MHz) of the 200-800 MHz Eleven feed (polarization B)

8/17/07

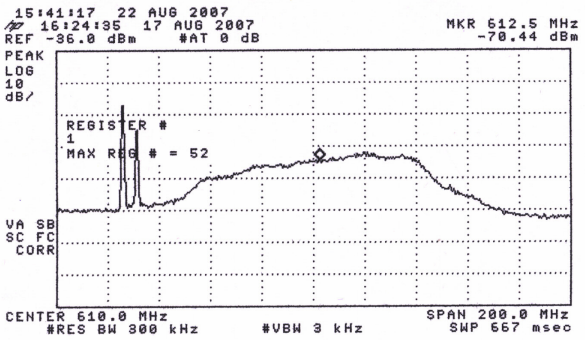

Source: Virgo

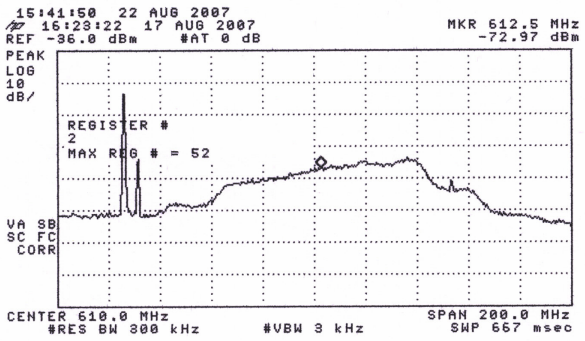

Frequency	Deflection	Expected
612.5 MHz	2.5 dB	3.8 dB

ON-Source and OFF-source Spectrum analyzer plots for Eleven feed+C02 antenna